SEISMIC RESPONSE CONTROL OF COUPLED STRUCTURES USING PASSIVE NEGATIVE STIFFNESS CONNECTION

by

Sonia LONGJAM

A dissertation

submitted to the Hokkaido University

in partial fulfilment of the requirement for the degree of

Doctor of Philosophy

in the field of Architectural and Structural Design

August 10, 2022

北海道大学

HOKKAIDO UNIVERSITY

ACKNOWLEDGMENTS

First and foremost, I would like to express my deepest gratitude to my supervisor, Dr. **Kazutaka SHIRAI**, Associate Professor at Hokkaido University, whose constant guidance, support, and encouragement proved pivotal during my Ph.D. years. Throughout my doctoral study, he has been a constant source of wisdom and encouragement. His tremendous research perspective and experience have greatly aided and influenced my research and will continue to do so in the future. I am grateful for his time, kindness, and wisdom in guiding me through my Ph.D. journey.

I would like to extend my gratitude to my thesis committee members, Dr. **Taichiro OKAZAKI** and Dr. **Shunji KANIE**, for their insightful comments and encouragement. Their comments prompted me to broaden the scope of my research to include multiple perspectives. I am also grateful to Dr. **Masaru KIKUCHI**, Professor at Hokkaido University, for providing an excellent research environment in the Building Structure Control Laboratory.

I would like to express my heartfelt regards to Ms. **Emi KIRIMOTO**, who helped with official paperwork and provided mental support throughout my doctoral study. I would like to thank my lab members for providing me with valuable support: **Bote SHU**, **Marco GREGORIUS**, **Jun IBA**, and **Ji Hyun PARK**. I would like to extend my thanks to my friend, **Anand KONJENGBAM,** who has been there through thick and thin.

A special note of thanks to **my family** and **friends**: Words cannot express how grateful I am to my parents, sisters, relatives, and a handful of my friends for having faith in me, encouraging, and supporting me throughout this work.

Lastly, I would like to express my gratitude to **Hokkaido University** and the **Japan Society for the Promotion of Science (JSPS)** for the studentship that enabled me to conduct this thesis.

ABSTRACT

Coupled vibration control (CVC) system is a promising method formed by linking two or more adjacent buildings with a connecting mechanism to reduce the response under dynamic excitations such as earthquakes. A spring and/or a damping element as vibration controllers connecting a mainframe and a subframe represent a typical passive CVC system. Over the last years, a number of control techniques have been proposed for the structural protection of CVC systems against earthquakes. The control techniques include passive, active, and semiactive control strategies. Various vibration control devices, primarily energy dissipators, have been proposed and practically applied to reduce the CVC systems' seismic response. Negative stiffness, which exerts an opposing restoring force when the displacement increases, is considered a potential vibration control technique for structures. In the past decades, rapid progress has been made in researching and developing negative stiffness devices (NSDs) incorporated into individual buildings. However, research on the incorporation of NSDs into CVC structures is very limited and remains challenging, despite the increasing applications of coupled building control. There has been limited research on assessing the seismic control effectiveness of a passive or active negative stiffness as a connecting controller for CVC systems.

This thesis explores the behaviour and control efficiency of a passive NSD (PNSD) to improve the seismic resistance of coupled buildings. PNSD as a connecting element is installed between the mainframe and subframe, forming the CVC system. This work highlights four objectives to accomplish the aim: (1) to investigate the behaviour of PNSD as the vibration control device and optimal tuning of the CVC structures; (2) to examine the linear and nonlinear numerical response of adjacent single degree of freedom (SDOF) structures connected by PNSD; (3) to figure out the control performance of PNSD on multi degrees of freedom (MDOF) CVC systems; (4) to validate the analytical and numerical investigation of the effective control technique of PNSD on CVC system through experiments. In this dissertation, the optimal parameters to effectively reduce the seismic response of the CVC systems were established. The numerical investigation of the CVC system incorporated with PNSD was verified with the experimental data.

TABLE OF CONTENTS

Chapter III: Numerical investigation on control effects by negative stiffness connection for CVC buildings subjected to earthquakes

Chapter IV: Numerical analysis of the seismic controlled motion for coupled MDOF buildings by negative stiffness connection

LIST OF FIGURES

Chapter II: Analytical investigation of coupled vibration control structures incorporating negative stiffness connection based on the transfer function

Chapter III: Numerical investigation on control effects by negative stiffness connection for CVC buildings subjected to earthquakes

LIST OF TABLES

Chapter II: Analytical investigation of coupled vibration control structures incorporating negative stiffness connection based on the transfer function

Chapter III: Numerical investigation on control effects by negative stiffness connection for CVC buildings subjected to earthquakes

Chapter IV: Numerical analysis of the seismic controlled motion for coupled MDOF buildings by negative stiffness connection

Chapter V: Experimental investigation on the coupled vibration control structures using a passive negative stiffness device

LIST OF SYMBOLS

$A_{1,acc}$ amplitude of the absolute acceleration TF for the mainframe

$A_{1,disp}$ amplitude of the relative displacement TF for the mainframe

$A_{2,acc}$ amplitude of the absolute acceleration TF for the subframe

$A_{2,disp}$ amplitude of the relative displacement TF for the subframe

C_0 lateral viscous damping coefficient at the connecting portion

$C_{0,opt}$ optimal viscous damping coefficient at the connecting portion for minimizing the peak amplitude of the displacement TF for the mainframe of the CVC-SD model when $K_{0,opt}$ was set

$C_{0,ref}$ reference viscous damping coefficient at the connecting portion for minimizing the peak amplitude of the displacement TF for the mainframe of the CVC-D model

$h_{0,opt}$ optimal damping ratio of $C_{0,opt}$ when $K_{0,opt}$ was set for the CVC-SD model {i.e., $h_{0,opt} = C_{0,opt}/[2(M_1K_1)^{0.5}]$}

$h_{0,ref}$ reference damping ratio of $C_{0,ref}$ for the CVC-D model {i.e., $h_{0,ref} = C_{0,ref}/[2(M_1K_1)^{0.5}]$}

i imaginary unit

J_1 evaluation criteria for the response displacement

J_2 evaluation criteria for the response acceleration

J_3 evaluation criteria for the response displacement root mean square

K_0 lateral stiffness of the spring element at the connecting portion for the CVC-SD model

$K_{0,opt}$ optimal stiffness at the connecting portion for optimal tuning for the displacement TF of the mainframe for the CVC-SD model using Equation (16)

$(K_{0,opt}/K_1)$ optimal stiffness ratio for the CVC-SD model

K_1 lateral stiffness of the mainframe

K_2 lateral stiffness of the subframe

M_1 mass of the mainframe

M_2 mass of the subframe

N number of data

n story number

$PA_{1,acc,opt}$ peak amplitude of the acceleration TF for the mainframe when $K_{0,opt}$ and $C_{0,opt}$ were set for the CVC-SD model

$PA_{1,acc,ref}$ peak amplitude of the acceleration TF for the mainframe when $C_{0,ref}$ was set for the CVC-D model

$PA_{1,disp,opt}$ optimized peak amplitude of the displacement TF for the mainframe when $K_{0,opt}$ and $C_{0,opt}$ were set for the CVC-SD model

$PA_{1,disp,ref}$ peak amplitude of the displacement TF for the mainframe when $C_{0,ref}$ was set for the CVC-D model

$PA_{2,acc,opt}$ peak amplitude of the acceleration TF for the subframe when $K_{0,opt}$ and $C_{0,opt}$ were set for the CVC-SD model

$PA_{2,acc,ref}$ peak amplitude of the acceleration TF for the subframe when $C_{0,ref}$ was set for the CVC-D model

$PA_{2,disp,opt}$ peak amplitude of the displacement TF for the subframe when $K_{0,opt}$ and $C_{0,opt}$ were set for the CVC-SD model

$PA_{2,disp,ref}$ peak amplitude of the displacement TF for the subframe when $C_{0,ref}$ was set for the CVC-D model

$PA_{1,ns}$ peak seismic response acceleration for the mainframe of the CVC-NS model

$PA_{1,rc}$ peak seismic response acceleration for the mainframe of the CVC-R model

$PA_{1,SDOF}$ peak seismic response acceleration of experiment's SDOF-mainframe model

$PD_{1,ns}$ peak seismic response displacement for the mainframe of the CVC-NS model

$PD_{1,rc}$ peak seismic response displacement for the mainframe of the CVC-R model

$PD_{1,SDOF}$ peak seismic response displacement of experiment's SDOF-mainframe model

$PR_{1,acc,opt}$ peak seismic response acceleration for the mainframe of the CVC-SD model

$PR_{1,acc,ref}$ peak seismic response acceleration for the mainframe of the CVC-D model

$PR_{1,acc,SDOF}$ peak seismic response acceleration of the SDOF-mainframe model

$PR_{1,disp,opt}$ peak seismic response displacement for the mainframe of the CVC-SD model

$PR_{1,disp,ref}$ peak seismic response displacement for the mainframe of the CVC-D model

$PR_{1,disp,SDOF}$ peak seismic response displacement of the SDOF-mainframe model

RMS(x_1) root mean square of the response displacement

s Laplace variable (= $i\omega$)

t time

t_f	duration (= $N\Delta t$)
T_1	natural period of the mainframe for the state of the mainframe alone
T_2	natural period of the subframe for the state of the subframe alone
x_1	relative displacement from the ground of the mainframe in the time domain
X_1	relative displacement from the ground of the mainframe in the frequency domain
$x_1(t)$	response displacement of the mainframe
$\ddot{x}_1(t)$	response acceleration of the mainframe
x_2	relative displacement from the ground of the subframe in the time domain
X_2	relative displacement from the ground of the subframe in the frequency domain
x_G	displacement of the ground motion in the time domain
X_G	displacement of the ground motion in the frequency domain
$\ddot{x}_G(t)$	input acceleration
α	stiffness ratio (= K_2/K_1)
Δt	time interval
μ	mass ratio (= M_2/M_1)
ω	circular frequency
ω_1	natural circular frequency for the state of the mainframe alone

Chapter I

Introduction

1. Research background

Coupled Vibration Control (CVC) structures are systems formed by linking two or more adjacent buildings with different or same natural periods using a connecting mechanism for reducing vibration, such as earthquake responses [1,2]. CVC strategies have been proven viable approach for protecting adjacent structures by enhancing their seismic resistance [3–8]. The idea of CVC structures with a connecting device to reduce their dynamic response from external excitation is extensively utilized in the control theory [7–9].

Many experimental and numerical studies have proven that coupling the adjacent building employing damping devices improves the CVC systems' seismic performance. Over the last years, a number of control techniques have been proposed for the structural protection of CVC systems against earthquakes. The control techniques include passive, active, and semiactive control strategies [10–18]. Among the various types of passive damping devices, viscous or viscoelastic dampers, hysteretic dampers, and friction dampers, primarily energy dissipators, have been proposed, developed, and practically applied to reduce the seismic response of the CVC systems. Researchers have studied the efficacies of these devices [19–26].

Past research has shown that the controlling performance of CVC structures varies depending on the structural parameters, including the stiffness, damping coefficient at the connecting portion, and the mass and stiffness of the adjacent structures (i.e., mainframe and subframe). Thus, there exists optimal parameters to reduce the earthquake response effectively [27–31]. The control effects of passive CVC system can be evaluated based on the peak amplitude of the transfer function (TF) for the systems [27]. An optimal design formula based on the fixed-point theory [30] is often used to design seismic tuned mass dampers [31–32]. Based on the fixed-point theory of CVC buildings, Kageyama et al. [27] theoretically derived an optimal design formula for a connection spring at the connecting portion of CVC structures. Depending on the structural parameter conditions for the mainframe and subframe, there are cases in which it is sometimes difficult to

obtain an optimal tuning that minimizes the peak amplitude of the TF of CVC structures by using only positive or zero stiffness at the connecting portion. Therefore, despite the vast study base and increasing applications of coupled building control, more research on the effects of diverse building layouts and types of coupling elements is still needed.

Negative stiffness, which exerts an opposing restoring force when the displacement increases, may be used as a vibration control (VC) technique for civil, building, and mechanical structures [33]. In the past decades, rapid progress has been made in the research and development of negative stiffness devices (NSDs) and systems incorporating NSDs [34–39]. More recently, several VC systems with NSDs for seismic protection of structures have been studied [40–43]. The authors proposed a passive negative stiffness device (PNSD) made of curved leaf springs that use geometric nonlinearity to generate a negative restoring force characteristic by exploiting elastic snap-through buckling reversal phenomena [44]. They conducted shake table tests and demonstrated that adopting negative stiffness in a vibrating system decreases the equivalent stiffness, resulting in an increase in the apparent period during an earthquake.

It should be highlighted that all these studies on NSDs focus solely on the seismic response of the individual buildings. The incorporation of NSD for CVC structures has yet to be examined for a broad range of buildings and connector configurations. There has been limited research on assessing the seismic control effectiveness of a passive or active negative stiffness as the connecting controller for CVC system [45–48]. Upon incorporating negative stiffness and damper devices as the connecting portion of CVC structures, it is anticipated that the range of the optimal tuning conditions may be extended, which is usually challenging when using only positive or zero stiffness, as mentioned previously.

Based on the above literature, NSD as connecting vibration controller is expected to enhance the structural performances of the coupled structures. However, studies in this area are very limited and remain challenging. Therefore, the present study was conducted to understand the behavior of the NSD and its controlling efficiency. This study includes an analytical investigation for optimal tuning of CVC structures and to understand the

essential characteristics of negative stiffness as the connecting device. The CVC structures were formed by connecting two adjacent structures, namely mainframe and subframe, with a vibration control device(s). The mainframe was considered the target-controlled structure, whereas the subframe wasn't the target-controlled structure. The time history seismic response simulation of the linear and nonlinear CVC structures to evaluate the control effect by negative stiffness connection subjected to earthquakes was also computed. Experiments on incorporating the PNSD in CVC structures using the shake table test were performed to validate the analytical and numerical investigation.

2. Critical review

Although several studies have been done in the past about the coupling of adjacent buildings utilizing dampers as controllers, to the authors' knowledge, the implementation of NSD as a vibration controller for CVC models has not yet been fully clarified. There is much research on NSD as a vibration controller for individual buildings; however, the seismic response control effects of CVC adjacent structures incorporating PNSDs at the connecting portion remain unclear [40–48]. Therefore, research in this area is necessary.

Additionally, there are cases in which it is sometimes difficult to obtain an optimal tuning that minimizes the peak amplitude of the TF of CVC structures by using only positive or zero stiffness at the connecting portion. Based on previous research, it is anticipated that introducing NSD as a coupling mechanism may solve the limitation of optimal tuning conditions [27,44]. Extensive parametric studies are required to find optimum NSD properties for adjacent buildings with different stiffness ratios and mass ratios of the coupled structures.

Furthermore, available research needs to investigate further on the sensitivity of NSDs based on their design parameters. Investigation on the formulation of multi-degree of freedom CVC structures used for numerical studies on the seismic response control effects by incorporating PNSDs at the connecting portion under various dynamic excitation is required. Analytical models of the CVC structures for efficient vibration control and numerical and experimental study for negative stiffness devices are still in the infant stage. The analytical, numerical, and experimental investigation presented in this thesis is an appealing control technique for CVC structure. This study validates the effective technique of seismic response reduction of CVC structures by a passive NSD through simulation and experimental studies.

3. Objectives

This research aims to comprehend the control effect that the PNSD has on CVC structures to increase the connected buildings' seismic resistance. To accomplish this aim, the following objectives have been attained:

(1) To investigate the optimal tuning of the peak amplitude response of CVC models on incorporating of PNSD as the connecting vibration controller by establishing analytical models of two degree of freedom (2DOF) CVC structures.
(2) To evaluate the linear and nonlinear seismic response control of the 2DOF CVC systems linked with a PNSD.
(3) To perform the numerical investigation of linear seismic response control of the multi-degree of freedom (MDOF) CVC system connected by PNSD.
(4) To conduct a shake table test and experimentally validate the control effectiveness of the PNSD on CVC structures.

4. Methodology

In this study, the research methodology consisted of:

- Performing analytical investigation on the 2DOF CVC structures based on transfer function analysis.
- Numerical investigation on the linear and nonlinear seismic response analyses of 2DOF CVC structures.
- Investigating the numerical analysis of the linear seismic response of MDOF CVC structures.
- Conducting a shake table test to experimentally obtain the response and validate the vibration control effect of the PNSD on CVC systems under dynamic excitations.

5. Overview

In addition to the introductory chapter that clarifies the research background, critical review, and research objectives, the main body of this thesis consists of four chapters (Chapter II-V), with the sixth chapter addressing the conclusion and recommendations for future research. Therefore, this thesis is structured into six chapters, which can be summarized as follows:

Chapter I introduces the background and review of existing research on PNSD-based vibration control techniques for CVC systems.

Chapter II conducts an analytical investigation of a linear two-degrees-of-freedom (2DOF) vibrating system model representing a simplified coupled vibration-controlled building to ascertain the fundamental properties of PNSD on adjacent structures. Based on the transfer function (TF) of the model's relative displacement and absolute acceleration, the peak amplitude was investigated for the CVC system. For optimal tuning of the displacement TF for the mainframe, the optimal stiffness ratio and optimal viscous damping coefficient were calculated against various stiffness ratio (α) and mass ratio (μ). For comparison, a reference viscous damping coefficient for the connecting element that minimizes the peak amplitude of the displacement TF for the mainframe without the connecting spring element was numerically obtained. The analysis found that adopting negative stiffness in the connection elements enabled optimal tuning of the TF for the mainframe, even if it was impossible to achieve by positive or zero stiffness.

Chapter III inspects linear and nonlinear seismic response analyses of 2DOF CVC systems linked by PNSD to determine adjacent structures' dynamic characteristics and seismic responses. Four groups of numerical models having linear characteristics were used, i.e., SDOF mainframe models, SDOF subframe models, 2DOF CVC models with PNSD and damper as the connecting elements (CVC-SD), and 2DOF CVC models with damper as the connecting element (CVC-D). For the state of the mainframe alone, three natural periods were specified, and six combinations of α and μ were selected such that each group consisted of 18 cases of models. The optimization was done using the

mainframe displacement TF as a control target. The mainframe response was effectively controlled to a significant extent as a result. In addition, nonlinear earthquake response simulations were conducted using the CVC-SD, CVC-D, and SDOF-mainframe models.

Chapter IV discusses a study on the numerical investigation of the seismic controlled motion for multi-story coupled structures linked by negative stiffness connection. The analysis included the MDOF mainframe model and MDOF subframe model of equal heights with substantially different structural properties connected by vibration controller(s) subjected to various earthquake motions. The study indicates that the reduction in the structural responses of the CVC system subjected to input motions depends on the setting of the connecting elements. The negative stiffness's significant ability to control vibration as a connecting vibration controller of coupled models was observed.

Chapter V addresses shaking table tests carried out for obtaining the earthquake response of connected building models using a prototyped PNSD to study the vibration control effects experimentally. The CVC model used in this experiment was of one mass system of mainframe and one mass system of a subframe. The CVC systems were examined by shaking table tests with/without the prototyped PNSD, subjected to sinusoidal and simulated earthquake waves. The result shows that PNSD exhibited negative stiffness over a displacement range. A reduction in the displacement response of the coupled structures occurred upon incorporating PNSD.

Chapter VI concludes the thesis and discusses the scope of future work. The results of the evaluations show that adopting PNSD in CVC structures can extend the range of optimal tuning conditions. The effective control performance of PNSD as a vibration controller of adjacent structures was understood. Evidently, the results show that PNSD can be considered as one of the potential vibration controllers for adjacent structures. Lastly, some directions for future work are listed.

6. Information details of the papers

Peer reviewed conference paper:

Longjam S, Shirai K (2021) Use of negative stiffness for coupled vibration control structures: an analytical investigation. *The 17th World Conference on Earthquake Engineering*, September 27–October 2, 2021, Sendai, Japan.

Published peer reviewed journal paper:

Longjam S, Shirai K (2022) Numerical investigation of earthquake response reduction effects by negative stiffness connection for adjacent building structures. *Structures*, Vol. **38**, 672-688. https://doi.org/10.1016/j.istruc.2022.01.078

7. References

[1] Basili M, De Angelis M (2017) Vibration analysis and models of adjacent structures controlled by magnetorheological dampers. *Shock and Vibration*. Article ID 9596382. https://doi.org/10.1155/2017/9596382

[2] Zhu H, Iemura H (2000) A study of response control on the passive coupling element between two parallel structures. *Structural Engineering and Mechanics*. **9**(4):383–396. https://doi.org/10.12989/sem.2000.9.4.383

[3] Xu YL, He Q, Ko JM (1999) Dynamic response of damper-connected adjacent buildings under earthquake excitation. *Engineering Structures*, **21**(2):135–148. https://doi.org/10.1016/S0141-0296(97)00154-5

[4] Tubaldi E (2015) Dynamic behavior of adjacent buildings connected by linear viscous/viscoelastic dampers. *Structural Control and Health Monitoring*, **22**(8):1086–1102. https://doi.org/10.1002/stc.1734

[5] Jankowski R, Mahmoud S (2016) Linking of adjacent three-storey buildings for mitigation of structural pounding during earthquakes. *Bulletin of Earthquake Engineering*, **14**(11):3075–3097. https://doi.org/10.1007/s10518-016-9946-z

[6] Tubaldi E, Gioiella L, Scozzese F, Ragni L, Dall'Asta A (2020) A design method for viscous dampers connecting adjacent structures. *Frontiers in Built Environment*, **6**:25. https://doi.org/10.3389/fbuil.2020.00025

[7] Minami S, Yamazaki S, Toyama K, Tahara K (2004) Experimental study on coupled vibration control structures. *The 13th World Conference on Earthquake Engineering*, Paper No. 2351, August 1–6, 2004, Vancouver, B.C., Canada.

[8] Palacios-Quiñonero F, Rubió-Massegú J, Rossell JM, Karimi HR (2014) Vibration control for adjacent structures using local state information. *Mechatronics*, **24**(4):336–344. http://dx.doi.org/10.1016/j.mechatronics.2013.08.001

[9] Zhang WS, Xu YL (2000) Vibration analysis of two buildings linked by Maxwell model-defined fluid dampers. *Journal of Sound and Vibration*, **233**(5):775–796. https://doi.org/10.1006/jsvi.1999.2735

[10] Bharti SD, Dumne SM, Shrimali MK (2010) Seismic response analysis of adjacent buildings connected with MR dampers. *Engineering Structures*, **32**(8):2122–2133. https://doi.org/10.1016/j.engstruct.2010.03.015

[11] Uz ME, Hadi MNS (2014) Optimal design of semi active control for adjacent buildings connected by MR damper based on integrated fuzzy logic and multi-objective genetic algorithm. *Engineering Structures*, **69**:135–148. https://doi.org/10.1016/j.engstruct.2014.03.006

[12] Guenidi Z, Abdeddaim M, Ounis A, Shrimali MK, Datta TK (2017) Control of adjacent buildings using shared tuned mass damper. *Procedia Engineering*, **199**:1568–1573. https://doi.org/10.1016/j.proeng.2017.09.059

[13] Al-Fahdawi OAS, Barroso LR, Soares RW (2018) Utilizing the adaptive control in mitigating the seismic response of adjacent buildings connected with MR dampers. *2018 Annual American Control Conference (ACC)*:912–917. https://doi.org/10.23919/ACC.2018.8431135

[14] Ndemanou BP, Nbendjo BRN (2018) Fuzzy magnetorheological device vibration control of the two Timoshenko cantilever beams interconnected under earthquake excitation. *The Structural Design of Tall and Special Buildings*, **27**(17):e1541. https://doi.org/10.1002/tal.1541

[15] Al-Fahdawi OAS, Barroso LR, Soares RW (2019) Simple adaptive control method for mitigating the seismic responses of coupled adjacent buildings considering parameter variations. *Engineering Structures*, **186**:369–381. https://doi.org/10.1016/j.engstruct.2019.02.025

[16] Al-Fahdawi OAS, Barroso LR, Soares RW (2019) Semi-active adaptive control for enhancing the seismic performance of nonlinear coupled buildings with smooth hysteretic behavior. *Engineering Structures*, **191**:536–548. https://doi.org/10.1016/j.engstruct.2019.04.078

[17] Al-Fahdawi OAS, Barroso LR (2021) Adaptive neuro-fuzzy and simple adaptive control methods for full three-dimensional coupled buildings subjected to bi-directional seismic excitations. *Engineering Structures*, **232**:111798. https://doi.org/10.1016/j.engstruct.2020.111798

[18] Ohtori Y, Christenson RE, Spencer Jr. BF, Dyke SJ (2004) Benchmark control problems for seismically excited nonlinear buildings. *Journal of Engineering Mechanics*, **130**(4): 366–385. https://doi.org/10.1061/(ASCE)0733-9399(2004)130:4(366)

[19] Ni YQ, Ko JM, Ying ZG (2001) Random seismic response analysis of adjacent buildings coupled with non-linear hysteretic dampers. *Journal of Sound and Vibration*, **246**(3):403–417. https://doi.org/10.1006/jsvi.2001.3679

[20] Ying ZG, Ni YQ, Ko JM (2003) Stochastic optimal coupling-control of adjacent building structures. *Computers & Structures*, **81**(30–31):2775–2787. https://doi.org/10.1016/S0045-7949(03)00332-8

[21] Christenson RE, Spencer Jr BF, Johnson EA, Seto K (2006) Coupled building control considering the effects of building/connector configuration. *Journal of structural engineering*, ASCE, **132**(6):853–863. https://doi.org/10.1061/(ASCE)0733-9445(2006)132:6(853)

[22] Basili M, De Angelis M, Fraraccio G (2013) Shaking table experimentation on adjacent structures controlled by passive and semi-active MR dampers. *Journal of Sound and Vibration*, **332**(13):3113–3133. https://doi.org/10.1016/j.jsv.2012.12.040

[23] Basili M, De Angelis M, Pietrosanti D (2019) Defective two adjacent single degree of freedom systems linked by spring-dashpot-inerter for vibration control. *Engineering Structures*, **188**:480–492. https://doi.org/10.1016/j.engstruct.2019.03.030

[24] De Domenico D, Qiao H, Wang Q, Zhu Z, Marano G (2020) Optimal design and seismic performance of Multi‐Tuned Mass Damper Inerter (MTMDI) applied to adjacent high‐rise buildings. *The Structural Design of Tall and Special Buildings*, **29**(14):e1781. https://doi.org/10.1002/tal.1781

[25] Kazemi F, Miari M, Jankowski R (2021) Investigating the effects of structural pounding on the seismic performance of adjacent RC and steel MRFs. *Bulletin of Earthquake Engineering*, **19**(1):317–343. https://doi.org/10.1007/s10518-020-00985-y

[26] Lu L, Xu J, Zhou Y, Lu W, Spencer Jr BF (2021) Viscous inertial mass damper (VIMD) for seismic responses control of the coupled adjacent buildings. *Engineering Structures*, **233**:111876. https://doi.org/10.1016/j.engstruct.2021.111876

[27] Kageyama M, Yasui Y, Seto K (2000) The principal solutions of connecting spring and damper for optimum vibration control under several criteria. *Journal of Structural and Construction Engineering*, AIJ, **65**(529):97−104. **(in Japanese)** https://doi.org/10.3130/aijs.65.97

[28] Zhu H, Wen Y, Iemura H (2001) A study on interaction control for seismic response of parallel structures. *Computers & Structures*, **79**(2):231−242. https://doi.org/10.1016/S0045-7949(00)00119-X

[29] Zhu HP, Ge DD, Huang X (2011) Optimum connecting dampers to reduce the seismic responses of parallel structures. *Journal of Sound and Vibration*, **330**(9): 1931–1949. https://doi.org/10.1016/j.jsv.2010.11.016

[30] Den Hartog JP (1956) Mechanical vibrations, 4th ed. McGraw-Hill, New York.

[31] Shirai K, Park J (2020) Use of scrap tire pads in vibration control system for seismic response reduction of buildings. *Bulletin of Earthquake Engineering*, **18**(5): 2497−2521. https://doi.org/10.1007/s10518-020-00787-2

[32] Sano T, Shirai K, Yoshida O, Nishikage T (2021) Assessment of a seismic tuned mass damper with friction fail-safe mechanism for the vibration control of high-rise buildings. *Structural Control and Health Monitoring*:e2831. https://doi.org/10.1002/stc.2831

[33] Li H, Li Y, Li J (2020) Negative stiffness devices for vibration isolation applications A review. *Advances in Structural Engineering*, **23**(8):1739−1755. https://doi.org/10.1177/1369433219900311

[34] Mizuno T, Toumiya T, Takasaki M (2003) Vibration isolation system using negative stiffness. *JSME International Journal*, Series C, **46**(3):807−812. https://doi.org/10.1299/jsmec.46.807

[35] Iemura H, Kouchiyama O, Toyooka A, Shimoda I (2008) Development of the friction-based passive negative stiffness damper and its verification tests using shaking table. *The 14th World Conference on Earthquake Engineering*, October 12−17, 2008, Beijing, China.

[36] Nagarajaiah S, Pasala DTR, Reinhorn A, Constantinou M, Sirilis AA, Taylor D (2013) Adaptive negative stiffness: a new structural modification approach for seismic protection. *Advanced Materials Research*, **639**–**640**:54−66. https://doi.org/10.4028/www.scientific.net/AMR.639-640.54

[37] Sarlis AA, Pasala DTR, Constantinou MC, Reinhorn AM, Nagarajaiah S, Taylor DP (2013) Negative stiffness device for seismic protection of structures. *Journal of Structural Engineering*, ASCE, **139**(7):1124−1133. https://doi.org/10.1061/(ASCE)ST.1943-541X.0000616

[38] Walsh KK, Boso, E., Steinberg EP, Haftman JT, Littell WN (2018) Variable negative stiffness device for seismic protection of building structures through apparent weakening. *Journal of Engineering Mechanics*, **144**(9):04018090. https://doi.org/10.1061/(ASCE)EM.1943-7889.0001512

[39] Zhou P, Liu M, Li H (2020) A passive negative stiffness damper in series with a flexible support: Theoretical and experimental study. *Structural Control and Health Monitoring*, **27**(9):e2594. https://doi.org/10.1002/stc.2594

[40] Nagarajaiah S, Sen D (2020) Apparent-weakening by adaptive passive stiffness shaping along the height of multistory building using negative stiffness devices and dampers for seismic protection. *Engineering Structures*, **220**:110754. https://doi.org/10.1016/j.engstruct.2020.110754

[41] Shi X, Zhao F, Yan Z, Zhu S, Li JY (2021) High‐performance vibration isolation technique using passive negative stiffness and semiactive damping. *Computer‐Aided Civil and Infrastructure Engineering*, **36**(8):1034–1055. https://doi.org/10.1111/mice.12681

[42] Salvatore A, Carboni B, Lacarbonara W (2021) Nonlinear dynamic response of an isolation system with superelastic hysteresis and negative stiffness. *Nonlinear Dynamics*. https://doi.org/10.1007/s11071-021-06666-y

[43] Walsh KK, Sallar G, Haftman JT, Steinberg EP (2021) Resetting passive stiffness damper with passive negative stiffness device for seismic protection of structures. *Structural Control and Health Monitoring*, **28**(8):e2774. https://doi.org/10.1002/stc.2774

[44] Shirai K, Noro S, Walsh KK (2021) Shake table testing of a passive negative stiffness device with curved leaf springs for seismic response mitigation of structures. *Structural Control and Health Monitoring*, **28**(7):e2736. https://doi.org/10.1002/stc.2736

[45] Yamada Y, Ikawa N, Yokoyama H, Tachibana E (1994) Active control of structures using the joining member with negative stiffness. *The First World Conference on Structural Control*, TP2, Vol. 2, 41–49, 1994, California, USA.

[46] Ikawa N, Yamada Y, Yokoyama H, Tachibana E (1996) Active control system of coupled structures with a negative stiffness. *Journal of Structural Engineering*, AIJ, Vol. **42B**: 629–634. **(in Japanese)**

[47] Shimizu K, Kurino H (2009) Fundamental study of structural control with negative stiffness connection. Part 1: Study of applicability of negative stiffness. *Summaries of Technical Papers of Annual Meeting*, AIJ:453–454. **(in Japanese)**

[48] Kurino H, Shimizu K (2009) Fundamental study of structural control with negative stiffness connection. Part 2: Feasibility study utilizing variable damping device. *Summaries of Technical Papers of Annual Meeting*, AIJ:455–456. **(in Japanese)**

Chapter II

Analytical investigation of coupled vibration control structures incorporating negative stiffness connection based on the transfer function

Conference paper:

(1) Longjam S, Shirai K (2021) Use of negative stiffness for coupled vibration control structures: an analytical investigation. *The 17th World Conference on Earthquake Engineering*, September 27–October 2, 2021, Sendai, Japan.

Journal paper:

(1) Longjam S, Shirai K (2022) Numerical investigation of earthquake response reduction effects by negative stiffness connection for adjacent building structures. *Structures*, Vol. **38**, 672-688. https://doi.org/10.1016/j.istruc.2022.01.078

The contents of this Chapter II have been taken from the above journal and conference papers except for the Sections 1 (Introduction) and 5 (Conclusions), in which some modifications have been made.

1. Introduction

Different vibration controllers are employed in coupled vibration control (CVC) systems to protect the structures against dynamic excitation such as earthquakes. These vibration controllers are the supplemental connecting structural elements in the form of stiffness and damping devices. A spring and/or a damping element connecting a mainframe and a subframe represent a typical passive CVC system [1–4]. Extensive research on CVC structures, mainly using energy dissipators as connecting elements, has been practically implemented, and the efficacies of these devices on CVC structures have been studied [5–16].

Structural parameters, including the stiffness and damping coefficient at the connecting portion and the mass and stiffness of the mainframe and subframe, affect the controlling performance of CVC structures. As a result, optimal parameters exist to effectively reduce the seismic response [17–20]. The peak amplitude of the transfer function (TF) for the systems can be used to evaluate the control effects of PNSD on CVC structures [18]. An optimal design technique based on the fixed-point theory [21] is often utilized to design seismic tuned mass dampers [22,23]. Theoretically, Kageyama et al. [18] leveraged the fixed-point theory to derive an optimal design formula for a connection spring and a viscous damping element at the connecting portion of a passive CVC structure. While research on the coupling of structures using only positive or zero stiffness has been developed extensively, research on obtaining an optimal tuning that minimizes the peak amplitude of the TF of CVC structures is very limited.

Negative stiffness exerts a negative restoring force with the increase in the displacement, which has the potential to be adopted as a vibration control (VC) technique for structures [24]. The study of negative stiffness devices (NSDs) and systems incorporating NSDs have advanced significantly during the past few decades [25–30]. It is expected that if negative stiffness is implemented together with a damper device at the connecting portion of CVC adjacent building structures, then the limitation of optimum tuning conditions may be extended. However, limited work has been carried out on

assessing the response control effectiveness of a passive or active negative stiffness connecting controller for CVC structures [33–36]. More in-depth research in this area is necessary to effectively overcome the limitation of optimum tuning conditions.

This study investigates the control strategies of coupled structures incorporating passive negative stiffness as the connecting spring element between the mainframe and subframe. An analytical control solution using TF analysis is assessed with a parametric study to examine the basic characteristics of negative stiffness as the vibration controller of a CVC system. A brief description of various NSDs is provided in Section 2 to grasp the concept of the negative stiffness mechanism. Section 3 describes the proposed approach for accomplishing the objective using a linear 2DOF vibrating system model that represents a simplified coupled vibration-controlled building. The analytical investigation's results and discussion are presented in Section 4. Finally, the conclusion derived from this study is summarized in Section 5.

The description of Sections 2-5 is an excerpt from the authors' work [37]. In this study, the authors numerically investigated the effectiveness of negative stiffness as an extensive study on the former analytical investigation of the CVC structures incorporated with negative stiffness as the connecting spring element [38]. For a better understanding, the detailed description of the analytical investigation of a linear two-degree-of-freedom (2DOF) system, representing a simplified coupled vibration-controlled building model, is vividly explained in this chapter.

2. Description of passive negative stiffness devices

This section describes the concept and operation of two passive NSDs that were already proposed by other researchers. In general, negative stiffness works in opposition to positive stiffness, and produces a decreased (i.e., negative) restoring force with the progression of the displacement of the device. A passive NSD using a vertical pre-compressed spring has been developed and studied [27,28,31]. This NSD comprises a pivot plate, a lever, top and bottom chevrons, a pre-loaded spring, gap spring assemblies, and double-hinged columns. In a small displacement range, the NSD generates a total stiffness of approximately zero or slightly larger than zero. When the NSD deforms, the device produces a force that assists motion, i.e., negative stiffness. However, as the NSD deforms, the magnitude of negative stiffness is reduced, leading to positive stiffness at a larger displacement.

Another passive NSD using curved leaf springs has been proposed by one of the authors [32]. This PNSD consists of two curved leaf springs rigidly connected to a pair of beams. The curved leaf springs are pre-compressed such that the strain energy stored leads to an initial negative stiffness before the onset of snap-through buckling. When exceeding a certain displacement, snap-through buckling occurs, resulting in an increase of negative restoring force. This PNSD has a displacement-dependent restoring force characteristic with both negative and positive stiffness; it offers a positive restoring force to resist further deformation once the device's displacement limit is reached. Although the above passive NSD has nonlinearity that depends on the device's displacement, in the present study, PNSD with linear characteristics was supposed for simplicity and used in the subsequent sections.

3. Methods of transfer function analysis

3.1. Analytical models

The linear two-degrees-of-freedom (2DOF) systems shown in Figs. 2a and 2b, assuming simplified CVC structures (Fig. 1), were adopted as the analytical models in the TF analysis. The mainframe (Fig. 2c) and subframe (Fig. 2d) of vibrating systems, representing a pair of adjacent structures, were horizontally connected to each other by a spring element and a viscous damping element at the connection portion. Negative stiffness, as well as positive or zero stiffness, was applied for the connecting spring element. This study aimed to understand the basic characteristics of the response control effects of adjacent buildings with negative stiffness connection using a passive NSD. Response control for the first modal vibration of the mainframe was intended. To this end, the 2DOF model was adopted for simplicity. The supposed building was a building where the first vibration mode was predominant and the stiffness distribution in the height direction was continuous, in each of the mainframe and subframe. The mainframe and subframe were simplified into the SDOF systems and linked by the connection elements. In general, the location in the structural height of the connecting elements affects the control performance of CVC structures. The present study assumed cases of SDOF models where the equivalent height (i.e., the position of the equivalent mass point) of the first mode for the mainframe and subframe was approximately the same, and the mainframe and subframe were horizontally connected at the same floor level close to the equivalent height.

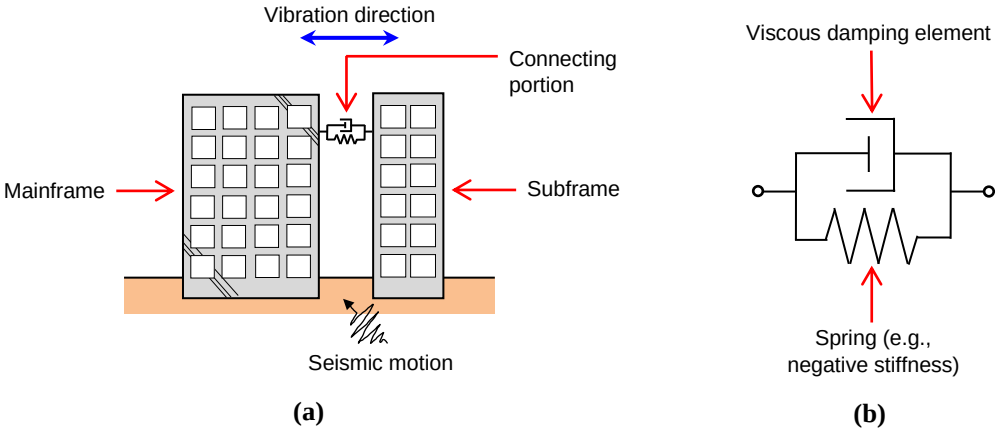

Fig. 1 Conceptual diagram of a coupled vibration control (CVC) building structure: **(a)** elevation view of whole system; and **(b)** enlarged view of connecting portion consisting of a spring and a viscous damping element

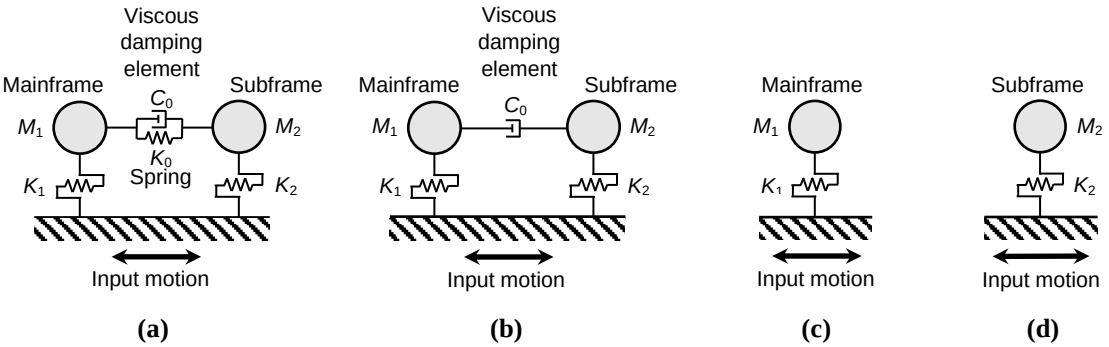

Fig. 2 Analytical models considered: **(a)** optimal-controlled coupled 2DOF model (CVC-SD model); **(b)** reference-controlled coupled 2DOF model (CVC-D model); **(c)** mainframe alone (SDOF-mainframe model); and **(d)** subframe alone (SDOF-subframe model)

3.2. Investigated CVC models and structural parameters

Two CVC models with different connection types, referred as CVC-SD and CVC-D models, were considered, as shown in Figs. 2a and 2b. The CVC-SD model (Fig. 2a) was the 2DOF system connected with both the stiffness element (i.e., spring) and the viscous damping element (i.e., dashpot) at the connecting portion (expressed by Equations (1) through (15)). On the other hand, the mainframe and subframe of the CVC-D model (Fig. 2b) were the same as those of the CVC-SD model, but the connecting element in the CVC-D model consisted of a dashpot alone (i.e., without the negative, or positive stiffness contribution). The equation of motion and the amplitude of the TF for the CVC-D model can be obtained by substituting $K_0 = 0$ into Equations (1) through (15). The TFs for the mainframe and subframe were compared for these two CVC models.

For each of the CVC models, two structural parameters of the 2DOF system, α and μ, were investigated, where α (= K_2/K_1) is the stiffness ratio (i.e., ratio of the lateral stiffness of the subframe to that of the mainframe, and μ (= M_2/M_1) is the mass ratio (i.e., ratio of the mass of the subframe to that of the mainframe). The considered ranges of these two parameters were $0 \le \alpha \le 2$ and $0 \le \mu \le 2$. Table 1 lists the combination values of α and μ investigated in this section.

The equations of motion for the mainframe and subframe, respectively, connected by the spring and viscous damping elements of the 2DOF-CVC system (Fig. 2a) can be expressed as follows:

$$M_1(\ddot{x}_1+\ddot{x}_G)+C_0(\dot{x}_1-\dot{x}_2)+K_1x_1+K_0(x_1-x_2) = 0 , \quad (1)$$

$$M_2(\ddot{x}_2+\ddot{x}_G)+C_0(\dot{x}_2-\dot{x}_1)+K_2x_2+K_0(x_2-x_1) = 0 , \quad (2)$$

where x_1, x_2, and x_G are the lateral relative displacement from the ground for the mainframe, subframe, and ground motion, respectively, in the time domain; M_1 and M_2 are the mass of the mainframe and subframe, respectively; K_1 and K_2 are the lateral stiffness of the mainframe and subframe, respectively; and K_0 and C_0 are the lateral stiffness and viscous damping coefficient of the connecting elements, respectively.

Equations (1) and (2) can be also expressed in matrix form as follows:

$$\begin{bmatrix} M_1 & 0 \\ 0 & M_2 \end{bmatrix} \begin{bmatrix} \ddot{x}_1+\ddot{x}_G \\ \ddot{x}_2+\ddot{x}_G \end{bmatrix} + \begin{bmatrix} C_0 & -C_0 \\ -C_0 & C_0 \end{bmatrix} \begin{bmatrix} \dot{x}_1 \\ \dot{x}_2 \end{bmatrix} + \begin{bmatrix} K_1+K_0 & -K_0 \\ -K_0 & K_2+K_0 \end{bmatrix} \begin{bmatrix} x_1 \\ x_2 \end{bmatrix} = \begin{bmatrix} 0 \\ 0 \end{bmatrix}. \quad (3)$$

Using the Laplace transform, the equations of motion in the frequency domain can be expressed as follows:

$$M_1(s^2X_1+s^2X_G)+C_0(sX_1-sX_2)+K_1X_1+K_0(X_1-X_2) = 0\,, \quad (4)$$

$$M_2(s^2X_2+s^2X_G)+C_0(sX_2-sX_1)+K_2X_2+K_0(X_2-X_1) = 0\,, \quad (5)$$

where X_1, X_2, and X_G are the lateral relative displacement from the ground for the mainframe, subframe, and ground motion, respectively, in the frequency domain; s is the Laplace variable (= $i\omega$); i is an imaginary unit, and ω is the circular frequency.
Solving Equations (4) and (5) for X_1 and X_2 yields the following:

$$X_1 = -\frac{s^2[-(sC_0+K_0)M_2-M_1(K_2+K_0+s(C_0+sM_2)]X_G}{(sC_0+K_0)^2-[K_1+K_0+s(C_0+sM_1)][K_0+K_2+s(C_0+sM_2)]}\,, \quad (6)$$

$$X_2 = -\frac{s^2[(K_1+s^2M_1)M_2+sC_0(M_1+M_2)+K_0(M_1+M_2)]X_G}{(K_2K_0+s^2K_2M_1+s^2K_0M_1+s^2K_0M_2+s^4M_1M_2+K_1(K_0+K_2+s^2M_2)+sC_0[K_1+K_2+s^2(M_1+M_2)]}\,. \quad (7)$$

The amplitude of the TF for the relative displacement of the mainframe, $A_{1,\mathrm{disp}}$, and subframe, $A_{2,\mathrm{disp}}$, can be expressed as follows:

$$A_{1,\mathrm{disp}} = \frac{|X_1|}{|X_G|}\,, \quad (8)$$

$$= \sqrt{\frac{M_1^2M_2^2\omega^8+\{C_0^2(M_1+M_2)^2-2M_1M_2[K_2M_1+K_0(M_1+M_2)]\}\,\omega^6+\{[K_2M_1+K_0(M_1+M_2)]^2\}\omega^4}{\begin{matrix}M_1^2M_2^2\omega^8+\{C_0^2(M_1^2+M_2^2)+2M_1M_2[C_0^2-(K_0+K_2)M_1-(K_0+K_1)M_2]\}\omega^6+\{K_2^2M_1^2+K_0[4K_1M_1M_2+K_0(M_1+M_2)^2\\ ]+K_1(K_1+2K_0)M_2^2-2C_0^2(K_1+K_2)(M_1+M_2)+2K_2M_1[2K_1M_2+K_0(M_1+2M_2)]\}\omega^4+\{C_0^2(K_1+K_2)^2\\ -2[K_0K_2+K_1(K_0+K_2)][K_2M_1+K_1M_2+K_0(M_1+M_2)]\}\omega^2+[K_0K_2+K_1(K_0+K_2)]^2\end{matrix}}}, \quad (9)$$

$$A_{2,\mathrm{disp}} = \frac{|X_2|}{|X_G|}\,, \quad (10)$$

$$= \sqrt{\frac{\begin{array}{c} M_1^2M_2^2\omega^8+\{C_0^2(2M_1+M_1^2+M_2^2)-2M_1M_2(K_1M_2+K_0(M_1+M_2))\}\omega^6+\{M_2(K_1^2M_2+2K_0K_1(M_1+M_2) \\ +K_0^2(2M_1+M_1^2+M_2))\}\omega^4 \end{array}}{\begin{array}{c} M_1^2M_2^2\omega^8+\{C_0^2(M_1+M_2)^2-2M_1M_2[K_2M_1+K_1M_2+K_0(M_1+M_2)]\}\omega^6-\{K_2^2M_1^2+K_1^2M_2^2+K_0^2(M_1+M_2)^2+2K_1K_0M_2 \\ (2M_1+M_2)+2C_0^2[K_1(M_1-M_2)-K_2(M_1+M_2)]+2K_2M_1[2K_1M_2+K_0(M_1+2M_2)]\}\omega^4+\{C_0^2(K_1+K_2)^2 \\ -2[K_0K_2+K_1(K_0+K_2)][K_2M_1+K_1M_2+K_0(M_1+M_2)]\}\omega^2+[K_0K_2+K_1(K_0+K_2)]^2 \end{array}}} \quad (11)$$

In addition, the amplitudes of the TF for the absolute acceleration of the mainframe, $A_{1,\mathrm{acc}}$, and subframe, $A_{2,\mathrm{acc}}$, can be expressed as follows:

$$A_{1,\mathrm{acc}} = \frac{\left|s^2X_1+s^2X_G\right|}{\left|s^2X_G\right|}, \quad (12)$$

$$= \sqrt{\frac{\begin{array}{c} K_1^2M_2^2\omega^4+\{C_0^2(K_1+K_2)^2-2K_1M_2[K_0K_2+K_1(K_0+K_2)]\}\omega^2+[K_0K_2+K_1(K_0+K_2)]^2 \end{array}}{\begin{array}{c} M_1^2M_2^2\omega^8+\{C_0^2(M_1+M_2)^2-2M_1M_2(K_2M_1+K_1M_2+K_0(M_1+M_2))\}\omega^6-\{2K_2^2M_1^2+K_1^2M_2^2+K_0^2(M_1+M_2)^2+2K_0K_1M_2 \\ (2M_1+M_2)+2C_0^2(K_1(M_1-M_2)-K_2(M_1+M_2))+2K_2M_1(2K_1M_2+K_0(M_1+2M_2))\}\omega^4+\{C_0^2(K_1+K_2)^2 \\ -2(K_0K_2+K_1(K_0+K_2))(K_2M_1+K_1M_2+K_0(M_1+M_2))\}\omega^2+[K_0K_2+K_1(K_0+K_2)]^2 \end{array}}}, \quad (13)$$

$$A_{2,\mathrm{acc}} = \frac{\left|s^2X_2+s^2X_G\right|}{\left|s^2X_G\right|}, \quad (14)$$

$$= \sqrt{\frac{\begin{array}{c} K_2^2M_1^2\omega^4+\{C_0^2(K_1+K_2)^2-2K_2M_1[K_1K_2+K_0(K_1+K_2)]\}\omega^2+[K_1K_2+K_0(K_1+K_2)]^2 \end{array}}{\begin{array}{c} M_1^2M_2^2\omega^8-\{C_0^2(M_1+M_2)^2+2M_1M_2[K_2M_1-K_1M_2-K_0(M_1+M_2)]\}\omega^6+\{K_2^2M_1^2+K_1^2M_2^2+K_0^2(M_1+M_2)^2+2K_1K_0M_2 \\ (2M_1+M_2)-2C_0^2(K_1+K_2)(M_1+M_2)+2K_2M_1[2K_1M_2+K_0(M_1+2M_2)]\}\omega^4+\{C_0^2(K_1+K_2)^2 \\ -2[K_2K_0+K_1(K_2+K_0)][K_2M_1+K_1M_2+K_0(M_1+M_2)]\}\omega^2+[K_0K_2+K_1(K_0+K_2)]^2 \end{array}}}. \quad (15)$$

4. Results of transfer function analysis

4.1. Optimal stiffness and damping characteristics

Since the CVC-SD model had linear characteristics and a single damping element, the fixed-point theory [21] can be adopted to determine the optimal parameters of the connecting elements (i.e., optimal spring stiffness, $K_{0,opt}$, and optimal viscous damping coefficient, $C_{0,opt}$) that minimize the peak amplitude of the TF of the system. Based on the fixed-point theory, Kageyama et al. [18] proposed a theoretical formula for optimal tuning and damping conditions for a CVC system connected by a spring and a viscous damping element. The formula of the optimal connection stiffness ($K_{0,opt}$) that minimizes the peak amplitude of the displacement TF for the mainframe of the CVC-SD model can be expressed as follows:

$$K_{0,\mathrm{opt}} = \frac{(\alpha-\mu)(-2-\mu+\alpha\mu)}{2(1+\alpha)(1+\mu)^2} K_1 \ . \tag{16}$$

In the present study, Equation (16) was used to determine the optimal stiffness ratio, $K_{0,opt}/K_1$, for the optimal tuning of the displacement TF for the mainframe of the CVC-SD model. Then, the optimal damping coefficient ($C_{0,opt}$) was determined such that the peak amplitude of the displacement TF for the mainframe ($K_0 = K_{0,opt}$) was minimized for the CVC-SD model. The calculated values of $K_{0,opt}/K_1$ against the given α and μ are shown in Table 1. In the several combinations of the given α and μ, negative values of $K_{0,opt}/K_1$ were obtained. These negative values of $K_{0,opt}/K_1$ indicated that negative stiffness may be required at the connecting portion for optimal tuning to minimize the peak amplitude of the TF. In the TF analysis (Section 3), the inherent damping of the mainframe and subframe was set to zero. The main reason for this is that the optimal stiffness formula (Equation (16)) has been derived based on the fixed-point theory from the condition of undamped state for the mainframe and subframe.

Figures 3 and 4 illustrate the response amplitudes of the TF for the displacement and acceleration, respectively, for the CVC-SD model ($\alpha = 0.1$, $\mu = 0.02$, and $K_0 = K_{0,opt}$). In these figures, cases when C_0 = zero, $C_{0,opt}$, and infinity are depicted. In addition, the

horizontal axis in these figures is a normalized circular frequency (= ω/ω_1), where ω_1 is the natural circular frequency for the state of the mainframe alone. As shown in Fig. 3a, by setting $K_0 = K_{0,opt}$ (i.e., for the case of a negative stiffness of $K_{0,opt}/K_1 = -0.0705$), the amplitude of the two fixed-points showed the same height, indicating an optimal tuning was obtained for the displacement TF of the mainframe. Moreover, by setting $C_0 = C_{0,opt}$, a significant reduction in the peak amplitude was achieved compared with the cases with C_0 = zero and infinity. As shown in Figs. 3b and 4, by giving $K_{0,opt}$ and $C_{0,opt}$, the peak amplitude of the TF for the displacement of the subframe (Fig. 3b) and the acceleration of the mainframe and subframe (Figs. 4a and 4b) was reduced compared with the corresponding cases with C_0 = zero and infinity.

Figure 5 pictures a two-dimensional (2D) contour diagram of calculated $K_{0,opt}/K_1$ with respect to α and μ. The calculated $K_{0,opt}/K_1$ varied between positive and negative values depending on the parameters α and μ. It was observed that in the given range of α and μ, negative stiffness was required to achieve an optimal tuning when $\mu < \alpha$. In addition, when $\alpha = \mu$, a zero value of $K_{0,opt}/K_1$ was obtained. This was likely because the mainframe and subframe had the same individual natural period when $\alpha = \mu$, resulting in the same vibration behavior and no relative displacement between the mainframe and subframe.

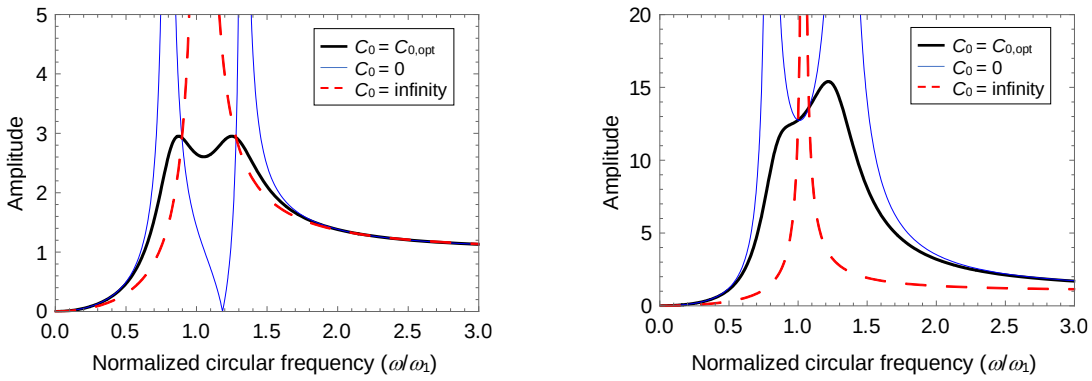

Fig. 3 Amplitude of the relative displacement transfer function (TF) for the CVC-SD model (α = 0.1, μ = 0.02, and $K_0 = K_{0,opt}$): **(a)** mainframe; and **(b)** subframe

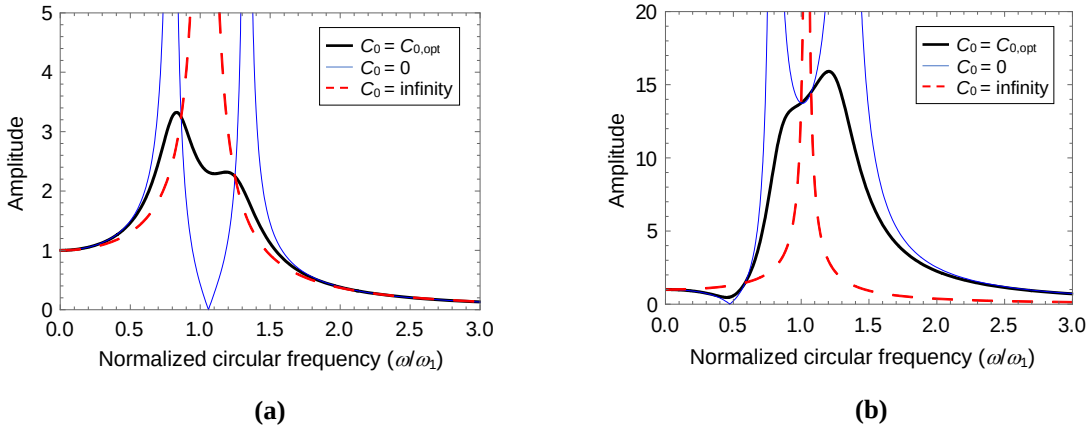

Fig. 4 Amplitude of the absolute acceleration TF for the CVC-SD model (α = 0.1, μ = 0.02, and $K_0 = K_{0,opt}$): **(a)** mainframe; and **(b)** subframe

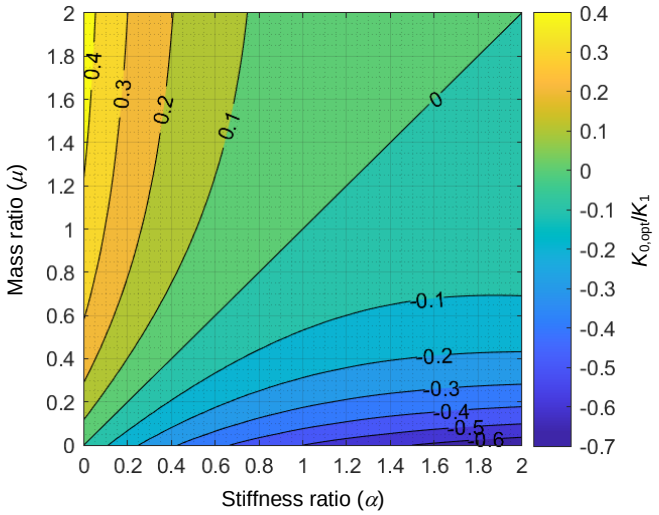

Fig. 5 Two-dimensional (2D) contour diagram of the optimal stiffness ratio ($K_{0,opt}/K_1$) at the connecting portion with respect to the stiffness ratio (α) and the mass ratio (μ)

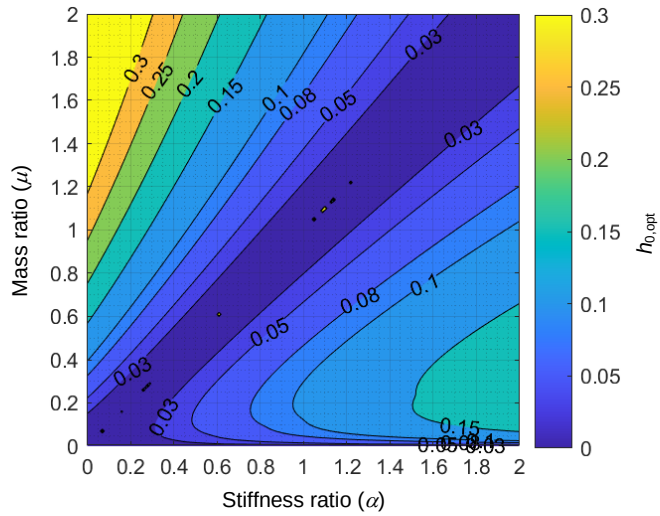

Fig. 6 Two-dimensional (2D) contour diagram of the optimal damping ratio ($h_{0,opt}$) at the connecting portion with respect to α and μ

The subsequent investigations adopted the combinations of α and μ where negative stiffness (i.e., a negative value of $K_{0,opt}/K_1$) was required as the optimal stiffness, taken from Table 1. Table 2 gives an optimal damping ratio, $h_{0,opt}$, obtained based on the optimization of the peak amplitude of the displacement TF for the mainframe when $K_{0,opt}$ was set for the CVC-SD model. Here, $h_{0,opt}$ was calculated as $h_{0,opt} = C_{0,opt}/[2(M_1K_1)^{0.5}]$. In addition, for the CVC-D model, the reference damping ratio, $h_{0,ref}$, was calculated as $h_{0,ref} = C_{0,ref}/[2(M_1K_1)^{0.5}]$, where $C_{0,ref}$ is a reference viscous damping coefficient at the connecting portion for minimizing the peak amplitude of the displacement TF for the mainframe of the CVC-D model. The obtained $h_{0,ref}$ is shown in Table 2. Moreover, a reduction index of the damping ratios calculated as $1 – (h_{0,opt}/h_{0,ref})$ is listed in Table 2. The optimal damping ratio ($h_{0,opt}$) was clearly reduced when a negative stiffness ($K_{0,opt}$) was applied at the connection portion for the CVC-SD model, as compared to the reference damping ratio ($h_{0,ref}$) for the CVC-D model without negative stiffness. A 2D contour diagram of $h_{0,opt}$ with respect to α and μ is depicted in Fig. 6. The diagram shows that $h_{0,opt}$ is dependent on the parameters α and μ.

Table 1 Combination list of α and μ, along with $K_{0,opt}/K_1$

α	μ	$K_{0,opt}/K_1$
0.1	0.02	−0.0705
0.2	0.02	−0.1453
0.2	0.1	−0.0716
0.5	0.25	−0.1133
1.0	0.5	−0.1111
2.0	0.5	−0.1667
0.2	0.2	0
1.0	1.0	0
0.02	0.2	0.1346
0.1	0.2	0.0688
0.5	1.0	0.1042
0.5	2.0	0.1667

Table 2 Optimal connecting stiffness ratio along with optimal and reference viscous damping ratios

α	μ	$K_{0,opt}/K_1$	$h_{0,opt}$	$h_{0,ref}$	$1-(h_{0,opt}/h_{0,ref})$
0.1	0.02	−0.0705	0.0063	0.0367	0.828
0.2	0.02	−0.1453	0.0135	0.0772	0.825
0.2	0.1	−0.0716	0.0149	0.0406	0.633
0.5	0.25	−0.1133	0.0421	0.0783	0.463
1.0	0.5	−0.1111	0.0750	0.1114	0.326
2.0	0.5	−0.1667	0.1696	0.2406	0.295

4.2 Control effects by negative stiffness connection

In order to understand the control effects by negative stiffness for the CVC-SD model, the values of $PA_{1,disp,opt}$, $PA_{2,disp,opt}$, $PA_{1,acc,opt}$, and $PA_{2,acc,opt}$ were examined. Here, $PA_{1,disp,opt}$ and $PA_{2,disp,opt}$ are the optimized peak amplitude of the displacement TF for the mainframe and the corresponding peak amplitude of the displacement TF for the subframe, respectively, and $PA_{1,acc,opt}$ and $PA_{2,acc,opt}$ are the peak amplitude of the acceleration TF for the mainframe and subframe, respectively, when $K_{0,opt}$ and $C_{0,opt}$ were set for the CVC-SD model. Figures 7 through 10 show 2D contour diagrams of $PA_{1,disp,opt}$, $PA_{2,disp,opt}$, $PA_{1,acc,opt}$, and $PA_{2,acc,opt}$ with respect to α and μ. Each contour line is cut off when the value exceeds 20. In Fig. 7, under the optimized condition, $PA_{1,disp,opt}$ varied depending on α and μ. Here, $PA_{1,disp,opt}$ generally increased as α decreased and μ increased (when $\mu < \alpha$) in the given range of α and μ. A similar tendency to that shown in Fig. 7 was observed in Figs. 8 through 10. However, a comparison at the same values of α and μ revealed that the obtained peak amplitudes for the displacement of the subframe ($PA_{2,disp,opt}$) and the acceleration of the subframe ($PA_{2,acc,opt}$) were generally greater than that for the displacement of the mainframe ($PA_{1,disp,opt}$). In addition, the peak amplitude of the acceleration of the mainframe ($PA_{1,acc,opt}$) was generally greater than that of the displacement of the mainframe ($PA_{1,disp,opt}$). This is because the optimization in the present study was conducted by targeting the displacement TF for the mainframe.

Tables 3 and 4 give $PA_{1,disp,opt}$ and $PA_{2,disp,opt}$, respectively, calculated for the cases of α and μ where negative stiffness was required for the optimal tuning. Reference peak amplitudes of the displacement TF for the mainframe, $PA_{1,disp,ref}$, and subframe, $PA_{2,disp,ref}$, are also shown in these tables. Here, $PA_{1,disp,ref}$ and $PA_{2,disp,ref}$ are the peak amplitudes of the displacement TF for the mainframe and subframe, respectively, when $C_{0,ref}$ was set for the CVC-D model. Then, reduction indices were calculated as $1 - (PA_{1,disp,opt} / PA_{1,disp,ref})$ and $1 - (PA_{2,disp,opt} / PA_{2,disp,ref})$ and are listed in Tables 3 and 4. A significant reduction in the peak amplitude of the mainframe was achieved by applying negative stiffness connection (the CVC-SD model) compared to the case with zero stiffness connection (the CVC-D model). For the mainframe, the reduction index increased as α and μ decreased (Table 3). In other words, the "relative" control effects for the mainframe

achieved by negative stiffness connection became clearer when the stiffness and mass of the subframe were small as compared to those of the mainframe.

Similarly, Tables 5 and 6 show $PA_{1,acc,opt}$ and $PA_{2,acc,opt}$, respectively, along with the corresponding $PA_{1,acc,ref}$ and $PA_{2,acc,ref}$. Here, $PA_{1,acc,ref}$ and $PA_{2,acc,ref}$ are the reference peak amplitudes of the acceleration TF for the mainframe and subframe, respectively, when $C_{0,ref}$ was set for the CVC-D model. In addition, corresponding reduction indices obtained as $1 - (PA_{1,acc,opt}/PA_{1,acc,ref})$ and $1 - (PA_{2,acc,opt}/PA_{2,acc,ref})$ are given in these tables. Since the optimization in the present analysis was focused on the control for the mainframe, the obtained reduction indices for the subframe [i.e., $1 - (PA_{2,disp,opt}/PA_{2,disp,ref})$ and $1 - (PA_{2,acc,opt}/PA_{2,acc,ref})$] were lesser than those for the mainframe [i.e., $1 - (PA_{1,disp,opt}/PA_{1,disp,ref})$ and $1 - (PA_{1,acc,opt}/PA_{1,acc,ref})$].

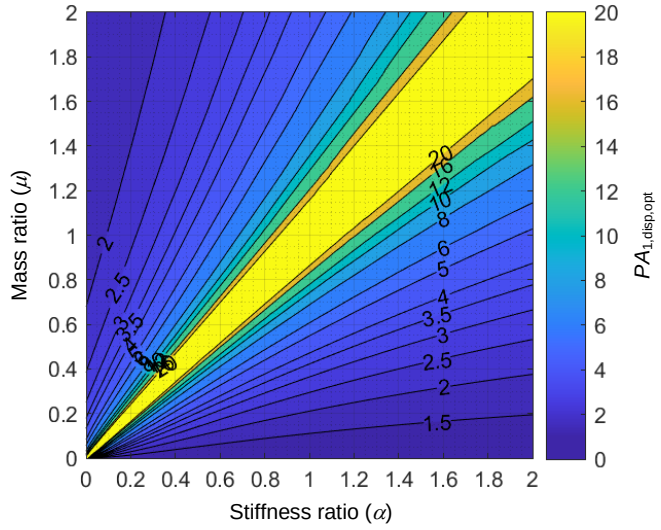

Fig. 7 Two-dimensional (2D) contour diagram of the peak amplitude of the relative displacement TF for the mainframe ($PA_{1,disp,opt}$)

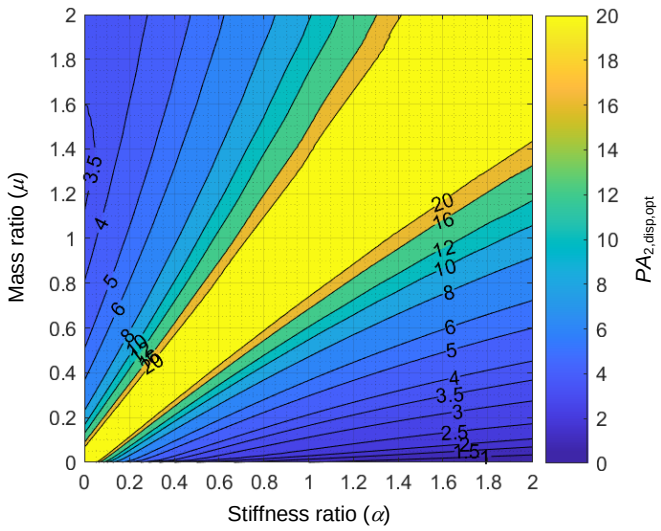

Fig. 8 Two-dimensional (2D) contour diagram of the peak amplitude of the relative displacement TF for the subframe ($PA_{2,disp,opt}$)

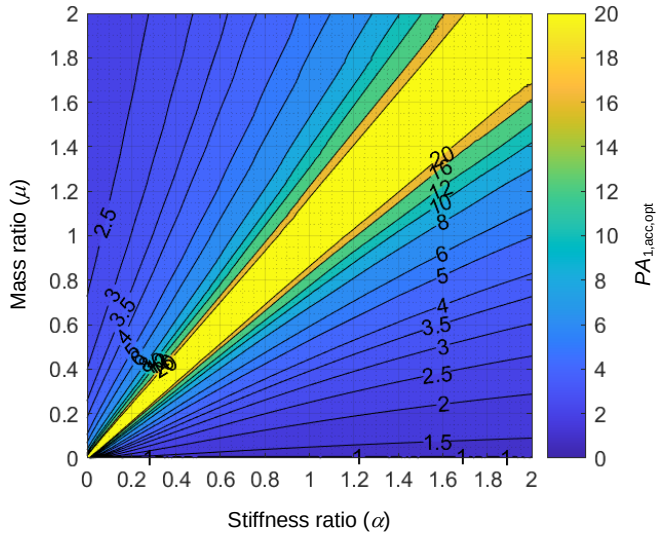

Fig. 9 Two-dimensional (2D) contour diagram of the peak amplitude of the absolute acceleration TF for the mainframe ($PA_{1,acc,opt}$)

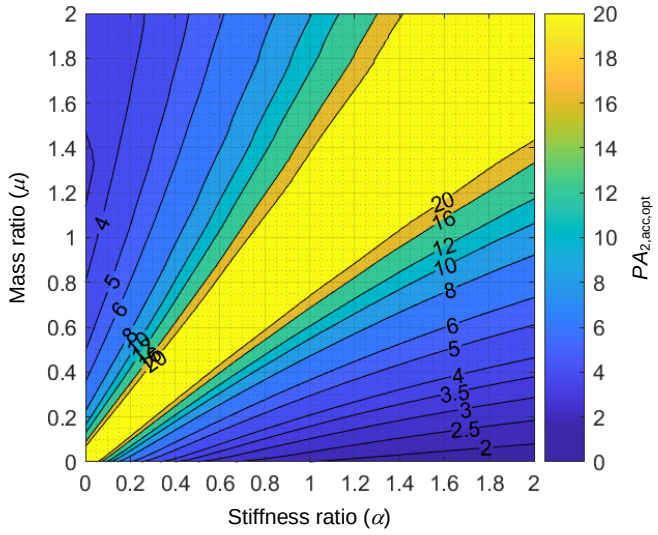

Fig. 10 Two-dimensional (2D) contour diagram of the peak amplitude of the absolute acceleration TF for the subframe ($PA_{2,acc,opt}$)

Table 3 Peak amplitude of relative displacement TF for mainframe

α	μ	$PA_{1,\mathrm{disp,opt}}$	$PA_{1,\mathrm{disp,ref}}$	$1-(PA_{1,\mathrm{disp,opt}}/PA_{1,\mathrm{disp,ref}})$
0.1	0.02	2.95	26.50	0.889
0.2	0.02	1.69	12.33	0.863
0.2	0.1	5.53	23.00	0.760
0.5	0.25	4.48	11.00	0.593
1.0	0.5	4.34	7.00	0.380
2.0	0.5	2.39	3.00	0.204

Table 4 Peak amplitude of relative displacement TF for subframe

α	μ	$PA_{2,\mathrm{disp,opt}}$	$PA_{2,\mathrm{disp,ref}}$	$1-(PA_{2,\mathrm{disp,opt}}/PA_{2,\mathrm{disp,ref}})$
0.1	0.02	15.40	18.38	0.162
0.2	0.02	7.14	8.36	0.147
0.2	0.1	16.56	15.94	−0.039
0.5	0.25	10.21	7.53	−0.357
1.0	0.5	8.69	5.05	−0.721
2.0	0.5	4.30	3.05	−0.409

Table 5 Peak amplitude of absolute acceleration TF for mainframe

α	μ	$PA_{1,\mathrm{acc,opt}}$	$PA_{1,\mathrm{acc,ref}}$	$1-(PA_{1,\mathrm{acc,opt}}/PA_{1,\mathrm{acc,ref}})$
0.1	0.02	3.32	26.50	0.875
0.2	0.02	2.00	12.33	0.838
0.2	0.1	5.90	23.00	0.744
0.5	0.25	4.81	11.00	0.563
1.0	0.5	4.62	7.01	0.341
2.0	0.5	2.63	3.05	0.138

Table 6 Peak amplitude of absolute acceleration TF for subframe

α	μ	$PA_{2,acc,opt}$	$PA_{2,acc,ref}$	$1-(PA_{2,acc,opt}/PA_{2,acc,ref})$
0.1	0.02	15.91	19.10	0.167
0.2	0.02	7.61	9.09	0.162
0.2	0.1	16.84	16.66	−0.010
0.5	0.25	10.21	8.26	−0.236
1.0	0.5	8.68	5.65	−0.537
2.0	0.5	4.23	3.00	−0.410

5. Conclusions

In this chapter, the control effects by negative stiffness connection between the mainframe and subframe for CVC adjacent structures were numerically assessed based on a TF analysis. The following conclusions could be observed:

1) Adopting negative stiffness in the connecting elements enabled an optimal tuning for minimizing the peak amplitude of the displacement TF for the mainframe, even in the cases in which it was impossible to achieve only by positive or zero stiffness. Thus, adopting negative stiffness in CVC structures can extend the range of optimal tuning conditions.

2) When optimal tuning and optimal damping coefficient were given by incorporating optimal negative stiffness, the peak amplitude of the TF of the mainframe of the CVC-SD model was significantly decreased, as compared with that for the CVC-D model without negative stiffness and with only a viscous damping element.

3) The optimal damping coefficient required for minimizing the peak amplitude of the displacement TF of the mainframe of the CVC-SD model with optimal negative stiffness was reduced compared to the CVC-D model without negative stiffness.

Further research includes time history seismic response simulations using linear and nonlinear CVC models with different natural periods and structural parameters under various earthquake motions for assessing the response control effectiveness on CVC structures.

Acknowledgments

The present study was supported by the Kajima Foundation 2021 Research Grant and the Japan Society for the Promotion of Science Grant-in-Aid for JSPS Research Fellow.

References

[1] Xu YL, He Q, Ko JM (1999) Dynamic response of damper-connected adjacent buildings under earthquake excitation. *Engineering Structures*, **21**(2):135–148. https://doi.org/10.1016/S0141-0296(97)00154-5

[2] Tubaldi E (2015) Dynamic behavior of adjacent buildings connected by linear viscous/viscoelastic dampers. *Structural Control and Health Monitoring*, **22**(8):1086–1102. https://doi.org/10.1002/stc.1734

[3] Jankowski R, Mahmoud S (2016) Linking of adjacent three-storey buildings for mitigation of structural pounding during earthquakes. *Bulletin of Earthquake Engineering*, **14**(11):3075–3097. https://doi.org/10.1007/s10518-016-9946-z

[4] Tubaldi E, Gioiella L, Scozzese F, Ragni L, Dall'Asta A (2020) A design method for viscous dampers connecting adjacent structures. *Frontiers in Built Environment*, **6**:25. https://doi.org/10.3389/fbuil.2020.00025

[5] Minami S, Yamazaki S, Toyama K, Tahara K (2004) Experimental study on coupled vibration control structures. *The 13th World Conference on Earthquake Engineering*, Paper No. 2351, August 1–6, 2004, Vancouver, B.C., Canada.

[6] Palacios-Quiñonero F, Rubió-Massegú J, Rossell JM, Karimi HR (2014) Vibration control for adjacent structures using local state information. *Mechatronics*, **24**(4):336–344. http://dx.doi.org/10.1016/j.mechatronics.2013.08.001

[7] Zhang WS, Xu YL (2000) Vibration analysis of two buildings linked by Maxwell model-defined fluid dampers. *Journal of Sound and Vibration*, **233**(5):775–796. https://doi.org/10.1006/jsvi.1999.2735

[8] Ni YQ, Ko JM, Ying ZG (2001) Random seismic response analysis of adjacent buildings coupled with non-linear hysteretic dampers. *Journal of Sound and Vibration*, **246**(3):403–417. https://doi.org/10.1006/jsvi.2001.3679

[9] Ying ZG, Ni YQ, Ko JM (2003) Stochastic optimal coupling-control of adjacent building structures. *Computers & Structures*, **81**(30–31):2775–2787. https://doi.org/10.1016/S0045-7949(03)00332-8

[10] Christenson RE, Spencer Jr BF, Johnson EA, Seto K (2006) Coupled building control considering the effects of building/connector configuration. *Journal of structural engineering*, ASCE, **132**(6):853–863. https://doi.org/10.1061/(ASCE)0733-9445(2006)132:6(853)

[11] Basili M, De Angelis M, Fraraccio G (2013) Shaking table experimentation on adjacent structures controlled by passive and semi-active MR dampers. *Journal of Sound and Vibration*, **332**(13):3113–3133. https://doi.org/10.1016/j.jsv.2012.12.040

[12] Basili M, De Angelis M (2017) Vibration analysis and models of adjacent structures controlled by magnetorheological dampers. *Shock and Vibration*. Article ID 9596382. https://doi.org/10.1155/2017/9596382

[13] Basili M, De Angelis M, Pietrosanti D (2019) Defective two adjacent single degree of freedom systems linked by spring-dashpot-inerter for vibration control. *Engineering Structures*, **188**:480–492. https://doi.org/10.1016/j.engstruct.2019.03.030

[14] De Domenico D, Qiao H, Wang Q, Zhu Z, Marano G (2020) Optimal design and seismic performance of Multi‐Tuned Mass Damper Inerter (MTMDI) applied to adjacent high‐rise buildings. *The Structural Design of Tall and Special Buildings*, **29**(14):e1781. https://doi.org/10.1002/tal.1781

[15] Kazemi F, Miari M, Jankowski R (2021) Investigating the effects of structural pounding on the seismic performance of adjacent RC and steel MRFs. *Bulletin of Earthquake Engineering*, **19**(1):317–343. https://doi.org/10.1007/s10518-020-00985-y

[16] Lu L, Xu J, Zhou Y, Lu W, Spencer Jr BF (2021) Viscous inertial mass damper (VIMD) for seismic responses control of the coupled adjacent buildings. *Engineering Structures*, **233**:111876. https://doi.org/10.1016/j.engstruct.2021.111876

[17] Zhu H, Iemura H (2000) A study of response control on the passive coupling element between two parallel structures. *Structural Engineering and Mechanics*. **9**(4):383–396. https://doi.org/10.12989/sem.2000.9.4.383

[18] Kageyama M, Yasui Y, Seto K (2000) The principal solutions of connecting spring and damper for optimum vibration control under several criteria. *Journal of Structural and Construction Engineering*, AIJ, **65**(529):97–104. **(in Japanese)** https://doi.org/10.3130/aijs.65.97

[19] Zhu H, Wen Y, Iemura H (2001) A study on interaction control for seismic response of parallel structures. *Computers & Structures*, **79**(2):231–242. https://doi.org/10.1016/S0045-7949(00)00119-X

[20] Zhu HP, Ge DD, Huang X (2011) Optimum connecting dampers to reduce the seismic responses of parallel structures. *Journal of Sound and Vibration*, **330**(9): 1931–1949. https://doi.org/10.1016/j.jsv.2010.11.016

[21] Den Hartog JP (1956) Mechanical vibrations, 4th ed. McGraw-Hill, New York.

[22] Shirai K, Park J (2020) Use of scrap tire pads in vibration control system for seismic response reduction of buildings. *Bulletin of Earthquake Engineering*, **18**(5): 2497–2521. https://doi.org/10.1007/s10518-020-00787-2

[23] Sano T, Shirai K, Yoshida O, Nishikage T (2021) Assessment of a seismic tuned mass damper with friction fail-safe mechanism for the vibration control of high-rise buildings. *Structural Control and Health Monitoring*:e2831. https://doi.org/10.1002/stc.2831

[24] Li H, Li Y, Li J (2020) Negative stiffness devices for vibration isolation applications A review. *Advances in Structural Engineering*, **23**(8):1739–1755. https://doi.org/10.1177/1369433219900311

[25] Mizuno T, Toumiya T, Takasaki M (2003) Vibration isolation system using negative stiffness. *JSME International Journal*, Series C, **46**(3):807–812. https://doi.org/10.1299/jsmec.46.807

[26] Iemura H, Kouchiyama O, Toyooka A, Shimoda I (2008) Development of the friction-based passive negative stiffness damper and its verification tests using shaking table. *The 14th World Conference on Earthquake Engineering*, October 12–17, 2008, Beijing, China.

[27] Nagarajaiah S, Pasala DTR, Reinhorn A, Constantinou M, Sirilis AA, Taylor D (2013) Adaptive negative stiffness: a new structural modification approach for seismic protection. *Advanced Materials Research*, **639**–**640**:54–66. https://doi.org/10.4028/www.scientific.net/AMR.639-640.54

[28] Sarlis AA, Pasala DTR, Constantinou MC, Reinhorn AM, Nagarajaiah S, Taylor DP (2013) Negative stiffness device for seismic protection of structures. *Journal of Structural Engineering*, ASCE, **139**(7):1124–1133. https://doi.org/10.1061/(ASCE)ST.1943-541X.0000616

[29] Walsh KK, Boso, E., Steinberg EP, Haftman JT, Littell WN (2018) Variable negative stiffness device for seismic protection of building structures through apparent weakening. *Journal of Engineering Mechanics*, **144**(9):04018090. https://doi.org/10.1061/(ASCE)EM.1943-7889.0001512

[30] Zhou P, Liu M, Li H (2020) A passive negative stiffness damper in series with a flexible support: Theoretical and experimental study. *Structural Control and Health Monitoring*, **27**(9):e2594. https://doi.org/10.1002/stc.2594

[31] Nagarajaiah S, Sen D (2020) Apparent-weakening by adaptive passive stiffness shaping along the height of multistory building using negative stiffness devices and dampers for seismic protection. *Engineering Structures*, **220**:110754. https://doi.org/10.1016/j.engstruct.2020.110754

[32] Shirai K, Noro S, Walsh KK (2021) Shake table testing of a passive negative stiffness device with curved leaf springs for seismic response mitigation of structures. *Structural Control and Health Monitoring*, **28**(7):e2736. https://doi.org/10.1002/stc.2736

[33] Yamada Y, Ikawa N, Yokoyama H, Tachibana E (1994) Active control of structures using the joining member with negative stiffness. *The First World Conference on Structural Control*, TP2, Vol. 2, 41–49, 1994, California, USA.

[34] Ikawa N, Yamada Y, Yokoyama H, Tachibana E (1996) Active control system of coupled structures with a negative stiffness. *Journal of Structural Engineering*, AIJ, Vol. **42B**: 629–634. **(in Japanese)**

[35] Shimizu K, Kurino H (2009) Fundamental study of structural control with negative stiffness connection. Part 1: Study of applicability of negative stiffness. *Summaries of Technical Papers of Annual Meeting*, AIJ:453–454. **(in Japanese)**

[36] Kurino H, Shimizu K (2009) Fundamental study of structural control with negative stiffness connection. Part 2: Feasibility study utilizing variable damping device. *Summaries of Technical Papers of Annual Meeting*, AIJ:455–456. **(in Japanese)**

[37] Longjam S, Shirai K (2022) Numerical investigation of earthquake response reduction effects by negative stiffness connection for adjacent building structures. *Structures*, Vol. **38**, 672-688. https://doi.org/10.1016/j.istruc.2022.01.078

[38] Longjam S, Shirai K (2021) Use of negative stiffness for coupled vibration control structures: an analytical investigation. *The 17th World Conference on Earthquake Engineering*, September 27–October 2, 2021, Sendai, Japan.

Chapter III

Numerical investigation on control effects by negative stiffness connection for CVC buildings subjected to earthquakes

Longjam S, Shirai K (2022) Numerical investigation of earthquake response reduction effects by negative stiffness connection for adjacent building structures. *Structures*, Vol. **38**, 672-688. https://doi.org/10.1016/j.istruc.2022.01.078

The contents of this Chapter III have been taken from the above journal paper except for the Sections 1 (Introduction) and 4 (Conclusions), in which some modifications have been made.

1. Introduction

CVC of structures is a promising method to mitigate earthquake response by connecting two or more vibrating structural systems. The CVC techniques have emerged as an efficient way to reduce the seismic response and effective control of the adjacent structures against earthquakes. These coupled vibration techniques as passive, semi-active, and active [1–19] in the form of a spring and/or a damping vibration controller device [20–24], mainly using energy dissipators, have been proposed and practically employed as the supplemental connector of the CVC structures.

The negative stiffness device is an emerging vibration control device with the potential for incorporation into the CVC system. Negative stiffness works in opposition to positive stiffness and produces a decreased (i.e., negative) restoring force with the progression of the displacement of the device [25]. Research and development of negative stiffness devices (NSDs) and systems incorporating NSDs have progressed much in the past decades [26–32]. Optimal parameters such as stiffness and damping coefficient of the connecting portion and the structural parameters of the adjacent structures must be appropriately defined for effective vibration control of the CVC systems [33–39].

The authors investigated the basic characteristics of negative stiffness as the connecting element based on the TF of vibrating models representing simplified CVC structures [40]. The negative stiffness applied with a damper device as the connecting elements of CVC structures was expected to extend the optimum tuning conditions. The investigation demonstrated that the peak amplitude of the TF for the models could be utilized to evaluate the control effects on the CVC systems. In addition, limited research on incorporating a passive or active NSD as a connecting element in the CVC system for numerically assessing the response control effectiveness on CVC structures has been made available [41–44]. The seismic response control effects of PNSD at the connecting portion of CVC structures remain unclear.

This chapter demonstrates that PNSD with proper structural parameters could significantly reduce the seismic responses of CVC buildings. The study deals with a

numerical seismic analysis of CVC adjacent buildings. In Section 2, the methods of seismic response simulation using 18 cases of linear CVC system models are described, followed by subsections explaining the obtained results, response behavior, and evaluation criteria. The nonlinear seismic response simulation method of CVC systems of different natural periods and structural parameters are described in Section 3, followed by the subsections on the discussion and validation of the obtained results. Finally, the conclusion is discussed in Section 4. This study expands on the previous study in Chapter II by presenting findings based on the linear and nonlinear seismic response simulation.

2. Linear earthquake response simulation

A time history seismic response simulation was conducted using 2DOF and single-degree-of-freedom (SDOF) models to evaluate the control effects by negative stiffness connection on CVC buildings subjected to earthquakes.

2.1. Methods of linear seismic response simulation

2.1.1. Modeling of mainframe and subframe

In the response simulation, four groups of numerical models were used, namely CVC-SD, CVC-D, SDOF-mainframe, and SDOF-subframe models, as shown in Fig. 1. The CVC-SD models represented 2DOF models, the mainframe and subframe of which were connected by both spring (K_0) and dashpot (C_0) elements. The CVC-D models represented 2DOF models, in which only a dashpot (C_0) was placed between the mainframe and subframe. The SDOF-mainframe models and SDOF-subframe models represented the models for the state of the mainframe and subframe alone, respectively.

Each group consisted of 18 cases of models. All of the models had linear characteristics. The mainframe and subframe were common to each model in the corresponding groups and cases. Unlike the models used in the TF analysis (Chapter II Section 3), regarding the models used in the response simulation, a dashpot was set for each mainframe and subframe such that a damping factor of 2% was obtained for the state of the mainframe and subframe alone, respectively.

Table 1 gives the model properties for each case (common to each group, except $K_{0,opt}$, $C_{0,opt}$, and $C_{0,ref}$). For the mainframe, three natural periods for the state of the mainframe alone, T_1, were set as T_1 = 0.5, 1.0, and 2.0 s. The mainframe had a mass of M_1 = 1,000 t. The lateral stiffness of the mainframe (K_1) was given by T_1 and M_1. The structural parameters for the subframe were set using the stiffness ratio ($\alpha = K_2/K_1$) and the mass ratio ($\mu = M_2/M_1$), where K_2 is the lateral stiffness of the subframe, and M_2 is the mass of the subframe. The combinations of α and μ were set from Chapter II Table 2, where a negative stiffness connection was required for the optimal tuning based on the

TF analysis (Chapter II Section 3). Six combinations of α and μ were set for each T_1. The natural period of the subframe for the state of the subframe alone, T_2, was obtained from M_2 and K_2. As for the case name in Table 1, the symbols A, B, C, D, E, and F denote the combination of α and μ. The numbers 05, 10, and 20 denote T_1 = 0.5, 1.0, and 2.0 s, respectively. Thus, a total of 18 cases were prepared.

Note: In seismic response simulation, a dashpot was placed at both the mainframe and the subframe in each model such that a damping factor of 0.02 was obtained for the state of the mainframe and subframe alone

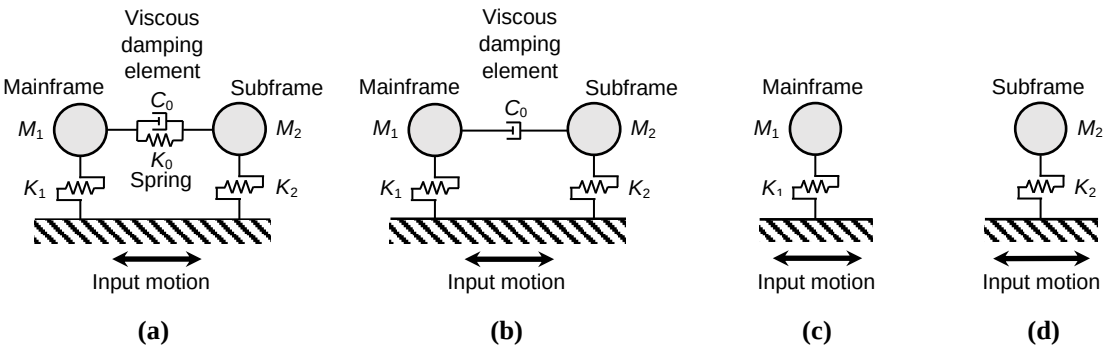

Fig. 1 Analytical models considered: **(a)** optimal-controlled coupled 2DOF model (CVC-SD model); **(b)** reference-controlled coupled 2DOF model (CVC-D model); **(c)** mainframe alone (SDOF-mainframe model); and **(d)** subframe alone (SDOF-subframe model)

Table 1 Properties of numerical models used in earthquake response simulation

Case	α	μ	T_1 (s)	T_2 (s)	M_1 (t)	K_1 (MN/m)	M_2 (t)	K_2 (MN/m)	$K_{0,opt}$ (MN/m)	$C_{0,opt}$ (MNs/m)	$C_{0,ref}$ (MNs/m)
A05	0.1	0.02	0.50	0.22	1000	157.91	20	15.79	−11.14	0.159	0.920
B05	0.2	0.02	0.50	0.16	1000	157.91	20	31.58	−5.74	0.340	1.938
C05	0.2	0.10	0.50	0.35	1000	157.91	100	31.58	−11.31	0.375	1.019
D05	0.5	0.25	0.50	0.35	1000	157.91	250	78.96	−17.90	1.057	1.964
E05	1.0	0.50	0.50	0.35	1000	157.91	500	157.91	−17.55	1.885	2.796
F05	2.0	0.50	0.50	0.25	1000	157.91	500	315.83	−26.32	4.263	6.040
A10	0.1	0.02	1.0	0.45	1000	39.48	20	3.95	−2.78	0.079	0.460
B10	0.2	0.02	1.0	0.32	1000	39.48	20	7.90	−5.74	0.170	0.969
C10	0.2	0.10	1.0	0.71	1000	39.48	100	7.90	−2.83	0.187	0.510
D10	0.5	0.25	1.0	0.71	1000	39.48	250	19.74	−4.47	0.529	0.982
E10	1.0	0.50	1.0	0.71	1000	39.48	500	39.48	−4.39	0.943	1.398
F10	2.0	0.50	1.0	0.50	1000	39.48	500	78.96	−6.58	2.132	3.020
A20	0.1	0.02	2.0	0.89	1000	9.87	20	0.99	−0.70	0.040	0.230
B20	0.2	0.02	2.0	0.63	1000	9.87	20	1.97	−1.43	0.085	0.484
C20	0.2	0.10	2.0	1.41	1000	9.87	100	1.97	−11.31	0.094	0.255
D20	0.5	0.25	2.0	1.41	1000	9.87	250	4.93	−1.12	0.264	0.491
E20	1.0	0.50	2.0	1.41	1000	9.87	500	9.87	−1.10	0.471	0.699
F20	2.0	0.50	2.0	1.00	1000	9.87	500	19.74	−1.64	1.066	1.510

2.1.2. Modeling of connecting stiffness and viscous damping element

In each CVC-SD model, the spring stiffness (K_0) and the viscous damping coefficient (C_0) at the connection portion were set using the same approach in Chapter II Section 3 (i.e., the TF-based method, where no damping factors were considered at the mainframe and subframe). First, the optimal stiffness ($K_{0,opt}$) was obtained using Chapter II Equation (16). Then, the optimal damping coefficient ($C_{0,opt}$) was determined such that the peak amplitude of the displacement TF of the mainframe (without damping at the mainframe and subframe) was minimized. The values of $K_{0,opt}$ and $C_{0,opt}$ for each CVC-SD model are shown in Table 1.

Regarding each CVC-D model, C_0 of the connection dashpot was set using the same approach in Chapter II Section 3. The reference damping coefficient ($C_{0,ref}$) was determined such that the peak amplitude of the displacement TF of the mainframe (no damping at the mainframe and subframe) was minimized. Table 1 shows the calculated $C_{0,ref}$ for each CVC-D model.

2.1.3. Input motions and analytical conditions

Five simulated earthquake waves and 10 observed seismic records were used for input motions. The peak ground acceleration (PGA) for each input motion is listed in Tables 2 and 3. The five simulated waves, namely Waves M1 through M5, were ground motions used in the literature [45]. The five simulated waves were made such that the response spectra were fitted to the same target response spectrum (damping factor: 0.05) but having different phase characteristics using random numbers. The 10 observed records consisted of El Centro 1940, Taft 1952, Hachinohe 1968, and Tohoku 1978 (provided by Building Performance Standardization Association [46]), and Kobe 1995 (provided by Japan Meteorological Agency [47]), for each NS and EW component. Each observed record was normalized such that the peak ground velocity (PGV) was set to be 0.5 m/s. Fig. 2 depicts the velocity response spectra (damping factor: 0.05) of the input motions. The numerical integration was based on the Newmark-β method (β = 0.25) with a time increment of 0.001 s for each case of the time history response simulation.

Table 2 Simulated earthquake waves

Input motion name	PGA (m/s^2)
Wave M1	4.19
Wave M2	3.80
Wave M3	3.39
Wave M4	3.39
Wave M5	3.14

Table 3 Observed seismic records (each PGV was normalized to 0.5 m/s)

Input motion name	Original record	PGA (m/s^2)
Elcn NS	1940 El Centro NS	5.100
Elcn EW	1940 El Centro EW	2.847
Taft NS	1952 Taft NS	4.863
Taft EW	1952 Taft EW	4.969
Hach NS	1968 Hachinohe NS	3.338
Hach EW	1968 Hachinohe EW	2.384
Tohk NS	1978 Tohoku NS	3.565
Tohk EW	1978 Tohoku EW	3.685
Kobe NS	1995 Kobe NS	4.460
Kobe EW	1995 Kobe EW	4.132

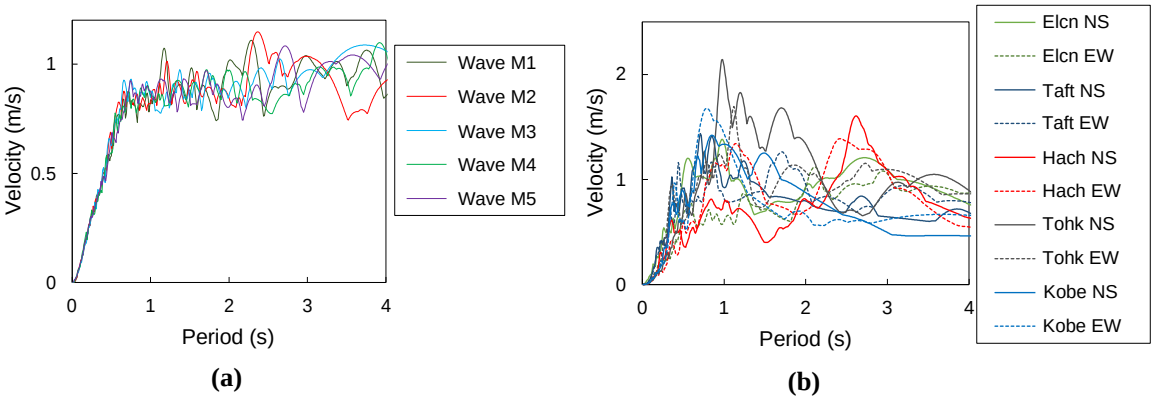

Fig. 2 Velocity response spectra of the input motions (damping factor of 5%): **(a)** simulated waves; and **(b)** observed records

2.2. Results of linear earthquake response simulation

2.2.1. Response behavior

Figures 3 and 4 illustrate the response hysteresis loops for the CVC-SD and CVC-D models, respectively (for the mainframe and the connecting portion, case A10, Wave M1 input,). Unlike the CVC-D model without connection springs (Fig. 4b), the connecting portion of the CVC-SD model incorporating the connection spring showed an elliptical loop with a negative slope by the effect of negative stiffness (Fig. 3b).

Figure 5 compares the time history response waveforms of the mainframe between the CVC-SD and CVC-D models for case A10 under Wave M1 input. For both the relative displacement (Fig. 5a) and absolute acceleration (Fig. 5b) responses of the mainframe, a decreased response was generally observed in the case with an optimal negative stiffness connection (the CVC-SD model), as compared to the case without an optimal negative stiffness connection (the CVC-D model), through the earthquake event. Also, the waveforms for the SDOF-mainframe model (case A10, Wave M1) are shown in Fig. 5. The time history response of the mainframe for the controlled cases (the CVC-SD and CVC-D models) was decreased compared to that of the uncontrolled case (the SDOF-mainframe model).

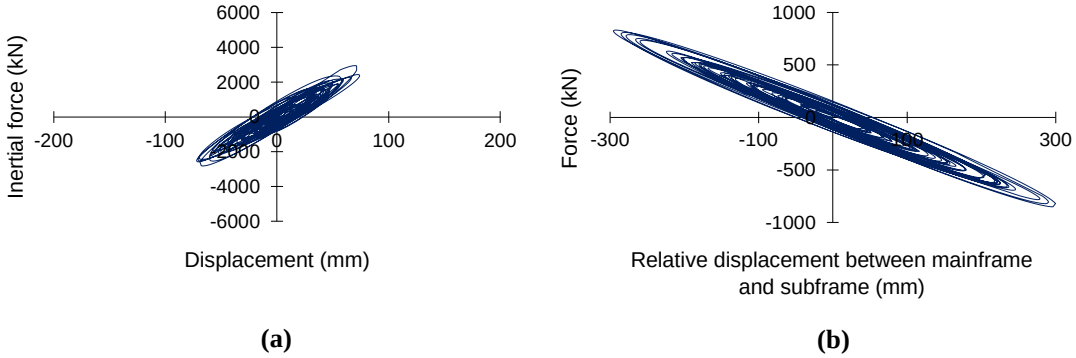

Fig. 3 Response hysteresis loops of the CVC-SD model (case A10, Wave M1 input): **(a)** mainframe; and **(b)** connecting portion (spring and damping elements)

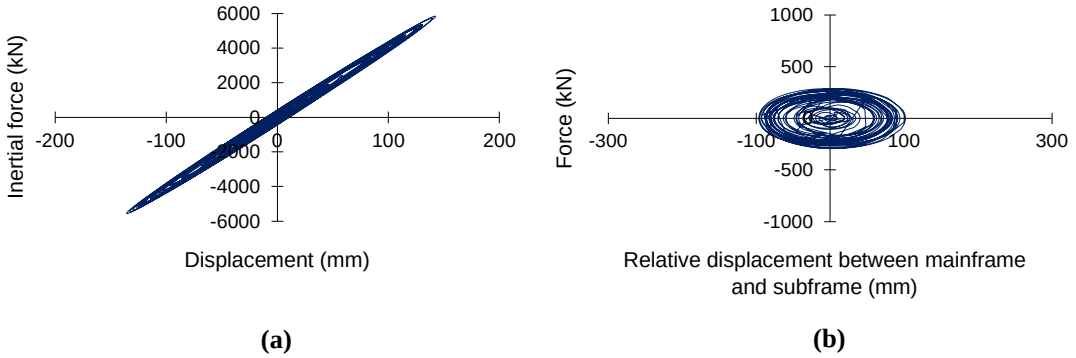

Fig. 4 Response hysteresis loops of the CVC-D model (case A10, Wave M1 input): **(a)** mainframe; and **(b)** connecting portion (damping element)

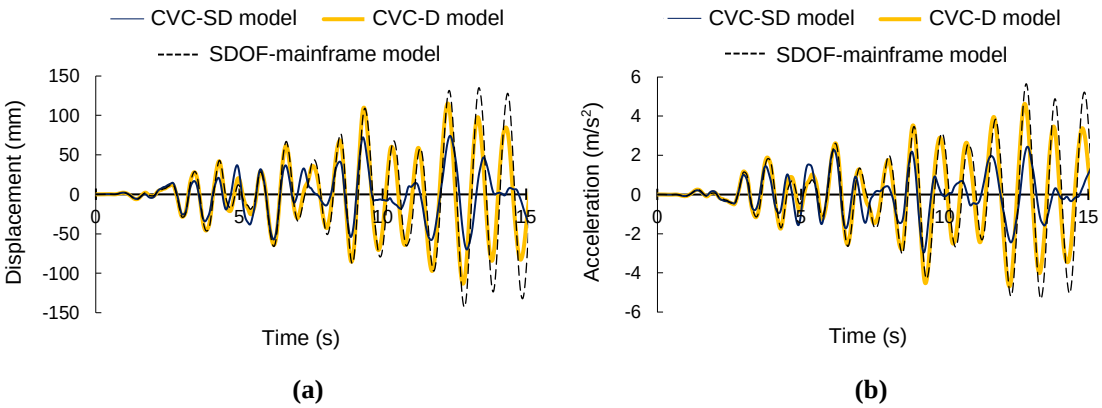

Fig. 5 Time history response waveforms of the mainframe for the controlled and uncontrolled models (case A10, Wave M1 input): **(a)** relative displacement; and **(b)** absolute acceleration

2.2.2. Peak response

Figure 6 compares the peak relative displacement responses of the mainframe between the CVC-SD and CVC-D models (case A10) under each input motion. The results showed that the obtained peak displacement of the mainframe for the CVC-SD models was decreased compared with those for the CVC-D models under all 15 inputs, except for the Elcn EW input. Similarly, the peak absolute acceleration responses of the mainframe for the CVC-SD and CVC-D models (case A10) under each input motion are plotted in Fig. 7. A reduction in the peak acceleration of the mainframe for the CVC-SD model was observed compared to that of the CVC-D model under every input motion. Also, the peak response displacement and acceleration (case A10) for the uncontrolled case (the SDOF-mainframe model) are shown in Figs. 6 and 7, respectively. The peak responses of the mainframe for the CVC-SD model were lesser than those of the uncontrolled case (the SDOF-mainframe model) for all input motions.

Figures 8a and 9a depict the peak response displacement reduction ratio averaged for the five simulated waves and 10 observed record inputs, respectively (for the mainframe and subframe, cases A10–F10). Here, the displacement reduction ratio was calculated as the ratio of the peak displacement of the CVC-SD model to that of the CVC-D model and was then averaged for the input motions. Similarly, Figs. 10a and 11a plot the peak response acceleration reduction ratios averaged for the five simulated waves and 10 observed record inputs, respectively. The acceleration reduction ratio was calculated as the ratio of the peak acceleration of the CVC-SD model to that of the CVC-D model and was then averaged for the input motions. The results indicated that both peak displacement and acceleration of the mainframe for the CVC-SD model were significantly reduced compared to those of the CVC-D model for cases A10 through F10. However, in general, the response reduction ratios of the subframe became larger than unity. This was because the parameter optimization for the connecting portion in the response simulation was done based on the displacement TF of the mainframe (Section 2.1). Also, Figs. 8b, 9b, 10b, and 11b show the ratios of the peak response of the mainframe and subframe for the CVC-SD model to that of the uncontrolled cases (the SDOF-mainframe and SDOF-subframe models). The response of the mainframe of the

CVC-SD model was significantly reduced in comparison with that of the uncontrolled case (the SDOF-mainframe model).

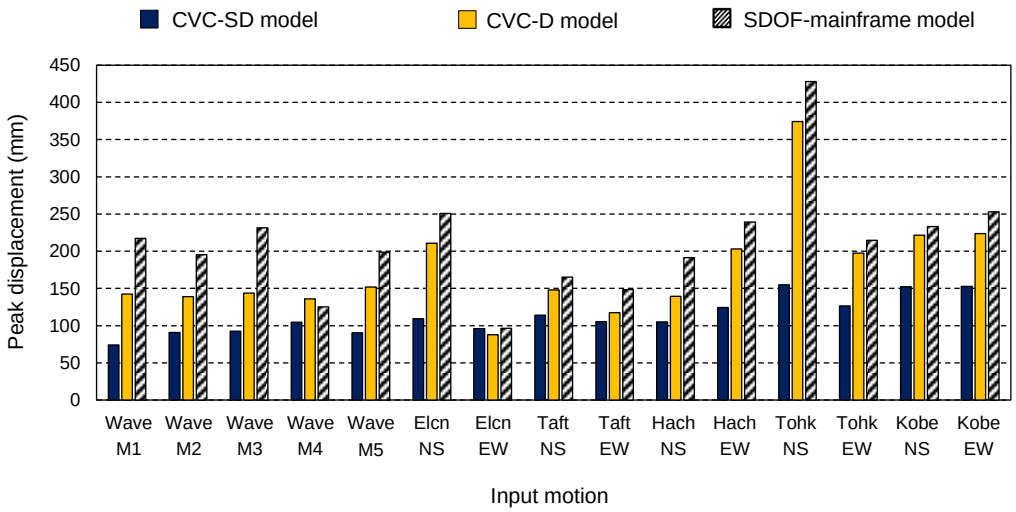

Fig. 6 Peak response displacement of the mainframe for the controlled and uncontrolled models (case A10)

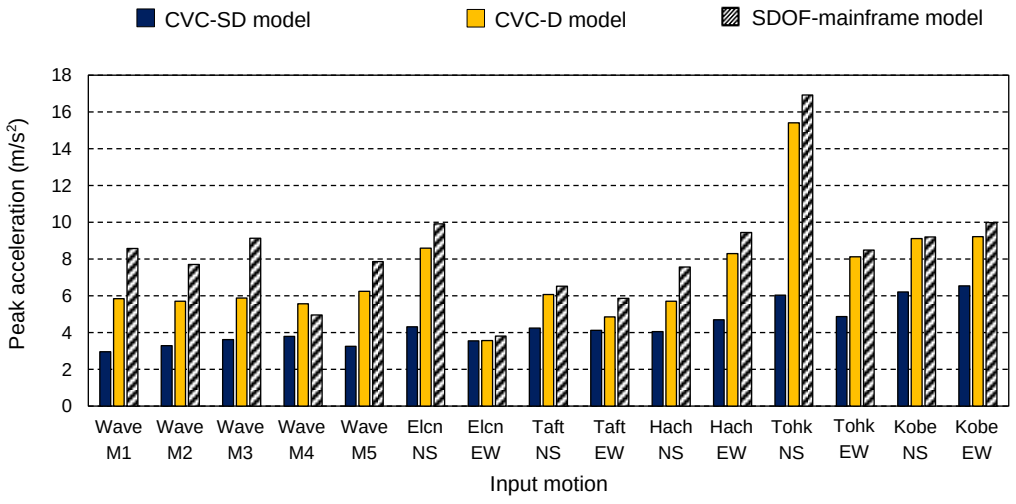

Fig. 7 Peak response acceleration of the mainframe for the controlled and uncontrolled models (case A10)

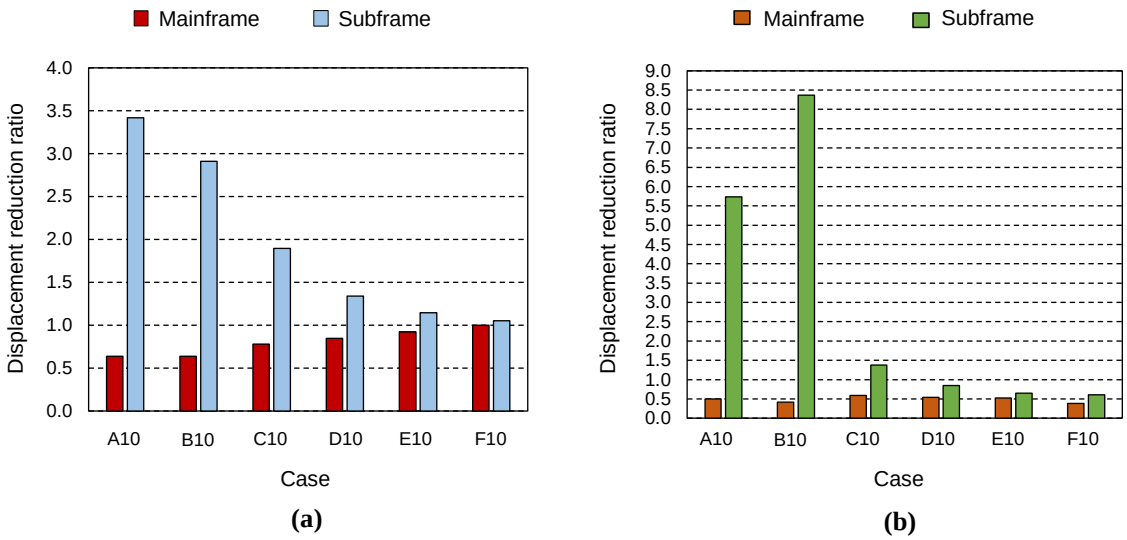

Fig. 8 Peak displacement response reduction ratios averaged for five simulated waves (mainframe and subframe, cases A10 to F10): **(a)** ratio of the CVC-SD model to the CVC-D model; and **(b)** ratio of the CVC-SD model to the SDOF model

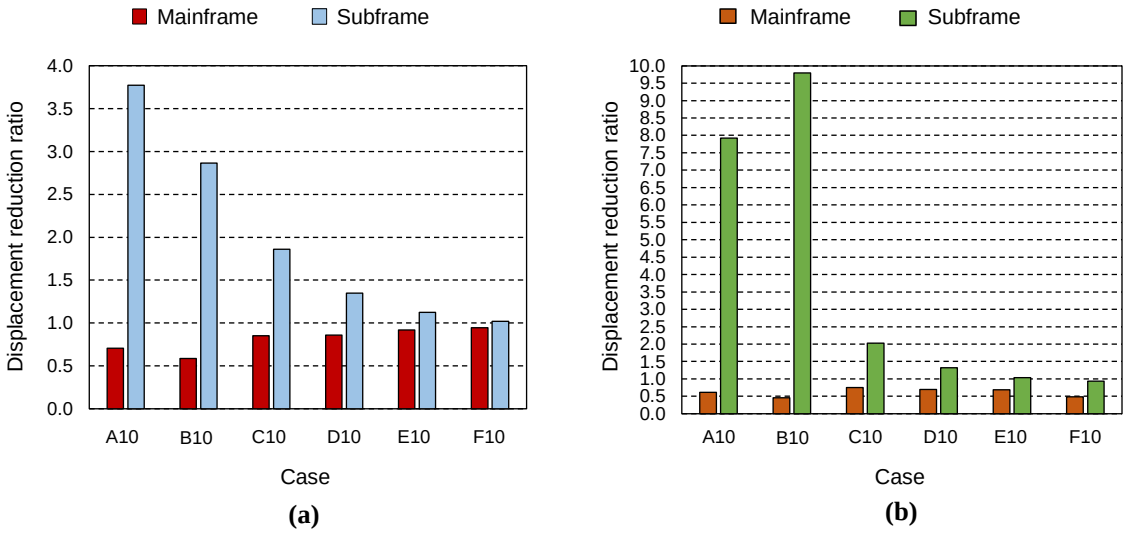

Fig. 9 Peak displacement response reduction ratios averaged for 10 observed records (mainframe and subframe, cases A10 to F10): **(a)** ratio of the CVC-SD model to the CVC-D model; and **(b)** ratio of the CVC-SD model to the SDOF model

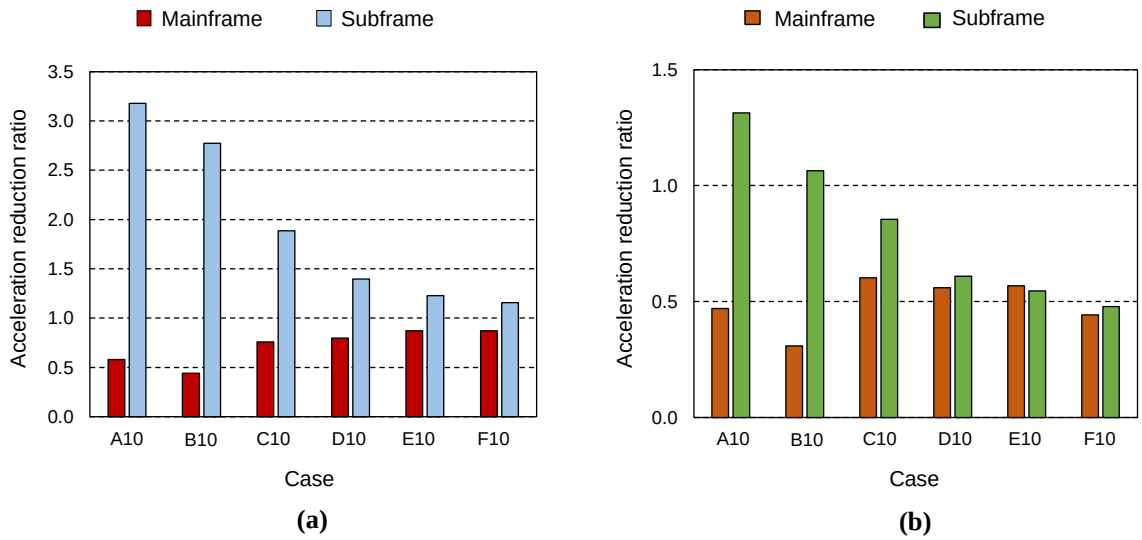

Fig. 10 Peak acceleration response reduction ratios averaged for five simulated waves (mainframe and subframe, cases A10 to F10): **(a)** ratio of the CVC-SD model to the CVC-D model; and **(b)** ratio of the CVC-SD model to the SDOF model

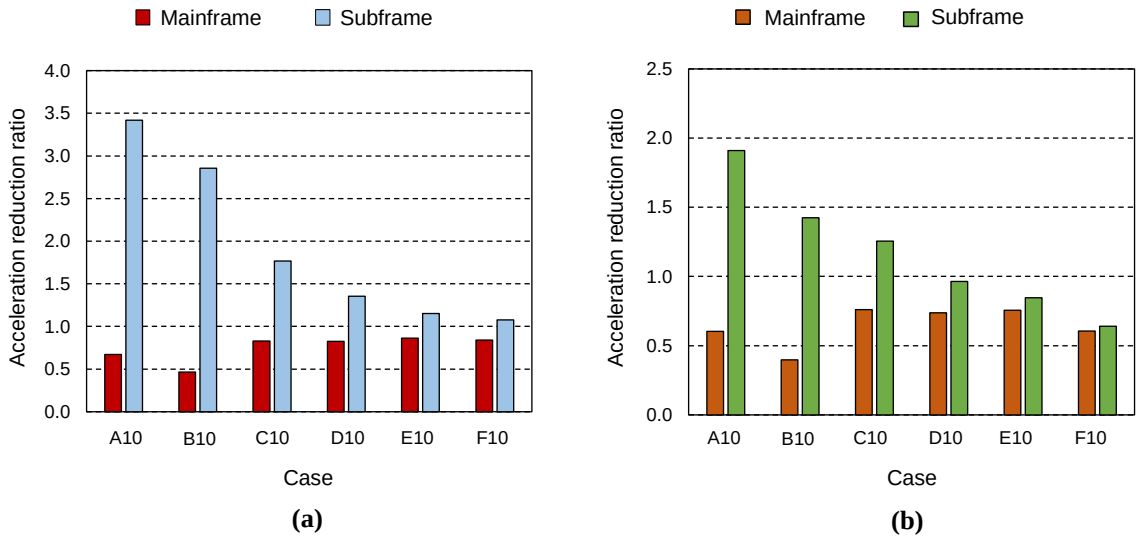

Fig. 11 Peak acceleration response reduction ratios averaged for 10 observed records (mainframe and subframe, cases A10 to F10): **(a)** ratio of the CVC-SD model to the CVC-D model; and **(b)** ratio of the CVC-SD model to the SDOF model

Tables 4 and 5 list the obtained peak response displacement of the mainframe averaged for the five simulated waves and the 10 observed records, respectively, for all 18 cases of the CVC-SD, CVC-D, and SDOF-mainframe models. In these Tables, $PR_{1,disp,opt}$, $PR_{1,disp,ref}$, and $PR_{1,disp,SDOF}$ denote the peak seismic response displacement of the mainframe for the CVC-SD, CVC-D, and SDOF-mainframe models, respectively. Similar to Tables 4 and 5, Tables 6 and 7 show the peak response acceleration of the mainframe averaged for the five simulated waves and the 10 observed records, respectively. Here, $PR_{1,acc,opt}$, $PR_{1,acc,ref}$, and $PR_{1,acc,SDOF}$ denote the peak seismic response acceleration of the mainframe for the CVC-SD, CVC-D, and SDOF-mainframe models, respectively. From these results, the peak displacement responses for the mainframe of the CVC-SD model were lower than those for the CVC-D and SDOF-mainframe models, except for the F05 and F20 cases (Tables 4 and 5). In addition, a decrease in the peak acceleration for the CVC-SD model was attained compared with the CVC-D and SDOF-mainframe models (Tables 6 and 7).

The displacement reduction index and the acceleration reduction index for the CVC-SD model compared with the CVC-D model were calculated as $1 - (PR_{1,disp,opt}/PR_{1,disp,ref})$ and $1 - (PR_{1,acc,opt}/PR_{1,acc,ref})$, respectively, and these reduction indices averaged for the input motions are shown in Tables 4 through 7. The displacement reduction indices yielded a promising result (Tables 4 and 5). In addition, a satisfactorily high acceleration reduction index was obtained (Tables 6 and 7).

Table 4 Peak displacement of mainframe for SDOF-mainframe, CVC-D, and CVC-SD models obtained from response simulation, along with reduction index (mean for five simulated waves)

Case	$PR_{1,\mathrm{disp,SDOF}}$ (m)	$PR_{1,\mathrm{disp,ref}}$ (m)	$PR_{1,\mathrm{disp,opt}}$ (m)	$1-(PR_{1,\mathrm{disp,opt}}/PR_{1,\mathrm{disp,ref}})$
A05	0.078	0.056	0.038	0.329
B05	0.078	0.045	0.032	0.288
C05	0.078	0.056	0.044	0.221
D05	0.078	0.046	0.040	0.134
E05	0.078	0.039	0.038	0.020
F05	0.078	0.028	0.029	−0.052
A10	0.194	0.143	0.090	0.364
B10	0.194	0.143	0.090	0.362
C10	0.194	0.141	0.110	0.222
D10	0.194	0.119	0.100	0.156
E10	0.194	0.106	0.097	0.079
F10	0.194	0.070	0.070	0.003
A20	0.356	0.293	0.180	0.383
B20	0.356	0.238	0.158	0.335
C20	0.356	0.291	0.217	0.251
D20	0.356	0.246	0.197	0.198
E20	0.356	0.220	0.196	0.111
F20	0.356	0.150	0.149	0.004

Table 5 Peak displacement of mainframe for SDOF-mainframe, CVC-D, and CVC-SD models obtained from response simulation, along with reduction index (mean for 10 observed records)

Case	$PR_{1,\mathrm{disp,SDOF}}$ (m)	$PR_{1,\mathrm{disp,ref}}$ (m)	$PR_{1,\mathrm{disp,opt}}$ (m)	$1-(PR_{1,\mathrm{disp,opt}}/PR_{1,\mathrm{disp,ref}})$
A05	0.074	0.062	0.048	0.221
B05	0.074	0.053	0.050	0.023
C05	0.074	0.062	0.052	0.160
D05	0.074	0.054	0.048	0.116
E05	0.074	0.049	0.046	0.055
F05	0.074	0.033	0.037	−0.116
A10	0.222	0.192	0.124	0.293
B10	0.222	0.168	0.092	0.413
C10	0.222	0.194	0.155	0.148
D10	0.222	0.173	0.145	0.140
E10	0.222	0.157	0.142	0.082
F10	0.222	0.106	0.099	0.055
A20	0.329	0.271	0.200	0.255
B20	0.329	0.236	0.161	0.306
C20	0.329	0.271	0.226	0.160
D20	0.329	0.246	0.214	0.122
E20	0.329	0.227	0.208	0.073
F20	0.329	0.168	0.170	−0.061

Table 6 Peak acceleration of mainframe for SDOF-mainframe, CVC-D, and CVC-SD models obtained from response simulation, along with reduction index (mean for five simulated waves)

Case	$PR_{1,acc,SDOF}$ (m/s^2)	$PR_{1,acc,ref}$ (m/s^2)	$PR_{1,acc,opt}$ (m/s^2)	$1-(PR_{1,acc,opt}/PR_{1,acc,ref})$
A05	12.400	9.247	5.541	0.401
B05	12.400	7.734	3.598	0.535
C05	12.400	9.187	6.774	0.264
D05	12.400	7.930	6.353	0.199
E05	12.400	7.029	6.352	0.095
F05	12.400	5.408	4.908	0.094
A10	7.648	5.852	3.383	0.420
B10	7.648	5.036	2.225	0.559
C10	7.648	5.810	4.398	0.242
D10	7.648	5.147	4.100	0.202
E10	7.648	4.787	4.161	0.129
F10	7.648	3.735	3.262	0.127
A20	3.521	2.999	1.710	0.427
B20	3.521	2.566	1.201	0.531
C20	3.521	2.998	2.199	0.262
D20	3.521	2.667	2.065	0.225
E20	3.521	2.505	2.106	0.159
F20	3.521	2.076	1.859	0.100

Table 7 Peak acceleration of mainframe for SDOF-mainframe, CVC-D, and CVC-SD models obtained from response simulation, along with reduction index (mean for 10 observed records)

Case	$PR_{1,acc,SDOF}$ (m/s^2)	$PR_{1,acc,ref}$ (m/s^2)	$PR_{1,acc,opt}$ (m/s^2)	$1-(PR_{1,acc,opt}/PR_{1,acc,ref})$
A05	11.646	10.182	6.588	0.343
B05	11.646	9.023	5.255	0.406
C05	11.646	10.273	8.200	0.201
D05	11.646	9.298	7.632	0.175
E05	11.646	8.658	7.543	0.122
F05	11.646	6.624	5.954	0.100
A10	8.772	7.898	4.868	0.329
B10	8.772	7.229	3.159	0.534
C10	8.772	8.024	6.253	0.172
D10	8.772	7.526	6.021	0.175
E10	8.772	7.218	6.186	0.137
F10	8.772	5.891	4.904	0.161
A20	3.252	2.795	1.905	0.307
B20	3.252	2.552	1.443	0.424
C20	3.252	2.802	2.271	0.183
D20	3.252	2.672	2.194	0.175
E20	3.252	2.584	2.222	0.134
F20	3.252	2.330	2.103	0.089

Overall, from the response simulation results, effective control performance for the response of the mainframe against various earthquakes was demonstrated by installation of negative stiffness as well as viscous damping at the connecting portion of the CVC models. This good performance with negative stiffness can be attained by a smaller viscous damping coefficient ($C_{0,\mathrm{opt}}$ in Table 1), as compared with that without negative stiffness ($C_{0,\mathrm{ref}}$ in Table 1).

In the present analysis, the optimization was done by using the mainframe displacement TF as a control target. As a result, a sufficient control effect was achieved for the mainframe response; on the other hand, an increase in the subframe response was observed. If both the mainframe and subframe displacements are used as control targets, the increase in subframe response may be mitigated, albeit with a deterioration in the control effect for the mainframe response. However, in the case where the subframe's mass is significantly smaller than the mainframe's mass, it is inferred that an increase in the response of the subframe may be unavoidable. When the response of the subframe is evaluated to be a large value, a sufficient deformation capacity needs to be ensured for the subframe.

2.2.3. Evaluation criteria

To evaluate the control performance of the CVC-SD and CVC-D models, evaluation criteria expressed as Equations (1)–(3) were used in reference to the literature [18,48].

$$J_1 = \frac{\max|x_1(t)|_C}{\max|x_1(t)|_U}, \tag{1}$$

$$J_2 = \frac{\max|\ddot{x}_1(t)+\ddot{x}_g(t)|_C}{\max|\ddot{x}_1(t)+\ddot{x}_g(t)|_U}, \tag{2}$$

$$J_3 = \frac{\mathrm{RMS}(x_1)_C}{\mathrm{RMS}(x_1)_U}, \tag{3}$$

where t is the time, $x_1(t)$ is the response displacement of the mainframe, $\ddot{x}_1(t)$ is the response acceleration of the mainframe, and $\ddot{x}_g(t)$ is the input acceleration. Subscript C denotes the controlled case (the CVC-SD and CVC-D models), and subscript U denotes the uncontrolled case (the SDOF-mainframe model). RMS(x_1) denotes the root mean square calculated as follows:

$$\mathrm{RMS}(x_1) = \sqrt{\frac{1}{t_f}\int_0^{t_f}[x_1(t)]^2 \mathrm{d}t}, \tag{4}$$

where t_f is the duration (= $N\Delta t$), N is the number of data, and Δt is the time interval.

The obtained evaluation criteria (J_1, J_2, and J_3) for the mainframe of the CVC-SD and CVC-D models are given in Tables 8 and 9. Here, each of J_1–J_3 was averaged for the input motions in each group (the simulated waves and observed records). From the results, the obtained evaluation criteria J_1–J_3 showed lesser values than unity, indicating a good seismic control performance.

Moreover, the evaluation criteria obtained from the present study were compared with corresponding evaluation criteria reported in a past study on semi-active control for

coupled adjacent buildings [18]. Summarized evaluation criteria from the literature [18] are as follows (for Building 1, intensity 0.5, averaged for three earthquakes): $J_1 = 0.75$, $J_2 = 1.02$, and $J_3 = 0.74$ by simple adaptive controller (SAC); and $J_1 = 0.78$, $J_2 = 0.89$, and $J_3 = 0.70$ by LQR controller. Although the building conditions and control methods considered are different between the literature [18] and the present study, thus direct comparison is just only for reference, the evaluation criteria obtained in the present study (Tables 8 and 9) were roughly comparable with the above summarized values of J_1–J_3 from the literature.

Table 8 Evaluation criteria for mainframe of controlled (CVC-SD and CVC-D) models obtained from response simulation (mean for five simulated waves)

Model	CVC-SD			CVC-D		
Case	J_1	J_2	J_3	J_1	J_2	J_3
A05	0.492	0.455	0.426	0.733	0.759	0.667
B05	0.418	0.295	0.406	0.589	0.638	0.515
C05	0.563	0.555	0.499	0.726	0.756	0.656
D05	0.515	0.520	0.451	0.601	0.654	0.522
E05	0.495	0.521	0.428	0.508	0.578	0.445
F05	0.377	0.403	0.321	0.358	0.446	0.287
A10	0.499	0.469	0.414	0.768	0.797	0.739
B10	0.413	0.308	0.362	0.639	0.691	0.591
C10	0.594	0.602	0.523	0.763	0.795	0.732
D10	0.543	0.560	0.469	0.647	0.709	0.604
E10	0.525	0.568	0.452	0.570	0.655	0.524
F10	0.382	0.442	0.362	0.382	0.509	0.329
A20	0.517	0.497	0.486	0.834	0.865	0.812
B20	0.451	0.346	0.430	0.684	0.747	0.659
C20	0.627	0.644	0.606	0.830	0.866	0.808
D20	0.568	0.602	0.546	0.708	0.778	0.673
E20	0.566	0.615	0.526	0.637	0.731	0.588
F20	0.424	0.540	0.385	0.427	0.600	0.383

Table 9 Evaluation criteria for mainframe of controlled (CVC-SD and CVC-D) models obtained from response simulation (mean for 10 observed records)

Model	CVC-SD			CVC-D		
Case	J_1	J_2	J_3	J_1	J_2	J_3
A05	0.666	0.585	0.479	0.855	0.885	0.747
B05	0.718	0.470	0.487	0.738	0.794	0.601
C05	0.728	0.722	0.561	0.861	0.895	0.741
D05	0.667	0.675	0.509	0.758	0.818	0.613
E05	0.638	0.670	0.488	0.680	0.766	0.532
F05	0.517	0.530	0.369	0.466	0.596	0.343
A10	0.611	0.602	0.399	0.864	0.898	0.739
B10	0.458	0.398	0.328	0.776	0.844	0.591
C10	0.747	0.759	0.529	0.875	0.914	0.733
D10	0.700	0.738	0.470	0.805	0.884	0.602
E10	0.689	0.756	0.450	0.746	0.870	0.517
F10	0.486	0.606	0.312	0.514	0.722	0.313
A20	0.625	0.612	0.391	0.838	0.874	0.699
B20	0.502	0.463	0.317	0.741	0.811	0.545
C20	0.710	0.725	0.497	0.839	0.879	0.689
D20	0.677	0.705	0.447	0.772	0.852	0.556
E20	0.661	0.717	0.430	0.720	0.834	0.482
F20	0.556	0.684	0.317	0.536	0.761	0.317

3. Nonlinear seismic response simulation

3.1. Methods

A nonlinear earthquake response simulation was conducted using the CVC-SD, CVC-D, and SDOF-mainframe models for Case C10 (α = 0.2, μ = 0.1, and T_1 = 1.0 s). A normal bilinear restoring force characteristic was adopted for the nonlinear spring of the mainframe. Except for the restoring force characteristic of the mainframe, the other parameters were the same as those used in the linear response simulation (Section 2.1). For the mainframe bilinear spring, the initial stiffness was the same as that in the linear model (Section 2.1), the yield base shear coefficient was 0.25, the second stiffness after yielding was 0.2 times the initial stiffness, and the unloading stiffness was the same as the initial stiffness. Waves M1–M5 were used for input motions, and three input multipliers of 0.5, 1.0, and 1.5 were adopted for each wave. Unlike the linear simulation (Section 2.1), a time increment of 0.0001 s was used in the nonlinear simulation.

3.2. Results

The obtained response displacement and acceleration for the nonlinear mainframe with respect to the input multiplier are shown in Figs. 12 and 13, respectively. Here, each value in the vertical axis was the mean for the five input motions. Figure 12a shows the peak response displacement ductility ratio of the mainframe calculated by dividing the peak response displacement with the yield displacement. Fig. 12b plots the ratio of the peak response displacement of the mainframe for the controlled case (the CVC-SD and CVC-D models) to that for the uncontrolled case (the SDOF-mainframe model). Also, Fig. 13 shows the peak response acceleration for the mainframe and the acceleration ratio of the controlled case to that of the uncontrolled case. From Fig. 12a, when the input multiplier was 0.5, the averaged displacement ductility ratio of the CVC-SD model was smaller than unity, indicating the mainframe was approximately within the elastic range. Under this input multiplier of 0.5, the CVC-SD model showed a significant reduction in the peak displacement and acceleration compared with the SDOF-mainframe model (Figs. 12 and 13). This was because the parameters of the connecting spring and damping elements (K_0 and C_0) were set based on the initial stiffness state of the mainframe. From Fig. 12b, the

averaged displacement ratios (CVC-SD model/SDOF-mainframe model) under the input multiplier of 1.0 and 1.5 increased compared to that under the input multiplier of 0.5; however, the ratios were smaller than unity, showing a control effect on the mainframe of the CVC-SD model.

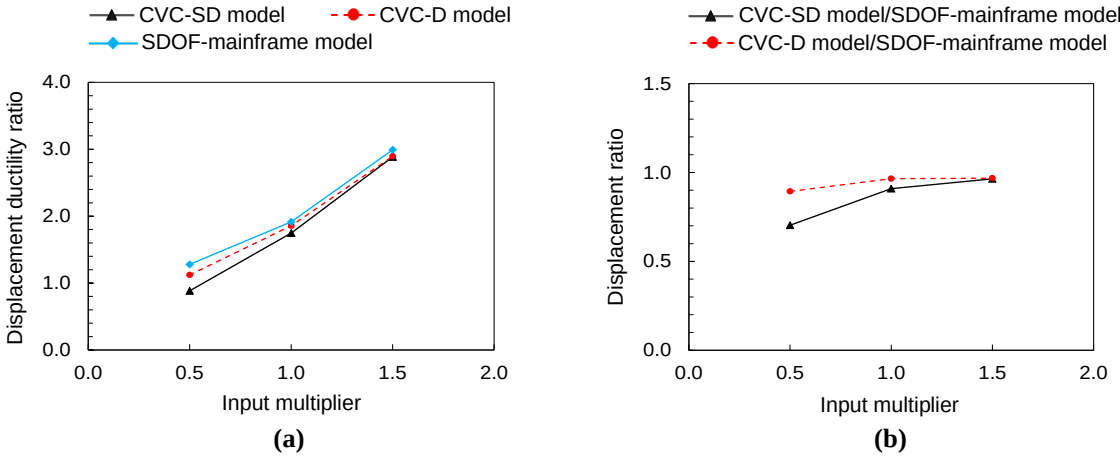

Fig. 12 Response displacement of the mainframe averaged for five simulated waves obtained from nonlinear simulation of the CVC-SD, CVC-D and SDOF-mainframe models (case C10, Waves M1–M5, input multipliers 0.5, 1.0, and 1.5): **(a)** displacement ductility ratio; and **(b)** displacement ratio

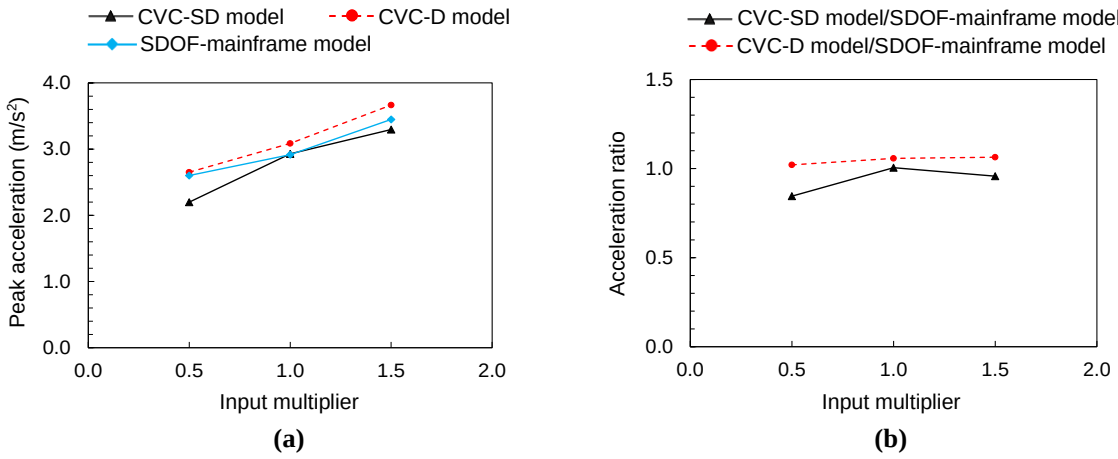

Fig. 13 Response acceleration of the mainframe averaged for five simulated waves obtained from nonlinear simulation of the CVC-SD, CVC-D and SDOF-mainframe models (case C10, Waves M1–M5, input multipliers 0.5, 1.0, and 1.5): **(a)** peak acceleration; and **(b)** acceleration ratio

4. Conclusions

In this chapter, numerical investigation on the control effects by negative stiffness connection between the mainframe and subframe for CVC adjacent structures were conducted based on a time history seismic response simulation. The following conclusions could be drawn:

1) An effective control performance for the response of the mainframe was achieved by installing the optimized negative stiffness and optimized damping elements at the connecting portion of the CVC-SD model under various earthquakes, including simulated waves and observed records.

2) The peak seismic response of the subframe for the CVC-SD model generally became larger as compared with that of the CVC-D model. This was because the optimization for the connecting portion was based on the displacement TF of the mainframe.

The study contributes to effective structural design for not only newly constructed coupled adjacent buildings but also aseismic retrofitting of existing mainframes by connecting with newly added subframes. Future research tasks include investigation using multi-story building models for both the mainframe and subframe of the CVC structures and optimization problems for the location in the height of the connection elements.

Acknowledgments

The present study was supported by the Kajima Foundation 2021 Research Grant and by the Japan Society for the Promotion of Science Grant-in-Aid for JSPS Research Fellow. The present earthquake response simulation used the observation records provided by the Japan Meteorological Agency and Building Performance Standardization Association of Japan.

References

[1] Palacios-Quiñonero F, Rubió-Massegú J, Rossell JM, Karimi HR (2014) Vibration control for adjacent structures using local state information. *Mechatronics*, **24**(4):336–344. http://dx.doi.org/10.1016/j.mechatronics.2013.08.001

[2] Zhang WS, Xu YL (2000) Vibration analysis of two buildings linked by Maxwell model-defined fluid dampers. *Journal of Sound and Vibration*, **233**(5):775–796. https://doi.org/10.1006/jsvi.1999.2735

[3] Ni YQ, Ko JM, Ying ZG (2001) Random seismic response analysis of adjacent buildings coupled with non-linear hysteretic dampers. *Journal of Sound and Vibration*, **246**(3):403–417. https://doi.org/10.1006/jsvi.2001.3679

[4] Ying ZG, Ni YQ, Ko JM (2003) Stochastic optimal coupling-control of adjacent building structures. *Computers & Structures*, **81**(30–31):2775–2787. https://doi.org/10.1016/S0045-7949(03)00332-8

[5] Christenson RE, Spencer Jr BF, Johnson EA, Seto K (2006) Coupled building control considering the effects of building/connector configuration. *Journal of structural engineering*, ASCE, **132**(6):853–863. https://doi.org/10.1061/(ASCE)0733-9445(2006)132:6(853)

[6] Basili M, De Angelis M, Fraraccio G (2013) Shaking table experimentation on adjacent structures controlled by passive and semi-active MR dampers. *Journal of Sound and Vibration*, **332**(13):3113–3133. https://doi.org/10.1016/j.jsv.2012.12.040

[7] Basili M, De Angelis M (2017) Vibration analysis and models of adjacent structures controlled by magnetorheological dampers. *Shock and Vibration*. Article ID 9596382. https://doi.org/10.1155/2017/9596382

[8] Basili M, De Angelis M, Pietrosanti D (2019) Defective two adjacent single degree of freedom systems linked by spring-dashpot-inerter for vibration control. *Engineering Structures*, **188**:480–492. https://doi.org/10.1016/j.engstruct.2019.03.030

[9] De Domenico D, Qiao H, Wang Q, Zhu Z, Marano G (2020) Optimal design and seismic performance of Multi‐Tuned Mass Damper Inerter (MTMDI) applied to adjacent high‐rise buildings. *The Structural Design of Tall and Special Buildings*, **29**(14):e1781. https://doi.org/10.1002/tal.1781

[10] Kazemi F, Miari M, Jankowski R (2021) Investigating the effects of structural pounding on the seismic performance of adjacent RC and steel MRFs. *Bulletin of Earthquake Engineering*, **19**(1):317–343. https://doi.org/10.1007/s10518-020-00985-y

[11] Lu L, Xu J, Zhou Y, Lu W, Spencer Jr BF (2021) Viscous inertial mass damper (VIMD) for seismic responses control of the coupled adjacent buildings. *Engineering Structures*, **233**:111876. https://doi.org/10.1016/j.engstruct.2021.111876

[12] Bharti SD, Dumne SM, Shrimali MK (2010) Seismic response analysis of adjacent buildings connected with MR dampers. *Engineering Structures*, **32**(8):2122–2133. https://doi.org/10.1016/j.engstruct.2010.03.015

[13] Uz ME, Hadi MNS (2014) Optimal design of semi active control for adjacent buildings connected by MR damper based on integrated fuzzy logic and multi-objective genetic algorithm. *Engineering Structures*, **69**:135–148. https://doi.org/10.1016/j.engstruct.2014.03.006

[14] Guenidi Z, Abdeddaim M, Ounis A, Shrimali MK, Datta TK (2017) Control of adjacent buildings using shared tuned mass damper. *Procedia Engineering*, **199**:1568–1573. https://doi.org/10.1016/j.proeng.2017.09.059

[15] Al-Fahdawi OAS, Barroso LR, Soares RW (2018) Utilizing the adaptive control in mitigating the seismic response of adjacent buildings connected with MR dampers. *2018 Annual American Control Conference (ACC)*:912–917. https://doi.org/10.23919/ACC.2018.8431135

[16] Ndemanou BP, Nbendjo BRN (2018) Fuzzy magnetorheological device vibration control of the two Timoshenko cantilever beams interconnected under earthquake excitation. *The Structural Design of Tall and Special Buildings*, **27**(17):e1541. https://doi.org/10.1002/tal.1541

[17] Al-Fahdawi OAS, Barroso LR, Soares RW (2019) Simple adaptive control method for mitigating the seismic responses of coupled adjacent buildings considering parameter variations. *Engineering Structures*, **186**:369–381. https://doi.org/10.1016/j.engstruct.2019.02.025

[18] Al-Fahdawi OAS, Barroso LR, Soares RW (2019) Semi-active adaptive control for enhancing the seismic performance of nonlinear coupled buildings with smooth hysteretic behavior. *Engineering Structures*, **191**:536–548. https://doi.org/10.1016/j.engstruct.2019.04.078

[19] Al-Fahdawi OAS, Barroso LR (2021) Adaptive neuro-fuzzy and simple adaptive control methods for full three-dimensional coupled buildings subjected to bi-directional seismic excitations. *Engineering Structures*, **232**:111798. https://doi.org/10.1016/j.engstruct.2020.111798

[20] Xu YL, He Q, Ko JM (1999) Dynamic response of damper-connected adjacent buildings under earthquake excitation. *Engineering Structures*, **21**(2):135–148. https://doi.org/10.1016/S0141-0296(97)00154-5

[21] Tubaldi E (2015) Dynamic behavior of adjacent buildings connected by linear viscous/viscoelastic dampers. *Structural Control and Health Monitoring*, **22**(8):1086–1102. https://doi.org/10.1002/stc.1734

[22] Jankowski R, Mahmoud S (2016) Linking of adjacent three-storey buildings for mitigation of structural pounding during earthquakes. *Bulletin of Earthquake Engineering*, **14**(11):3075–3097. https://doi.org/10.1007/s10518-016-9946-z

[23] Tubaldi E, Gioiella L, Scozzese F, Ragni L, Dall'Asta A (2020) A design method for viscous dampers connecting adjacent structures. *Frontiers in Built Environment*, **6**:25. https://doi.org/10.3389/fbuil.2020.00025

[24] Minami S, Yamazaki S, Toyama K, Tahara K (2004) Experimental study on coupled vibration control structures. *The 13th World Conference on Earthquake Engineering*, Paper No. 2351, August 1–6, 2004, Vancouver, B.C., Canada.

[25] Li H, Li Y, Li J (2020) Negative stiffness devices for vibration isolation applications A review. *Advances in Structural Engineering*, **23**(8):1739–1755. https://doi.org/10.1177/1369433219900311

[26] Mizuno T, Toumiya T, Takasaki M (2003) Vibration isolation system using negative stiffness. *JSME International Journal*, Series C, **46**(3):807–812. https://doi.org/10.1299/jsmec.46.807

[27] Iemura H, Kouchiyama O, Toyooka A, Shimoda I (2008) Development of the friction-based passive negative stiffness damper and its verification tests using shaking table. *The 14th World Conference on Earthquake Engineering*, October 12–17, 2008, Beijing, China.

[28] Nagarajaiah S, Pasala DTR, Reinhorn A, Constantinou M, Sirilis AA, Taylor D (2013) Adaptive negative stiffness: a new structural modification approach for seismic protection. *Advanced Materials Research*, **639**–**640**:54–66. https://doi.org/10.4028/www.scientific.net/AMR.639-640.54

[29] Sarlis AA, Pasala DTR, Constantinou MC, Reinhorn AM, Nagarajaiah S, Taylor DP (2013) Negative stiffness device for seismic protection of structures. *Journal of Structural Engineering*, ASCE, **139**(7):1124–1133. https://doi.org/10.1061/(ASCE)ST.1943-541X.0000616

[30] Walsh KK, Boso, E., Steinberg EP, Haftman JT, Littell WN (2018) Variable negative stiffness device for seismic protection of building structures through apparent weakening. *Journal of Engineering Mechanics*, **144**(9):04018090. https://doi.org/10.1061/(ASCE)EM.1943-7889.0001512

[31] Zhou P, Liu M, Li H (2020) A passive negative stiffness damper in series with a flexible support: Theoretical and experimental study. *Structural Control and Health Monitoring*, **27**(9):e2594. https://doi.org/10.1002/stc.2594

[32] Shirai K, Noro S, Walsh KK (2021) Shake table testing of a passive negative stiffness device with curved leaf springs for seismic response mitigation of structures. *Structural Control and Health Monitoring*, **28**(7):e2736. https://doi.org/10.1002/stc.2736

[33] Zhu H, Iemura H (2000) A study of response control on the passive coupling element between two parallel structures. *Structural Engineering and Mechanics*. **9**(4):383–396. https://doi.org/10.12989/sem.2000.9.4.383

[34] Kageyama M, Yasui Y, Seto K (2000) The principal solutions of connecting spring and damper for optimum vibration control under several criteria. *Journal of Structural and Construction Engineering*, AIJ, **65**(529):97–104. **(in Japanese)** https://doi.org/10.3130/aijs.65.97

[35] Zhu H, Wen Y, Iemura H (2001) A study on interaction control for seismic response of parallel structures. *Computers & Structures*, **79**(2):231–242. https://doi.org/10.1016/S0045-7949(00)00119-X

[36] Zhu HP, Ge DD, Huang X (2011) Optimum connecting dampers to reduce the seismic responses of parallel structures. *Journal of Sound and Vibration*, **330**(9): 1931–1949. https://doi.org/10.1016/j.jsv.2010.11.016

[37] Den Hartog JP (1956) Mechanical vibrations, 4th ed. McGraw-Hill, New York.

[38] Shirai K, Park J (2020) Use of scrap tire pads in vibration control system for seismic response reduction of buildings. *Bulletin of Earthquake Engineering*, **18**(5): 2497–2521. https://doi.org/10.1007/s10518-020-00787-2

[39] Sano T, Shirai K, Yoshida O, Nishikage T (2021) Assessment of a seismic tuned mass damper with friction fail-safe mechanism for the vibration control of high-rise buildings. *Structural Control and Health Monitoring*:e2831. https://doi.org/10.1002/stc.2831

[40] Longjam S, Shirai K (2021) Use of negative stiffness for coupled vibration control structures: an analytical investigation. *The 17th World Conference on Earthquake Engineering*, September 27–October 2, 2021, Sendai, Japan.

[41] Yamada Y, Ikawa N, Yokoyama H, Tachibana E (1994) Active control of structures using the joining member with negative stiffness. *The First World Conference on Structural Control*, TP2, Vol. 2, 41–49, 1994, California, USA.

[42] Ikawa N, Yamada Y, Yokoyama H, Tachibana E (1996) Active control system of coupled structures with a negative stiffness. *Journal of Structural Engineering*, AIJ, Vol. **42B**: 629–634. **(in Japanese)**

[43] Shimizu K, Kurino H (2009) Fundamental study of structural control with negative stiffness connection. Part 1: Study of applicability of negative stiffness. *Summaries of Technical Papers of Annual Meeting*, AIJ:453–454. **(in Japanese)**

[44] Kurino H, Shimizu K (2009) Fundamental study of structural control with negative stiffness connection. Part 2: Feasibility study utilizing variable damping device. *Summaries of Technical Papers of Annual Meeting*, AIJ:455–456. **(in Japanese)**

[45] Shirai K, Inoue N (2014) A seismic response estimation method for RC structures using random vibration theory. *Journal of Advanced Concrete Technology*, **12**(2):62–72. https://doi.org/10.3151/jact.12.62

[46] Building Performance Standardization Association. (**in Japanese**) (Access date: July 30, 2019) https://www.seinokyo.jp/jsh/top/

[47] Japan Meteorological Agency. (**in Japanese**) (Access date: July 30, 2019) https://www.data.jma.go.jp/svd/eqev/data/kyoshin/jishin/hyogo_nanbu/index.html

[48] Ohtori Y, Christenson RE, Spencer Jr. BF, Dyke SJ (2004) Benchmark control problems for seismically excited nonlinear buildings. *Journal of Engineering Mechanics*, **130**(4): 366–385. https://doi.org/10.1061/(ASCE)0733-9399(2004)130:4(366)

Chapter IV

Numerical analysis of the seismic controlled motions for coupled MDOF buildings by negative stiffness connection

1. Introduction

Negative stiffness generally functions in opposition to positive stiffness, generating a decreased (i.e., negative) restoring force as the device's displacement increases. Negative stiffness is considered one of the potential control strategies for building structures against dynamic action such as an earthquake. During the past few decades, considerable works have been done to explore negative stiffness devices (NSDs) and systems consisting NSDs [1–6].

A pseudo-negative-stiffness damper generating a negative-stiffness hysteresis loop was devised. The device's effectiveness was assessed on structures, including bridges and buildings subjected to seismic motions [2]. A passive NSD based on a vertical pre-compressed spring was proposed [3,4]. The device gave an approximately zero total stiffness in a small displacement range. Another passive NSD consisting of two curved leaf springs rigidly connected to a pair of beams was also proposed [7]. Before the occurrence of snap-through buckling, pre-compressed strain energy stored in the form of curved leaf springs creates an initial negative stiffness.

The mentioned past studies on NSD have solely depended on the seismic response of the individual structures. Limited research on adjacent structures linked by NSD has been made available [8–11]. An analytical and numerical investigation based on coupled structures formed by connecting two single degree of freedom structures, namely mainframe and subframe, were proposed as described in Chapters II and III. Different linear and nonlinear 2DOF-coupled systems, depending on structural parameters and natural periods of the connected structures, were adopted for seismic response analysis under various ground motions, including simulated waves and observed earthquake records. Effective control by the negative stiffness linking the mainframe and subframe, forming a coupled vibration control (CVC) structure, was observed.

This chapter investigates the control effects of negative stiffness connecting multi-degree of freedom (MDOF) mainframe and MDOF subframe, forming a CVC model, as a strategy for mitigation of vibration caused by earthquakes. Different settings of connecting portion were studied to compare the controlling performance of the connector on the CVC models. Various damping and negative stiffness values of the connecting vibration controllers were considered for the CVC structures against seismic ground motions.

2. Linear earthquake response simulation

2.1. Modeling of mainframe and subframe

For the objectives of the investigation, two adjacent structures namely, 6DOF-mainframe and 6DOF-subframe with structural parameters combination for the stiffness ratio ($\alpha = k_n^S/k_n^M$) of 0.2 and the mass ratio ($\mu = m_n^S/m_n^M$) of 0.10 for each nth story were considered. Fig.1 shows the individual MDOF models of the mainframe and subframe with the stories' mass lumped at the floor level. Table 1 shows the structural properties of the mainframe and subframe models to form MDOF CVC systems. A mass of 1000 t for each story of the mainframe was adopted. The floor-to-floor height of each storey equals to 4.0 meters. The viscous damping coefficient was set based on the stiffness proportional type damping with a damping factor of 0.02 for the first mode. The stiffness and damping values of each story of the mainframe were distributed in a proportion ratio of 2.0, 1.8, 1.6, 1.4, 1.2, and 1.0 from the bottom to the top story, such that the target first modal natural period of the mainframe (T = 0.72s) was achieved. The first modal natural period of the subframe was determined to be 0.51s. The stiffness and damping values of each story of the subframe were distributed based on the target structural parameters combination of α and μ of each story of the mainframe, as shown in Table 1. The primary study was based on simplified SDOF models adopted in Chapters II and III. Based on the equivalent heights and optimal design using equivalent vibration behavior of the SDOF-models, the analysis using MDOF-models was to be conducted. Therefore, MDOF-mainframe and MDOF-subframe models were linked by vibration control mechanism at their corresponding sixth floor, i.e., near the equivalent heights of the SDOF-models.

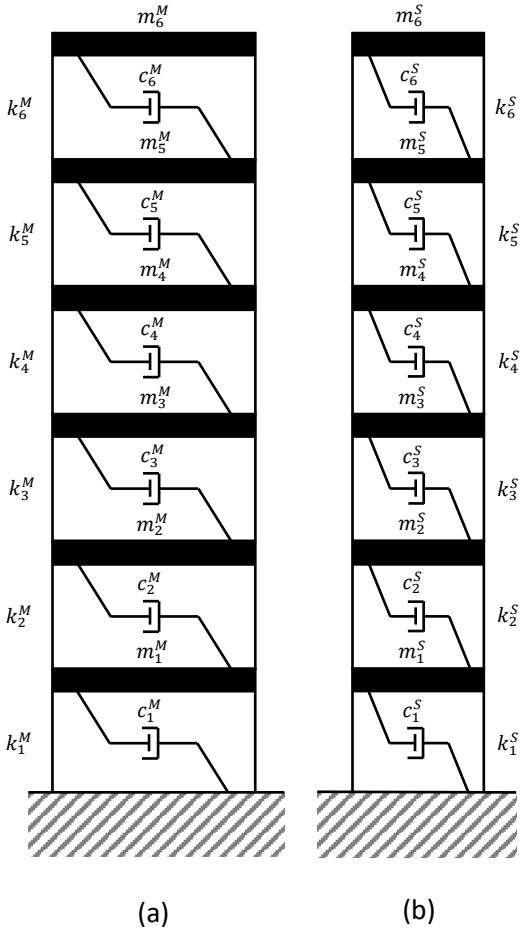

Fig. 1 Analytical models considered: **(a)** 6DOF mainframe and **(b)** 6DOF subframe

Table 1 Structural properties of the 6DOF mainframe and 6DOF subframe models

	Mainframe				Subframe	
Story, n	Mass, m_n^M (t)	Stiffness, k_n^M (N/m)	Damping coefficient, c_n^M (Ns/m)	Mass, m_n^S (t)	Stiffness, k_n^S (N/m)	Damping coefficient, c_n^S (Ns/m)
1	1000	1581768001.07	7250290.811	100	316353600.21	1025346.01
2	1000	1423591200.97	6525261.730	100	284718240.19	922811.41
3	1000	1265414400.86	5800232.649	100	253082880.17	820276.80
4	1000	1107237600.75	5075203.568	100	221447520.15	717742.20
5	1000	949060800.64	4350174.487	100	189812160.13	615207.60
6	1000	790884000.54	3625145.406	100	158176800.11	512673.00

Table 2 The K_0 and C_0 values of the connecting vibration controller in the CVC models

MDOF model name	Negative stiffness, K_0 (N/m)	Damping coefficient, C_0 (Ns/m)
CVC-D	0	1815505
CVC-S	-12378144	0
CVC-SD	-9796595	467044

2.2. Modeling of connecting stiffness and viscous damping element

The linear 6DOF mainframe and 6DOF subframe models shown in Fig. 1(a) were adopted as the individual MDOF models. The governing equation of motions of the MDOF CVC system can be expressed as follows [12,13]:

$$M\ddot{x} + C\dot{x} + Kx = -M\ddot{x}_G \tag{1}$$

where,

$$M = \begin{bmatrix} M_6^m & 0 \\ 0 & M_6^s \end{bmatrix} \tag{2}$$

$$M_6^m = \begin{bmatrix} m_1^M & \cdots & 0 \\ \vdots & \ddots & \vdots \\ 0 & \cdots & m_6^M \end{bmatrix}; M_6^s = \begin{bmatrix} m_1^S & \cdots & 0 \\ \vdots & \ddots & \vdots \\ 0 & \cdots & m_6^S \end{bmatrix}$$

$$K = \begin{bmatrix} K_6^m & 0 \\ 0 & K_6^s \end{bmatrix} \tag{3}$$

$$K_6^m = \begin{bmatrix} k_1^M + k_2^M & -k_2^M & \cdots & 0 \\ -k_2^M & \ddots & \ddots & \vdots \\ \vdots & \ddots & \ddots & -k_6^M \\ 0 & \cdots & -k_6^M & k_6^M \end{bmatrix}; K_6^s = \begin{bmatrix} k_1^S + k_2^S & -k_2^S & \cdots & 0 \\ -k_2^S & \ddots & \ddots & \vdots \\ \vdots & \ddots & \ddots & -k_6^S \\ 0 & \cdots & -k_6^S & k_6^S \end{bmatrix}$$

$$C = \begin{bmatrix} C_6^m & 0 \\ 0 & C_6^s \end{bmatrix} \tag{4}$$

$$C_6^m = \begin{bmatrix} c_1^M + c_2^M & -c_2^M & \cdots & 0 \\ -c_2^M & \ddots & \ddots & \vdots \\ \vdots & \ddots & \ddots & -c_6^M \\ 0 & \cdots & -c_6^M & c_6^M \end{bmatrix}; C_6^s = \begin{bmatrix} c_1^S + c_2^S & -c_2^S & \cdots & 0 \\ -c_2^S & \ddots & \ddots & \vdots \\ \vdots & \ddots & \ddots & -c_6^S \\ 0 & \cdots & -c_6^S & c_6^S \end{bmatrix}$$

These mainframe model and subframe model were linked using three different settings of the connecting portions, i.e., firstly, dashpot (damper) only with $K_0 = 0$ as the coupled vibration controller for the CVC-D model (in Section 2.2.1.), secondly, negative stiffness only with $C_0 = 0$ represented as CVC-S models (in Section 2.2.2.), and thirdly, negative stiffness ($K_0 \neq 0$) and dashpot ($C_0 \neq 0$) as connector defined the CVC-SD model (in Section 2.2.3.). The combination values of K_0 and C_0 were adopted based on the connecting types for each model, and the combination of α and μ are shown in Table 2. The analysis focused primarily on the negative stiffness device's control performance as a connecting element for the coupled structure. This investigation did not consider other aspects, such as the deformation limit of the negative stiffness device. The descriptions for each model are explained in the corresponding sub-sections (Sections 2.2.1. to 2.2.3).

2.2.1. CVC-D model linked by dashpot element

Firstly, the CVC-D model linked by the dashpot element was considered, as shown in Fig. 2. The linear 6DOF mainframe and 6DOF subframe models as described in Section 2.1. were adopted and linked at the sixth floor of each model by a dashpot represented as C_0. The equation of motion subjected to the excitation is expressed by Equation (1), where the damping matrix given in Equation (5) was used upon incorporating dashpot as the connecting element. The combination values of C_0 and K_0 corresponding to the adopted combination of structural parameters, α and μ, were used as shown in Table 2. The same mass matrix and stiffness matrix of the models shown in Equations (2) and (3) were used for the analysis.

$$C=\begin{bmatrix} c_1^M+c_2^M & -c_2^M & \cdots & \cdots & \cdots & \cdots & \cdots & 0 \\ -c_2^M & \ddots & \ddots & \ddots & \ddots & \ddots & \ddots & \vdots \\ \vdots & \ddots & c_5^M+c_6^M+C_0 & -c_6^M & \ddots & \ddots & -C_0 & \vdots \\ \vdots & \ddots & -c_6^M & c_6^M & \ddots & \ddots & \ddots & \vdots \\ \vdots & \ddots & \ddots & \ddots & c_1^S+c_2^S & -c_2^S & \ddots & \vdots \\ \vdots & \ddots & \ddots & \ddots & -c_2^S & \ddots & \ddots & \vdots \\ \vdots & \ddots & -C_0 & \ddots & \ddots & \ddots & c_5^S+c_6^S+C_0 & -c_6^S \\ 0 & \cdots & \cdots & \cdots & \cdots & \cdots & -c_6^S & c_6^S \end{bmatrix} \quad (5)$$

when $C_0 \neq 0$, i.e., dashpot (damper) is provided as the connecting element

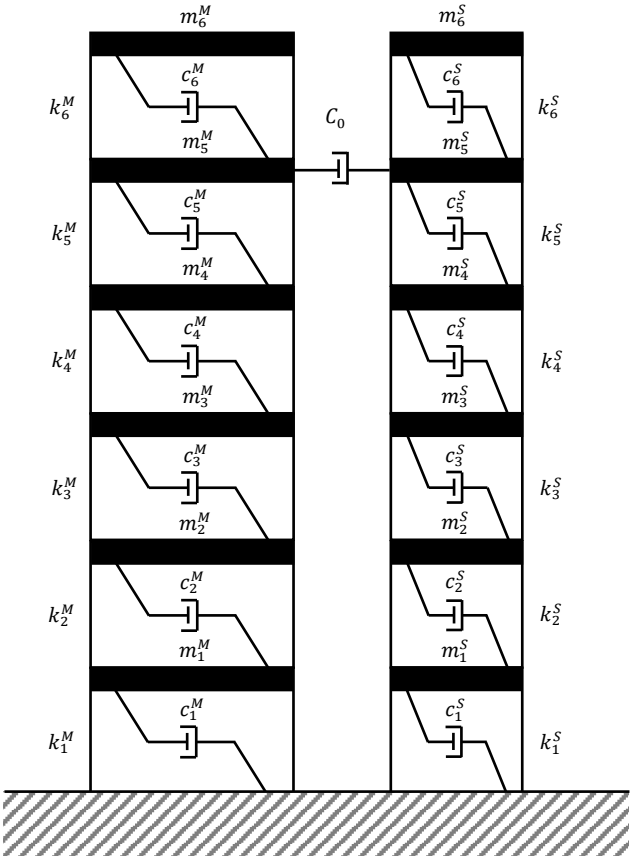

Fig. 2 Analytical CVC-D model with dashpot as connector

2.2.2. CVC-S model linked by negative stiffness element

Secondly, Fig. 3 shows the analytical CVC-S model where the mainframe and subframe were linked by a negative stiffness element as the connecting vibration controller. The same mainframe and subframe models as described in Section 2.1. were adopted. The negative stiffness element linked the mainframe and subframe at the sixth floor. In this case, Equations (1), (2), (4), and the stiffness matrix expressed in equation (6) were evaluated for the analysis. The corresponding negative stiffness value, K_0, for CVC-S model is given in Table 2.

$$K = \begin{bmatrix} k_1^M + k_2^M & -k_2^M & \cdots & \cdots & \cdots & \cdots & \cdots & 0 \\ -k_2^M & \ddots & \ddots & \ddots & \ddots & \ddots & \ddots & \vdots \\ \vdots & \ddots & k_5^M + k_6^M + K_0 & -k_6^M & \ddots & \ddots & -K_0 & \vdots \\ \vdots & \ddots & -k_6^M & k_6^M & \ddots & \ddots & \ddots & \vdots \\ \vdots & \ddots & \ddots & \ddots & k_1^S + k_2^S & -k_2^S & \ddots & \vdots \\ \vdots & \ddots & \ddots & \ddots & -k_2^S & \ddots & \ddots & \vdots \\ \vdots & \ddots & -K_0 & \ddots & \ddots & \ddots & k_5^S + k_6^S + K_0 & -k_6^S \\ 0 & \cdots & \cdots & \cdots & \cdots & \cdots & -k_6^S & k_6^S \end{bmatrix} \quad (6)$$

when $K_0 \neq 0$, i.e., negative stiffness spring is provided as the connecting element

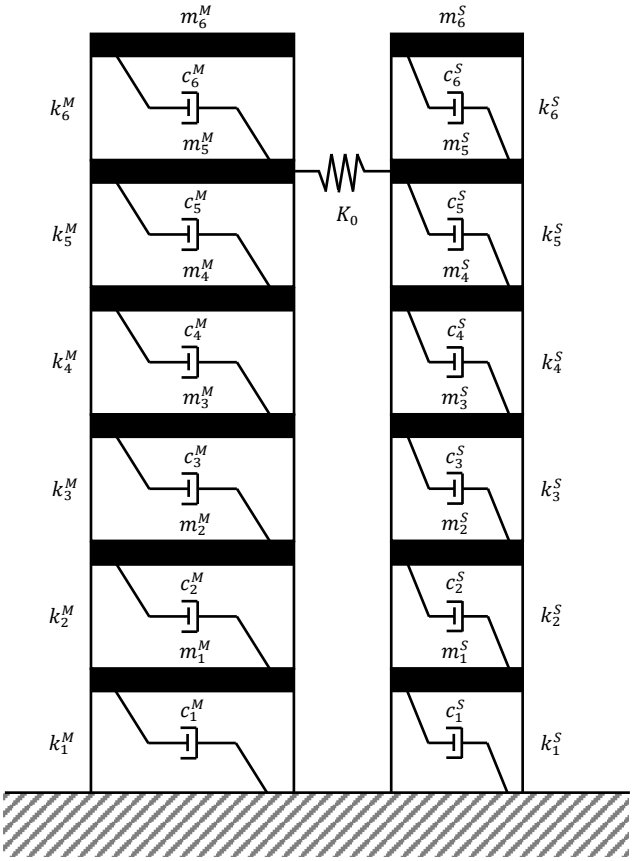

Fig. 3 Analytical CVC-S model with negative stiffness spring as connector

2.2.3. CVC-SD model linked by both dashpot and negative stiffness element

As shown in Fig. 4, in this setting of connecting portion, the CVC-SD model was formed by using both damper (dashpot) and negative stiffness elements as the connecting coupled vibration controller. The mainframe and subframe models as described in Section 2.1. were linked at the sixth floor of the mainframe and subframe by a damper and a negative stiffness element. Equation (1) was adopted as the equation of motion for the CVC model. The corresponding mass, damping, and stiffness matrices expressed by Equations (2), (5), and (6) respectively, were used for the linear analysis subjected to input motions. The combination values of C_0 and K_0 corresponding to CVC-SD model are shown in Table 2.

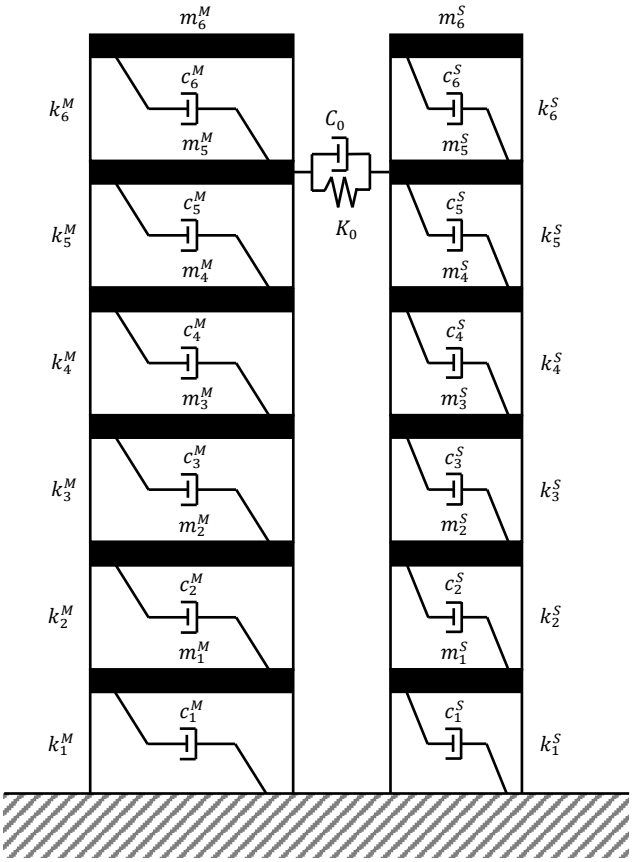

Fig. 4 Analytical CVC-SD model with dashpot and negative stiffness spring as connectors

2.3. Input motions and analytical conditions

For input motions, three simulated earthquake waves were used. Waves M1 through M3 represent the three simulated earthquake waves adopted from the literature [14]. For each time history response simulation, the numerical integration was based on the Newmark β method ($\beta = 0.25$) with a time increment of 0.001 s.

3. Results of linear earthquake response simulation

3.1. Peak response

Figures 5 and 6 show the story-wise relative peak displacement from the ground and absolute peak acceleration responses of the mainframe based on the different settings of connecting elements subjected to three simulated earthquakes (Waves M1-M3) input motions. Fig. 5 shows that the obtained peak displacement of each story of the mainframe for the CVC-S model was decreased compared to the mainframe model with no connection (uncontrolled model) under all the three input motions. Moreover, it was also observed that when the connecting portion consists of both negative stiffness element and dashpot, i.e., CVC-SD model, there was further improvement in the response reduction of the peak displacement of the mainframe. The peak displacement response of the mainframe for the CVC-SD model indicated better performances compared to the peak displacement response of the mainframe for the CVC-D models under each input motion.

Similarly, the peak absolute acceleration responses of the mainframe for the controlled CVC-S, CVC-SD, and CVC-D models under each input motion were plotted as shown in Fig. 6. Also, the peak acceleration response for the uncontrolled case (the MDOF-mainframe model) is shown in Fig. 6. Although a reduction in the peak acceleration response of the mainframe for the CVC-S model was obtained, the control effects in the peak acceleration response of the mainframe for the CVC-SD model was larger when compared to the responses of the mainframe for controlled cases, i.e., CVC-S and CVC-D models. Whereas, an increase in the subframe's responses was observed. This could be because when the subframe's mass is much less than the mainframe's mass, it is assumed that an increase in the subframe's reaction is inevitable. This also shows that

the subframe should have an adequate deformation capacity when the subframe's responses are evaluated as having a large value.

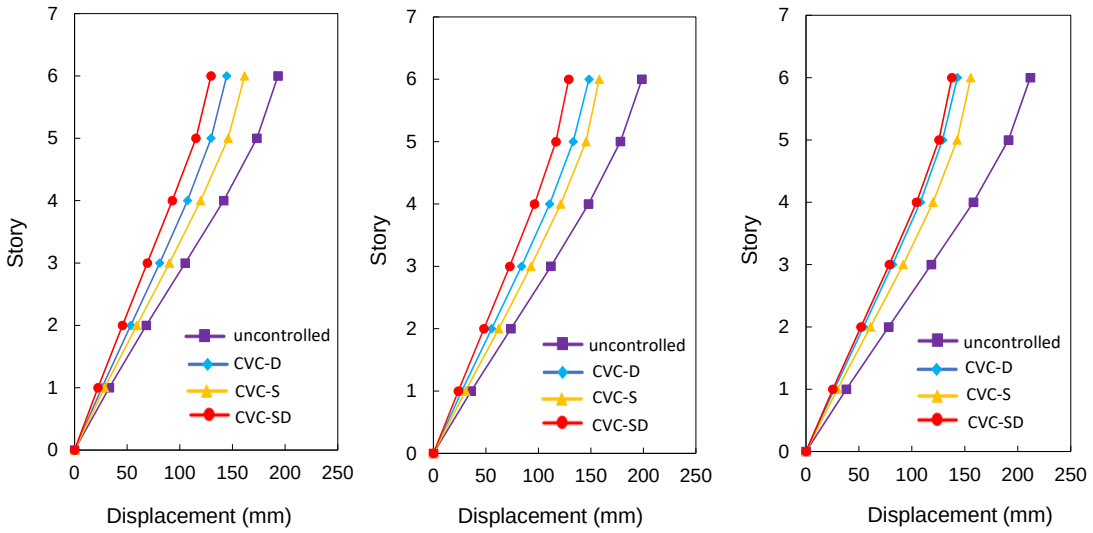

Fig. 5 Story wise peak displacement response of mainframe models based on the connecting elements of CVC model subjected to simulated earthquake **(a)** Wave M1, **(b)** Wave M2, and **(c)** Wave M3

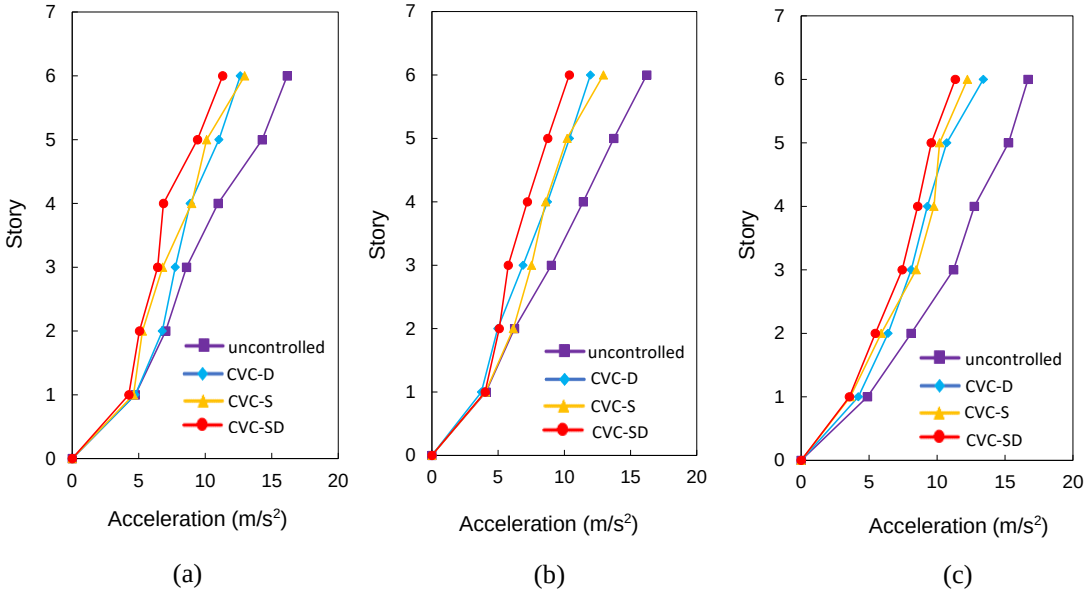

Fig. 6 Story wise peak acceleration response of mainframe models based on the connecting elements CVC model subjected to simulated earthquake **(a)** Wave M1, **(b)** Wave M2, and **(c)** Wave M3

3.2. Evaluation criteria

The control performance of controlled (CVC-SD and CVC-D) models was evaluated based on the evaluation criteria expressed in Equations (7)–(8) in reference to the literature [15,16].

$$J_1 = \frac{\max|x_j(t)|_C}{\max|x_j(t)|_U}, \tag{7}$$

$$J_2 = \frac{\max|\ddot{x}_j(t)+\ddot{x}_g(t)|_C}{\max|\ddot{x}_j(t)+\ddot{x}_g(t)|_U} \tag{8}$$

where t is the time, j^{th} is the number of floor level, $x_j(t)$ is the response displacement of the structures (mainframe and subframe) from the ground, $\ddot{x}_j(t)$ is the response acceleration of the structures, and $\ddot{x}_g(t)$ is the input acceleration. Subscript C denotes the controlled case (the CVC-SD and CVC-D models), and subscript U denotes the uncontrolled case (the MDOF-mainframe and the MDOF-subframe models).

J_1 and J_2 represent the evaluation criteria for the performance of the peak displacement and peak absolute acceleration responses. For a particular model, a smaller value of evaluation criteria implies a better performance and more reduction in responses of the models. The obtained J_1 and J_2 for the top floors of the mainframe and subframe for the CVC-SD and CVC-D models subjected to three input motions are given in Table 3. J_1 and J_2 were the averaged value for the three simulated waves (Waves M1–M3) input motions. The acquired evaluation criteria J_1 and J_2 of the mainframe for CVC-SD had less than unity values, indicating a good seismic control performance. The criteria also showed that the mainframe of the controlled models linked by negative stiffness and damper (CVC-SD model) performed better than that of the mainframe of the controlled models linked by damper solely (CVC-D model). However, the performance of the subframe for the CVC-SD model based on the displacement response (J_1) was greater than unity, but the subframe for CVC-SD performance based on acceleration response (J_2) was less than unity.

Table 3 Evaluation criteria for top floors of the controlled (CVC-SD and CVC-D) models subjected to simulated earthquake (mean for three simulated waves)

CVC models	CVC-SD		CVC-D	
	J_1	J_2	J_1	J_2
Mainframe	0.657	0.673	0.723	0.774
Subframe	1.213	0.945	0.838	0.585

4. Conclusions

This chapter numerically assessed the control effects of negative stiffness utilized as the vibration controller between the MDOF mainframe and MDOF subframe forming the MDOF CVC systems based on linear analysis.

The simulation results showed that combining the negative stiffness element with a supplemental damping element resulted in a significant control effect over the uncoupled/uncontrolled structures. Furthermore, the combination of connecting vibration controller elements resulted in a more significant response reduction of the peak displacement and acceleration of the mainframe for the CVC-SD model than the other controlled models with negative stiffness (CVC-S) or damping element (CVC-D) solely.

Overall, an effective control performance for the response of the mainframe against earthquakes was achieved upon installation of negative stiffness and damping elements at the connecting portion of the CVC models. However, a broader range of input motions, different structural parameters, and optimal connecting elements should be considered to better understand the control performance of the negative stiffness connection on the MDOF CVC system. Also, additional future work includes an investigation of the non-linear analysis of the MDOF CVC system.

References

[1] Mizuno T, Toumiya T, Takasaki M (2003) Vibration isolation system using negative stiffness. *JSME International Journal*, Series C, **46**(3):807–812. https://doi.org/10.1299/jsmec.46.807

[2] Iemura H, Kouchiyama O, Toyooka A, Shimoda I (2008) Development of the friction-based passive negative stiffness damper and its verification tests using shaking table. *The 14th World Conference on Earthquake Engineering*, October 12–17, 2008, Beijing, China.

[3] Nagarajaiah S, Pasala DTR, Reinhorn A, Constantinou M, Sirilis AA, Taylor D (2013) Adaptive negative stiffness: a new structural modification approach for seismic protection. *Advanced Materials Research*, **639**–**640**:54–66. https://doi.org/10.4028/www.scientific.net/AMR.639-640.54

[4] Sarlis AA, Pasala DTR, Constantinou MC, Reinhorn AM, Nagarajaiah S, Taylor DP (2013) Negative stiffness device for seismic protection of structures. *Journal of Structural Engineering*, ASCE, **139**(7):1124–1133. https://doi.org/10.1061/(ASCE)ST.1943-541X.0000616

[5] Walsh KK, Boso, E., Steinberg EP, Haftman JT, Littell WN (2018) Variable negative stiffness device for seismic protection of building structures through apparent weakening. *Journal of Engineering Mechanics*, **144**(9):04018090. https://doi.org/10.1061/(ASCE)EM.1943-7889.0001512

[6] Zhou P, Liu M, Li H (2020) A passive negative stiffness damper in series with a flexible support: Theoretical and experimental study. *Structural Control and Health Monitoring*, **27**(9):e2594. https://doi.org/10.1002/stc.2594

[7] Shirai K, Noro S, Walsh KK (2021) Shake table testing of a passive negative stiffness device with curved leaf springs for seismic response mitigation of structures. *Structural Control and Health Monitoring*, **28**(7):e2736. https://doi.org/10.1002/stc.2736

[8] Yamada Y, Ikawa N, Yokoyama H, Tachibana E (1994) Active control of structures using the joining member with negative stiffness. *The First World Conference on Structural Control*, TP2, Vol. 2, 41–49, 1994, California, USA.

[9] Ikawa N, Yamada Y, Yokoyama H, Tachibana E (1996) Active control system of coupled structures with a negative stiffness. *Journal of Structural Engineering*, AIJ, Vol. **42B**: 629–634. **(in Japanese)**

[10] Shimizu K, Kurino H (2009) Fundamental study of structural control with negative stiffness connection. Part 1: Study of applicability of negative stiffness. *Summaries of Technical Papers of Annual Meeting*, AIJ:453–454. **(in Japanese)**

[11] Kurino H, Shimizu K (2009) Fundamental study of structural control with negative stiffness connection. Part 2: Feasibility study utilizing variable damping device. *Summaries of Technical Papers of Annual Meeting*, AIJ:455–456. **(in Japanese)**

[12] Cimellaro, GP, & Lopez-Garcia D (2011) Algorithm for design of controlled motion of adjacent structures. *Structural Control and Health Monitoring*, **18**(2), 140-148.

[13] Jankowski R, Mahmoud S (2016) Linking of adjacent three-storey buildings for mitigation of structural pounding during earthquakes. *Bulletin of Earthquake Engineering*, **14**(11):3075–3097. https://doi.org/10.1007/s10518-016-9946-z

[14] Shirai K, Inoue N (2014) A seismic response estimation method for RC structures using random vibration theory. *Journal of Advanced Concrete Technology*, **12**(2):62–72. https://doi.org/10.3151/jact.12.62

[15] Al-Fahdawi OAS, Barroso LR, Soares RW (2019) Semi-active adaptive control for enhancing the seismic performance of nonlinear coupled buildings with smooth hysteretic behavior. *Engineering Structures*, **191**:536–548. https://doi.org/10.1016/j.engstruct.2019.04.078

[16] Ohtori Y, Christenson RE, Spencer Jr. BF, Dyke SJ (2004) Benchmark control problems for seismically excited nonlinear buildings. *Journal of Engineering Mechanics*, **130**(4): 366–385. https://doi.org/10.1061/(ASCE)0733-9399(2004)130:4(366)

Chapter V

Experimental investigation on the coupled vibration control structures using a passive negative stiffness device

1. Introduction

Over the past years, researchers have proposed and developed several vibration control (VC) techniques for the structural protection of CVC systems against dynamic excitation such as earthquakes. The control techniques include passive, active, and semiactive control strategies. To mitigate the seismic response of CVC systems, several VC devices, particularly energy dissipators, have been designed and practically implemented [1–12].

Negative stiffness that exerts an opposing restoring force when the displacement increases is considered a potential VC technique for building structures. Rapid progress has been made in researching and developing negative stiffness devices (NSDs) and individual buildings incorporating NSDs [13-18]. These NSDs are adopted in multi-story structures as a base isolation control method to reduce seismic loads. Although extensive analytical and experimental structural control research on NSDs has been conducted, little research on incorporating NSDs into CVC structures has been done. Despite the increasing applications of coupled building control, there has been limited research on assessing the seismic control effectiveness of a passive or active negative stiffness as a connecting vibration controller for CVC systems. The incorporation of NSDs as vibration controllers for CVC systems is relatively a new concept.

An extension of the range of optimal tuning was previously reported to achieve with the adoption of negative stiffness in CVC structures (Chapter II). The linear and non-linear responses of CVC structures incorporated with NSD were also numerically investigated by previous study (Chapters III and IV). In the present research, in Chapter V, an experiment on implementing NSD in a CVC system was conducted. Shaking table tests were carried out to obtain the earthquake responses of a connected building model using a prototyped passive negative stiffness device (PNSD) and the vibration control effects were studied experimentally. The organization of this Chapter V is as follows. Section 2 describes the functionality of the prototype PNSD specimen. Section 3 describes the criterion for the installation of the specimens. Section 4 contains the evaluation of the results. Conclusions with the findings from the study are drawn in Section 5.

2. Negative Stiffness Device for CVC model description

Negative stiffness exerts an opposing restoring force when the displacement increases, unlike the positive stiffness spring. The PNSD concept employed here is comparable to the device developed by Shirai et al. [19], except for the installation and corresponding specification. Shirai et al. [19] provided an in-depth overview of the PNSD. It should be emphasized that, in this study, the PNSD was utilized as a vibration controller that connect two adjacent structures in this work. For completeness, a shorter description of the PNSD development is included herein.

The schematic PNSD shown in Fig. 1 demonstrates how the device functions as a connecting vibration controller between two structures namely mainframe and subframe. The two curved leaf springs are pre-compressed and kept at a constant distance between the beams in the Z-direction. In Fig. 1(a), the dotted regions represent the curved leaf springs subjected to snap-through buckling during relative motion of the upper and lower beams in the X-direction. When the mainframe and subframe corresponding to the connected lower and upper beams moves in the opposite direction, as shown in Figs. 1b and 1c, snap-through buckling will occur in the curved regions depending on the movement of the mainframe in the left or right direction opposite to that of the subframe movement. The mainframe and subframe motions depend on the restoring force produced by the PNSD. It is important to note that forces are exerted on the beams in the increasing direction of the beam displacement when snap-through buckling occurs. This indicates the characteristics of negative restoring force known as negative stiffness through geometric non-linearity.

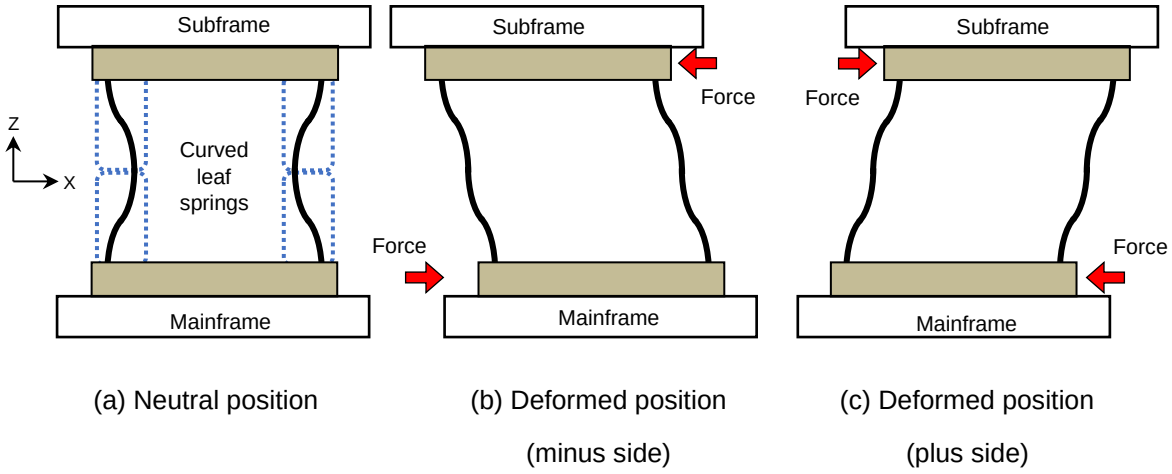

Fig. 1 Schematic diagram of passive negative stiffness device

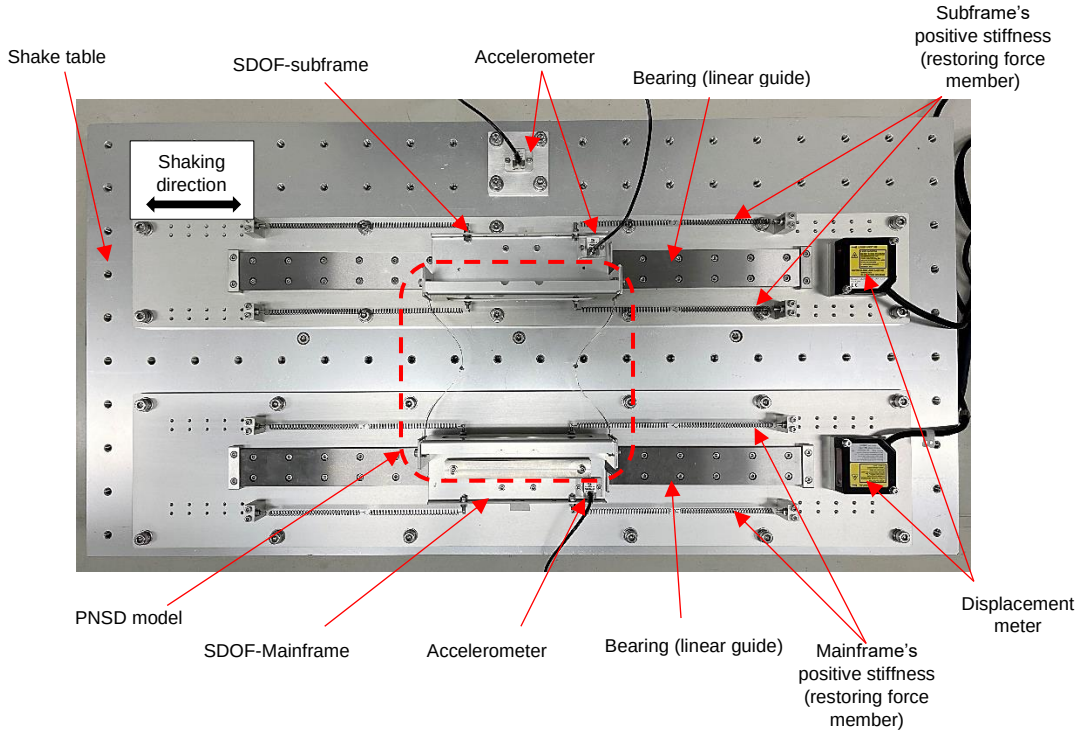

Fig. 2 Photograph of plan view of CVC system connected with PNSD mounted upon shaking table

3. Experimental Methods

3.1. Test Specimens

The CVC system consisting of one mass system of mainframe and one mass system of a subframe was manufactured. This CVC system with and without PNSD was mounted on the shaking table for experimentation. Also, a CVC system with a rigid connection (CVC-R) was tested. Each vibrating specimen (mainframe and subframe) was subjected to excitations. Fig. 2 illustrates the incorporation of the PNSD between the mainframe and subframe, forming the CVC system.

An SDOF-mainframe, an SDOF-subframe, two bearings (linear guides), and positive stiffness restoring members corresponding to the mainframe and subframe specimens together formed the vibrating parts of the CVC system model. The set up was designed to move in one horizontal direction of the shake table excitation (X-direction). The masses of the moving part, namely the mainframe (M_1) and subframe (M_2), were 0.945 kg and 0.468 kg, respectively, resulting in a mass ratio (μ) of 0.5. The two linear guides were installed in the excitation direction of the shake table. The positive restoring forces for the mainframe and subframe were generated by series and parallel connections of tension coil springs. With the application of an initial tensile deformation on them, these springs function in both the -X and +X directions without becoming loose.

3.2. Passive negative stiffness device

The production layout of the PNSD before it was pre-compressed is shown in Fig. 3. As mentioned in Section 2, the concept of PNSD is the same as that of the proposed device by Shirai et al. [19]. Each of the PNSD's curved leaf spring consisted of three plates which were formed such that the ends of the outer plates were bolted to the middle of the center plate. Two such springs were fabricated and pre-compressed between two rigid beams forming curvatures required for occurrence of snap through buckling phenomena. The PNSD was constructed such that both the leaf springs achieved initial curvature and were bilaterally symmetrical. Fig. 4 shows the PNSD adopted for the experimentation. The PNSD specimen's specification for the shake table test is shown in Table 1.

The moving masses, the SDOF-mainframe and SDOF-subframe, were mounted on the shaking table using the two bearings (linear guides). The PNSD was incorporated between these two moving masses forming a coupled system. The two linear guides were positioned on the shake table such that the inner span of the PNSD was maintained constant, i.e., 146 mm, during the shaking experiments. This study utilized the PNSD with a negative stiffness value of –0.00685 N/mm. This negative stiffness was determined by keeping the subframe in a fixed position and mainframe as the vibrating part only and subjected to sinusoidal input wave of frequency 1.0 Hz and displacement amplitude of 10 mm, 12 mm, 13 mm, and 15 mm. The detailed measurement of the negative stiffness is explained in Section 4.2.

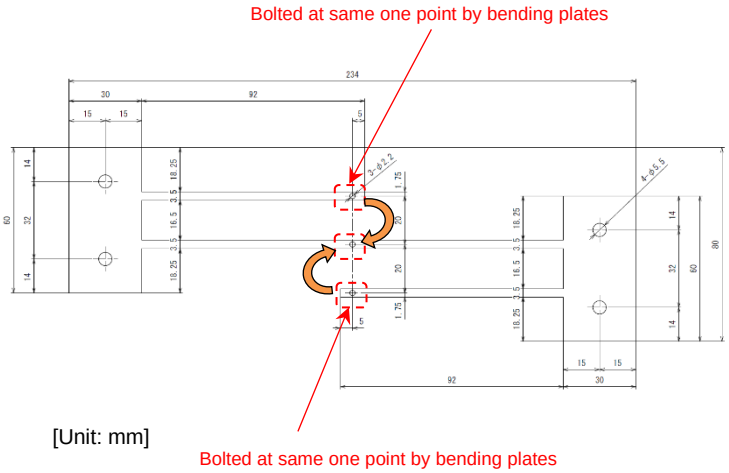

Fig. 3 Production layout of the PNSD before bending process

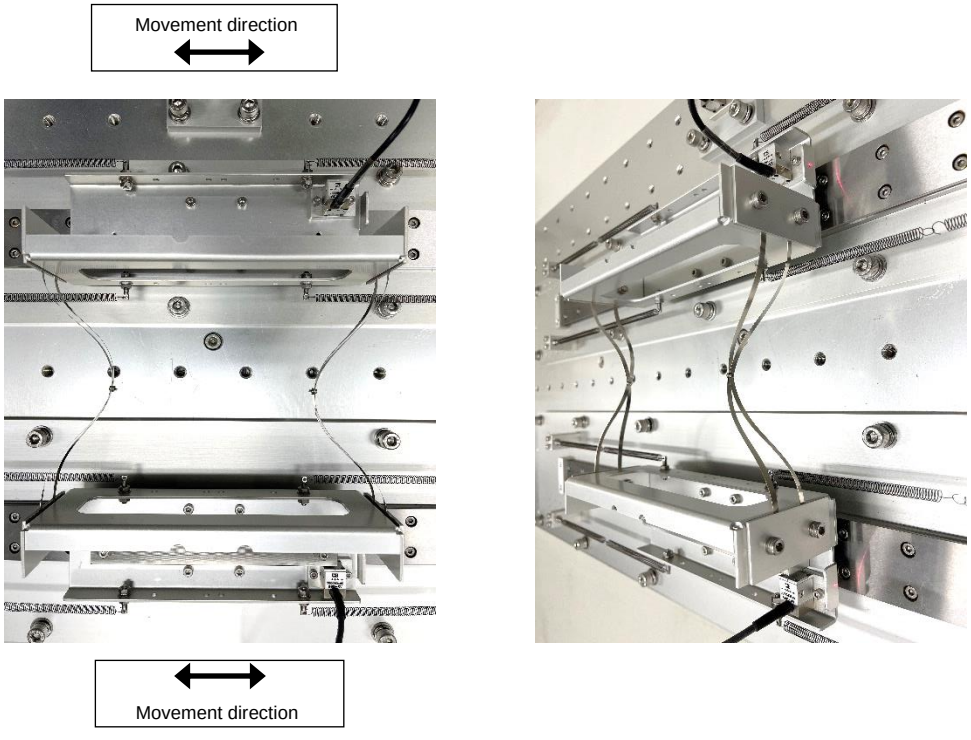

(a) Plan view (b) Side view

Fig. 4 Photograph of plan view and side view of the PNSD installed between mainframe and subframe

Table 1 Specification of the passive negative stiffness devices

Device name	Plate thickness (mm)	Plate width (mm)	Plate length (before bending) (mm)	Inner span of device (when installed) (mm)
PNSD	0.2	3.5	174	146

Table 2 Natural frequencies and damping factor of the vibrating specimens

Specimen name	Natural period (s)	Natural frequency (Hz)	Damping factor
SDOF-mainframe	0.953	1.05	0.15
SDOF-subframe	0.689	1.45	0.13
CVC-R's mainframe	0.833	1.20	0.17
CVC-R's subframe	0.832	1.20	0.17

3.3. Input motions

Sinusoidal waves and simulated earthquake waves were used as the input motions for the shake table test. The sinusoidal waves consisted of five cycles sine function with displacement amplitude of 10–15 mm and with three different frequencies, 1.0 Hz, 1.5 Hz, and 1.2 Hz roughly corresponding to the natural frequencies of the mainframe, subframe, and CVC-R models, respectively. A detailed description of the measurement of these natural frequencies is explained in Section 4.1. Five simulated waves (namely Wave S1 to S5) with a magnification factor of 0.30, 0.40, 0.45, and 0.50 times each wave were also used as input motions. Figs. 5(a) and (b) show the time history acceleration waveforms of the sinusoidal input waves for mainframe and subframe, respectively. Fig. 5(c) depicts the velocity response spectra of the mainframe (damping factor = 0.05) for the five simulated earthquakes (wave S1-S5) input motions with a magnification factor of 0.45.

3.4. Shaking table and vibration direction

The shaking table tests were carried out using a uniaxial shaking table with a maximum acceleration of 1.0 G, a maximum displacement of 100 mm, and a maximum payload of 1000 N. The assembled CVC system was mounted on the shaking table. The shaking tests were performed in the horizontal X-direction, as shown in Fig. 2.

3.5. Measurement

Two laser displacement meters were mounted on the shake table to measure the relative displacements for both mainframe and subframe specimens vibrated with the excitation of the shake table. The absolute accelerations of the shaking table and the vibrating mainframe and subframe specimens in the excitation direction were measured using strain gauge-type accelerometers. The acceleration and displacement data collected from the shaking table tests were smoothed using a moving average with a rectangular window of 0.035 seconds.

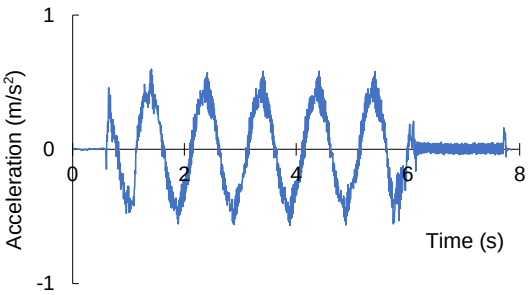

(a) Sinusoidal wave for mainframe (1.0 Hz, amplitude 10 mm)

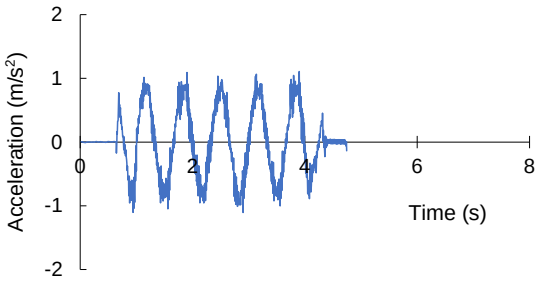

(b) Sinusoidal wave for subframe (1.5 Hz, amplitude 10 mm)

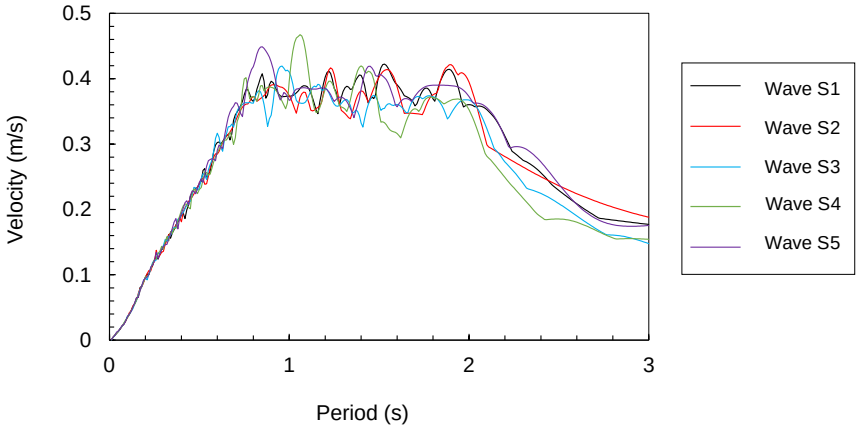

(c) Simulated earthquake waves of damping factor of 5% (magnification factor = 0.45)

Fig. 5 Time history acceleration and velocity response spectra of input motions

3.6. Experiment parameters and shaking conditions

The CVC model used in this experiment was of one mass system of mainframe and one mass system of a subframe. The CVC systems were examined by shaking table tests with/without the prototyped PNSD, subjected to two kinds of input motions, sinusoidal waves and simulated earthquake waves. After each excitation, the specimens were restored to the neutral position to remove any residual displacement, and the next excitation was continued.

4. Experimental results

4.1. Free vibration measurement

Prior to the shaking table test, free vibration measurements of the SDOF-mainframe, SDOF-subframe, and CVC-R system models were conducted to determine their corresponding natural frequencies and damping factors. Without employing the PNSD prototype, the mainframe and subframe specimens were each independently subjected to free vibration (i.e., with the positive stiffness restoring members alone). The free vibration was created by releasing the vibrating mainframe and subframe specimens, respectively, after providing the specimens an initial displacement of 40 mm. Similar procedures were followed for the CVC-R system. The time history displacement waveforms were used to calculate the specimens' natural frequencies and damping factors. The natural frequencies were computed using the time difference between the peak amplitude of the waves, and the damping factors were calculated using the logarithmic damping rate obtained from the amplitude ratio of the waveform's peaks. Table 2 displays the corresponding averaged natural frequencies and damping factor. The frequencies of the sinusoidal waves utilized in the shaking table experiments were set relatively to these natural frequencies, as detailed in Section 3.3. The relatively high value of the damping factors was accounted due to the resistance forces of the corresponding linear guides used as the bearings in the excitation direction.

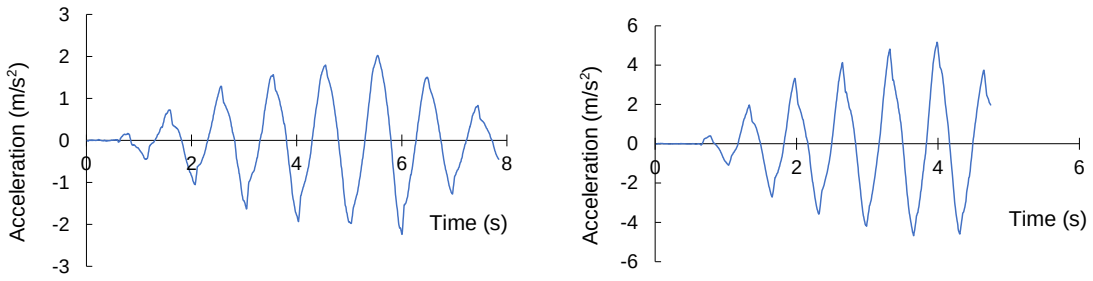

(a) Input frequency 1.0 Hz (b) Input frequency 1.5 Hz

Fig. 6 Time history acceleration response with input amplitude of 10 mm for **(a)** mainframe with frequency 1.0 Hz **(b)** subframe with frequency 1.5 Hz

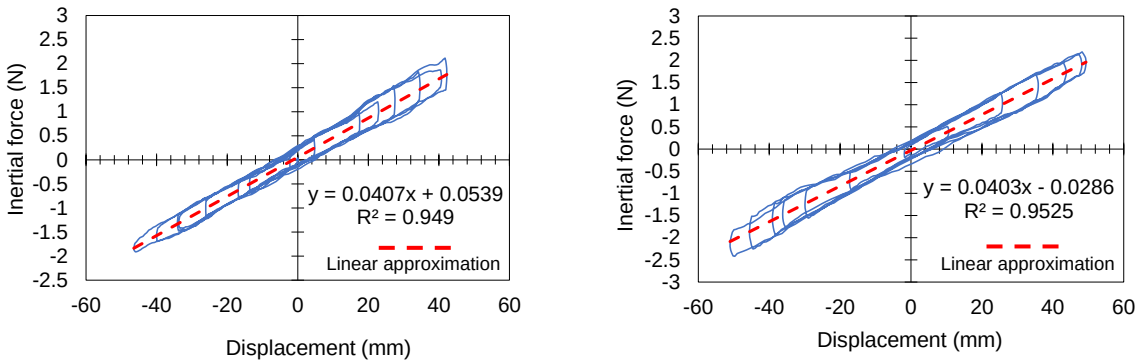

(a) (b)

Fig. 7 Response hysteresis loop without PNSD for **(a)** mainframe **(b)** subframe

4.2. Results of sinusoidal inputs

Figure 6 displays the time history response of the mainframe and subframe without PNSD subjected to sinusoidal waves with input displacement amplitudes of 10 mm and frequencies of 1.0 Hz and 1.5 Hz. Figs. 6(a) and (b) show the time history response acceleration of the mainframe and subframe, where gradual amplification of the responses due to resonances were observed up to around 5.99s for the mainframe's acceleration response and around 3.99s for the subframe's acceleration response. After 5.99s and 3.99s (Figs. 5(a) and (b) respectively), the amplitude of the input accelerations corresponding to the mainframe and subframe became nearly zero and damped free vibration of the acceleration responses were observed.

Figure 7 depicts the inertial force-displacement relationship's hysteresis loops. Due to the resistance of the corresponding linear guides used as bearings and the positive stiffness, a bilinear type of hysteresis loops could be seen (as described in Section 3.1). Figs. 7a and 7b also show a linear function estimated by the least-square approach, including the decision coefficient R^2. Therefore, the horizontal stiffness for the positive stiffness restoring members corresponding to the mainframe and subframe were determined to be K_1 = 0.0407 N/mm and K_2 = 0.0403 N/mm, respectively. Therefore, this study utilized the structural parameters combination for the stiffness ratio ($\alpha = K_2/K_1$) of 1.0 and the mass ratio ($\mu = M_2/M_1$) of 0.50.

The negative stiffness of PNSD was measured by keeping the subframe fixed and connected by the PNSD to the vibrating part consisting of the mainframe only that moves along the linear guide when subjected to sinusoidal waves input in the shaking table excitation direction. Figures 8(a) through 8(d) show the inertial force-displacement relationship of the vibrating system produced upon installation of PNSD subjected to the sinusoidal waves input of displacement amplitudes 10, 12, 13, and 15 mm, respectively with frequency of 1.0 Hz corresponding to the mainframe's natural frequency. From these hysteresis loops, the corresponding subtracted inertial force-displacement relationship of the PNSD obtained, including the linear guide's resistance force, is shown in Fig. 9. The

negative stiffness of PNSD was calculated by deducting the resistance force attributed to the linear guide used as the bearing.

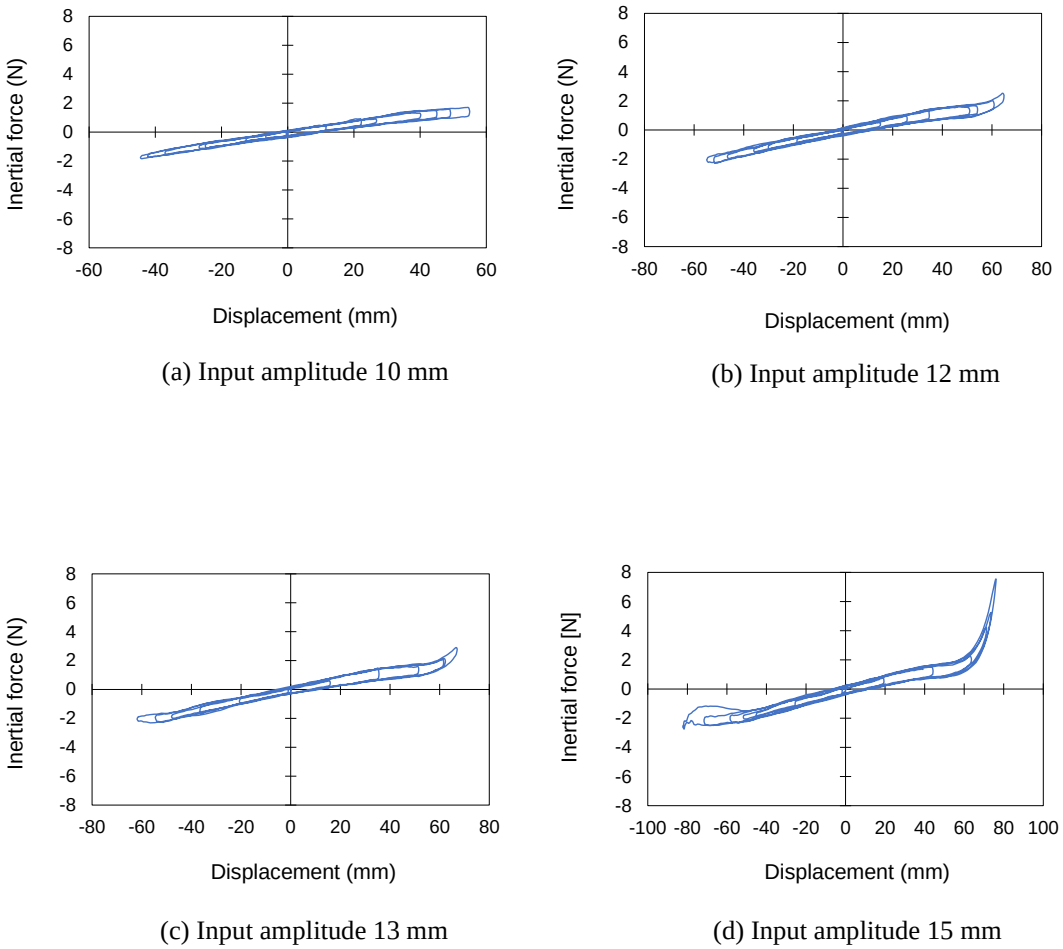

(a) Input amplitude 10 mm

(b) Input amplitude 12 mm

(c) Input amplitude 13 mm

(d) Input amplitude 15 mm

Fig. 8 Response hysteresis loops of SDOF-mainframe with PNSD with one end (SDOF-subframe) fixed for sinusoidal wave input (frequency 1.0 Hz)

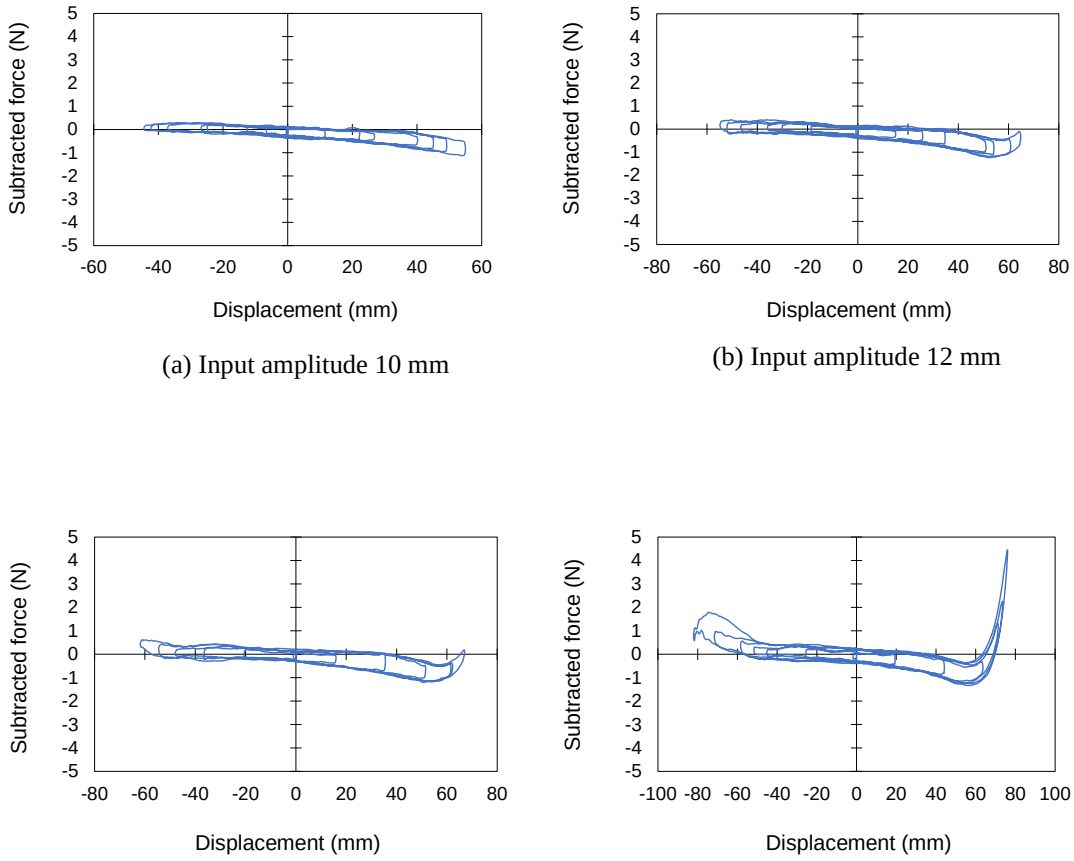

(a) Input amplitude 10 mm

(b) Input amplitude 12 mm

(c) Input amplitude 13 mm

(d) Input amplitude 15 mm

Fig. 9 Subtracted hysteresis loops of PNSD for sinusoidal wave input (frequency 1.0 Hz)

The subtracted hysteresis loops of 1.0 Hz and amplitude of 10, 12, 13, and 15 mm determined that the PNSD exhibited approximately constant negative equivalent stiffness over the range of displacement ±25 mm. The initial stiffness of PNSD was determined by subtracting the positive stiffness of the mainframe without PNSD, K_1 = 0.0407 N/mm, from the initial stiffness of the vibrating system with PNSD. The initial negative stiffness of the vibrating system with PNSD was determined by applying the least square approximation to the force-displacement data between displacement ±25 mm. The initial stiffness was determined to be 0.0336, 0.0339, 0.0343, and 0.0336 N/mm for corresponding 1.0 Hz and amplitudes of 10, 12, 13, and 15 mm, resulting in an average of K_{net} = 0.03385 N/mm. The initial negative stiffness of PNSD (K_{net}-K_1) was then calculated to be K_{ns} = –0.00685 N/mm. It is important to note that the PNSD's displacement limit occurred prior the device could undergo clear snap-through buckling.

As shown in Fig. 9, the maximum section force at zero response displacement was roughly 0.21 N for the PNSD. No significant increase in the section force occurred by adding PNSD to the vibrating component of the specimen, i.e., energy consumption by PNSD was small such as that due to friction between the leaf springs.

Figures 10 and 11 compare the time history response waveforms of the mainframe and subframe with and without PNSD under the sinusoidal wave input with a frequency of 1.0 Hz and an amplitude of 10 mm. A decreased response was generally observed for both the displacement and acceleration responses of the mainframe connected with PNSD, as compared to the responses without PNSD connection; on the other hand, an increase in the subframe's responses was observed, as demonstrated in Figs. 10(b) and 11(b).

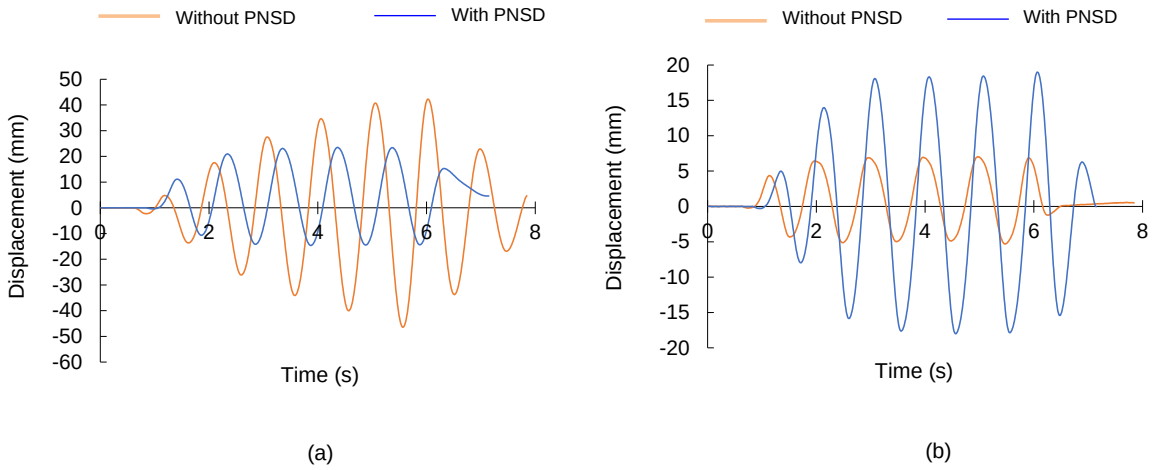

Fig. 10 Comparison of time history response displacement between with or without PNSD for sinusoidal wave inputs (Frequency 1.0 Hz, amplitude 10 mm) of (a) mainframe and (b) subframe

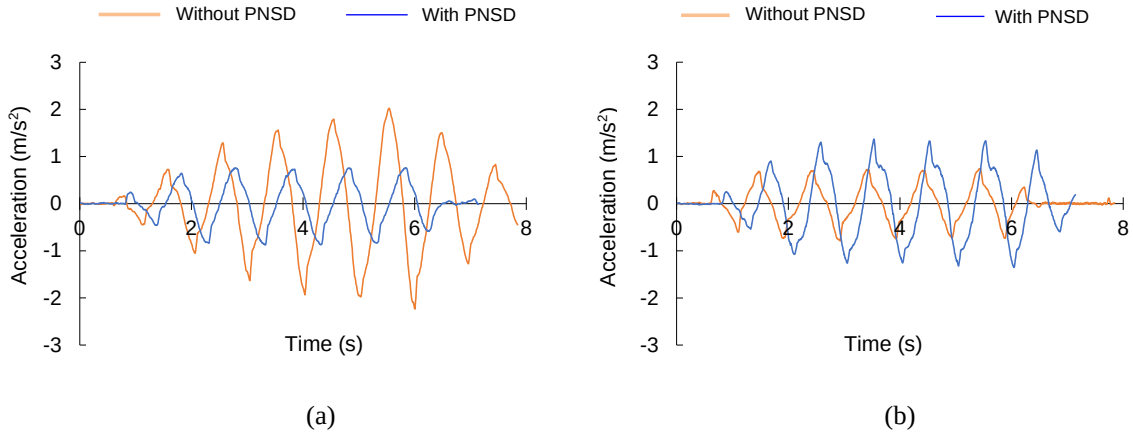

Fig. 11 Comparison of time history response acceleration between with or without PNSD for sinusoidal wave inputs (Frequency 1.0 Hz, amplitude 10 mm) of **(a)** mainframe and **(b)** subframe

4.3. Results of simulated earthquake inputs

Table 3 lists the obtained peak displacement response of the mainframe (averaged for the five simulated waves) for each of the magnification factors of 0.30, 0.40, 0.45, and 0.50 of the CVC-NS, CVC-R, and SDOF-mainframe models. In this Table 3, $PD_{1,ns}$, $PD_{1,rc}$, and $PD_{1,SDOF}$ denote the peak seismic displacement response of the mainframe for the CVC-NS, CVC-R, and SDOF-mainframe models, respectively. Similarly, Table 4 shows the peak acceleration response of the mainframe averaged for the five simulated earthquake waves. $PA_{1,ns}$, $PA_{1,rc}$, and $PA_{1,SDOF}$ denote the peak seismic response acceleration of the mainframe for the CVC-NS, CVC-R, and SDOF-mainframe models, respectively. These findings show that the peak displacement responses of the mainframe for the controlled CVC-NS model were lower than those for the uncontrolled SDOF-mainframe model (Table 3). Additionally, compared to the SDOF-mainframe model, the peak acceleration response for the CVC-NS model was reduced (Table 4).

The displacement reduction index and the acceleration reduction index for the CVC-NS model's mainframe compared with the SDOF-mainframe model were calculated as $1 - (PD_{1,ns}/PD_{1,SDOF})$ and $1 - (PA_{1,ns}/PA_{1,SDOF})$, respectively, and these reduction indices averaged for the five simulated earthquake input motions are shown in Tables 3 and 4. The displacement reduction indices yielded a promising result (Table 3). In addition, a satisfactorily high acceleration reduction index was obtained (Table 4).

Overall, from the response simulation results, an effective control performance for the response of the mainframe against various excitations was established upon incorporating negative stiffness at the connecting portion of the CVC models. Figs. 12 and 13 show the mainframe's displacement and acceleration response, respectively, with and without PNSD subjected to simulated earthquake input (Wave S1 ×0.45). From Fig. 12, it was also observed that incorporating the PNSD reduced the displacement response of the mainframe compared to the SDOF-displacement response of mainframe without the PNSD over the displacement range ±25 mm, where the PNSD exhibited approximately constant negative equivalent stiffness.

Figures 14a and 14b depict the peak response reduction ratio of displacement and acceleration (averaged for the five simulated waves), respectively for the mainframe and subframe corresponding to the magnification factors of 0.20, 0.30, 0.40, 0.45, and 0.50. The displacement reduction ratio was calculated from the ratio of the averaged peak displacement of the CVC-NS model to that of the SDOF model for the input motions. Similarly, the acceleration reduction ratio was calculated from the ratio of the averaged peak acceleration responses of the CVC-NS model to that of the SDOF model for the input motions. The results indicated that both peak displacement and acceleration responses of the mainframe for the CVC-NS model were significantly reduced compared to those of the SDOF-mainframe model for the corresponding input motion's magnification factors. However, in general, the response reduction ratios of the subframe became larger than unity.

Table 3 Peak displacement of mainframe for CVC-R, SDOF-mainframe, and CVC-NS models obtained from shaking table test, along with reduction index (mean for five simulated earthquake (S1-S5) waves)

Magnification factor	$PD_{1,rc}$ (mm)	$PD_{1,SDOF}$ (mm)	$PD_{1,ns}$ (mm)	$1-(PD_{1,ns}/PD_{1,SDOF})$
0.20	10.612	12.474	12.165	0.025
0.30	20.330	24.651	20.610	0.164
0.40	30.351	37.317	29.571	0.208
0.45	35.648	43.559	34.307	0.212
0.50	40.171	50.597	40.471	0.200

Table 4 Peak acceleration of mainframe for CVC-R, SDOF-mainframe, and CVC-NS models obtained from shaking table test, along with reduction index (mean for five simulated earthquake (S1-S5) waves)

Magnification factor	$PA_{1,rc}$ (m/s^2)	$PA_{1,SDOF}$ (m/s^2)	$PA_{1,ns}$ (m/s^2)	$1-(PA_{1,ns}/PA_{1,SDOF})$
0.20	0.747	0.669	0.540	0.193
0.30	1.358	1.336	0.946	0.292
0.40	1.983	1.776	1.312	0.261
0.45	2.324	2.115	1.544	0.270
0.50	2.607	2.417	1.829	0.243

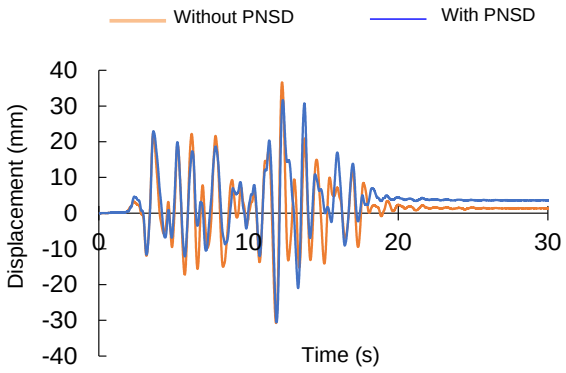

Fig. 12 Comparison of time history response displacement of mainframe between with or without PNSD for simulated earthquake input (Wave S1 ×0.45)

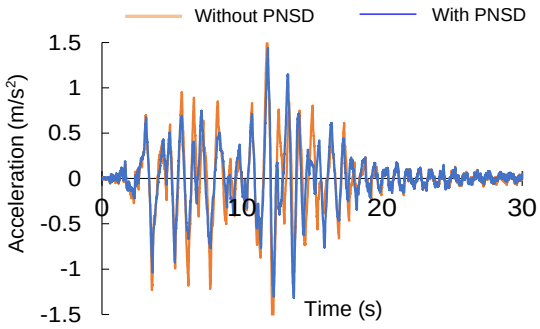

Fig. 13 Comparison of time history response acceleration of mainframe between with or without PNSD for simulated earthquake input (Wave S1 ×0.45)

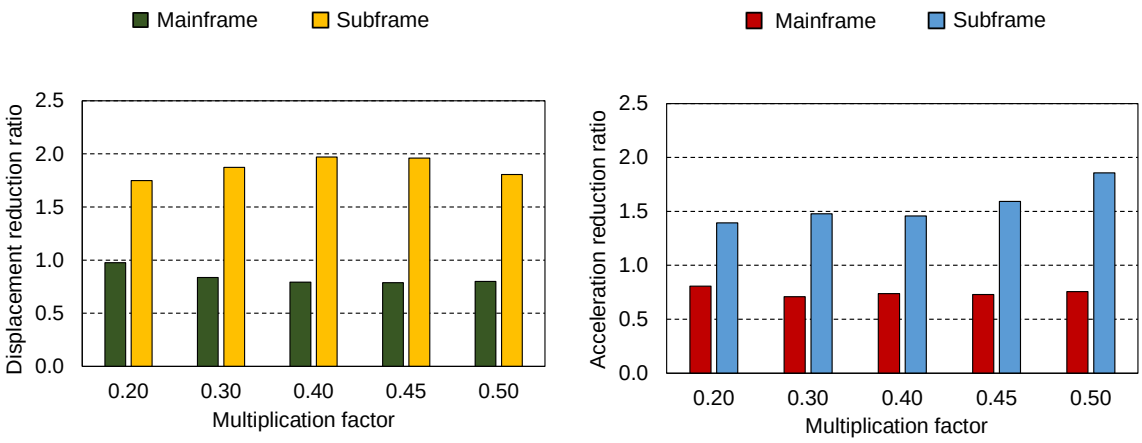

Fig. 14 Peak response reduction ratio (averaged for five simulate earthquakes waves) between CVC-NS models and SDOF-models based on **(a)** displacement response **(b)** acceleration response of mainframe and subframe

5. Conclusions

The effectiveness of negative stiffness as the connecting vibration controller for coupled structures was experimentally explored through a shake table testing. The operation, functionality, and design parameters of the PNSD and CVC system models were presented in detail. On a shaking table test that was subjected to various sinusoidal waveforms and simulated earthquake waves, the responses of the CVC specimens with and without the prototype PNSD were evaluated. The response performances of the vibrating specimens with and without PNSD and response characteristics, such as peak displacement and acceleration responses, were investigated.

With the addition of PNSD, a significant decrease in the displacement and acceleration responses of the CVC system's mainframe was observed. Finally, the study in this Chapter V validated the analytical and numerical results by conducting an experiment on CVC systems connected by prototype PNSD mounted on the shake table subjected to different excitations. The displacement limit of the PNSD was achieved before evident snap-through buckling, although the response decrease was still noticeable. Future research will be required to extend the results of this study by employing multi-story CVC structures subject to ground motions and PNSD with snap-through buckling phenomena with a larger displacement limit.

Acknowledgments

The funding supports by the Japan Society for the Promotion of Science Grant-in-Aid for JSPS Research Fellow, and the Kajima Foundation 2021 Research Grant are gratefully acknowledged.

References

[1] Minami S, Yamazaki S, Toyama K, Tahara K (2004) Experimental study on coupled vibration control structures. *The 13th World Conference on Earthquake Engineering*, Paper No. 2351, August 1–6, 2004, Vancouver, B.C., Canada.

[2] Palacios-Quiñonero F, Rubió-Massegú J, Rossell JM, Karimi HR (2014) Vibration control for adjacent structures using local state information. *Mechatronics*, **24**(4):336–344. http://dx.doi.org/10.1016/j.mechatronics.2013.08.001

[3] Zhang WS, Xu YL (2000) Vibration analysis of two buildings linked by Maxwell model-defined fluid dampers. *Journal of Sound and Vibration*, **233**(5):775–796. https://doi.org/10.1006/jsvi.1999.2735

[4] Ni YQ, Ko JM, Ying ZG (2001) Random seismic response analysis of adjacent buildings coupled with non-linear hysteretic dampers. *Journal of Sound and Vibration*, **246**(3):403–417. https://doi.org/10.1006/jsvi.2001.3679

[5] Ying ZG, Ni YQ, Ko JM (2003) Stochastic optimal coupling-control of adjacent building structures. *Computers & Structures*, **81**(30–31):2775–2787. https://doi.org/10.1016/S0045-7949(03)00332-8

[6] Christenson RE, Spencer Jr BF, Johnson EA, Seto K (2006) Coupled building control considering the effects of building/connector configuration. *Journal of structural engineering*, ASCE, **132**(6):853–863. https://doi.org/10.1061/(ASCE)0733-9445(2006)132:6(853)

[7] Basili M, De Angelis M, Fraraccio G (2013) Shaking table experimentation on adjacent structures controlled by passive and semi-active MR dampers. *Journal of Sound and Vibration*, **332**(13):3113–3133. https://doi.org/10.1016/j.jsv.2012.12.040

[8] Basili M, De Angelis M (2017) Vibration analysis and models of adjacent structures controlled by magnetorheological dampers. *Shock and Vibration*. Article ID 9596382. https://doi.org/10.1155/2017/9596382

[9] Basili M, De Angelis M, Pietrosanti D (2019) Defective two adjacent single degree of freedom systems linked by spring-dashpot-inerter for vibration control. *Engineering Structures*, **188**:480–492. https://doi.org/10.1016/j.engstruct.2019.03.030

[10] De Domenico D, Qiao H, Wang Q, Zhu Z, Marano G (2020) Optimal design and seismic performance of Multi‐Tuned Mass Damper Inerter (MTMDI) applied to adjacent high‐rise buildings. *The Structural Design of Tall and Special Buildings*, **29**(14):e1781. https://doi.org/10.1002/tal.1781

[11] Kazemi F, Miari M, Jankowski R (2021) Investigating the effects of structural pounding on the seismic performance of adjacent RC and steel MRFs. *Bulletin of Earthquake Engineering*, **19**(1):317–343. https://doi.org/10.1007/s10518-020-00985-y

[12] Lu L, Xu J, Zhou Y, Lu W, Spencer Jr BF (2021) Viscous inertial mass damper (VIMD) for seismic responses control of the coupled adjacent buildings. *Engineering Structures*, **233**:111876. https://doi.org/10.1016/j.engstruct.2021.111876

[13] Mizuno T, Toumiya T, Takasaki M (2003) Vibration isolation system using negative stiffness. *JSME International Journal*, Series C, **46**(3):807–812. https://doi.org/10.1299/jsmec.46.807

[14] Iemura H, Kouchiyama O, Toyooka A, Shimoda I (2008) Development of the friction-based passive negative stiffness damper and its verification tests using shaking table. *The 14th World Conference on Earthquake Engineering*, October 12–17, 2008, Beijing, China.

[15] Nagarajaiah S, Pasala DTR, Reinhorn A, Constantinou M, Sirilis AA, Taylor D (2013) Adaptive negative stiffness: a new structural modification approach for seismic protection. *Advanced Materials Research*, **639**–**640**:54–66. https://doi.org/10.4028/www.scientific.net/AMR.639-640.54

[16] Sarlis AA, Pasala DTR, Constantinou MC, Reinhorn AM, Nagarajaiah S, Taylor DP (2013) Negative stiffness device for seismic protection of structures. *Journal of Structural Engineering*, ASCE, **139**(7):1124–1133. https://doi.org/10.1061/(ASCE)ST.1943-541X.0000616

[17] Walsh KK, Boso, E., Steinberg EP, Haftman JT, Littell WN (2018) Variable negative stiffness device for seismic protection of building structures through apparent weakening. *Journal of Engineering Mechanics*, **144**(9):04018090. https://doi.org/10.1061/(ASCE)EM.1943-7889.0001512

[18] Zhou P, Liu M, Li H (2020) A passive negative stiffness damper in series with a flexible support: Theoretical and experimental study. *Structural Control and Health Monitoring*, **27**(9):e2594. https://doi.org/10.1002/stc.2594

[19] Shirai K, Noro S, Walsh KK (2021) Shake table testing of a passive negative stiffness device with curved leaf springs for seismic response mitigation of structures. *Structural Control and Health Monitoring*, **28**(7):e2736. https://doi.org/10.1002/stc.2736

Chapter VI

Conclusions

1. Research findings and conclusions

From this research, the following findings and conclusions can be drawn:

(1) The control effects of negative stiffness as the connecting element between the mainframe and subframe for the CVC model were analytically and numerically assessed based on a TF analysis. Optimal tuning for minimizing the peak amplitude of the displacement TF for the mainframe was observed, showing that adopting negative stiffness in CVC structures can extend the range of optimal tuning conditions.

(2) The optimal damping coefficient required for setting the connecting vibration controller with optimal negative stiffness of the CVC-SD model was reduced. The reduction in the peak amplitude of the displacement TF of the mainframe of the CVC-SD model was also observed compared to the CVC-D model without negative stiffness and damper only.

(3) The effective control performance for the negative stiffness as a vibration controller was numerically evaluated. Installing the optimized negative stiffness and optimized damping elements at the connecting portion of the CVC-SD model subjected to various earthquakes, including simulated waves and observed records, showed an effective control performance on the responses of the mainframe against vibration.

(4) Numerical investigation on combining the negative stiffness element with an additional damping element for linear multi-story coupled structures subjected to simulated earthquakes resulted in a significant vibration control effect compared with the uncoupled structures.

(5) Shaking table tests of coupled structures with negative stiffness as a connecting element were performed. The control effectiveness of negative stiffness as connecting vibration controller was proved through the experiments.

(6) The results show that PNSD can be considered as one of the potential vibration controllers for adjacent structures. The study contributes to effective structural design for newly constructed coupled adjacent buildings and aseismic retrofitting of existing mainframes by connecting with newly added subframes using PNSD.

2. Future work

The thesis explores the incorporation of negative stiffness as a vibration controller for coupled structures. The followings are some of the future research tasks recommended to be carried out:

(1) An investigation of analytical MDOF-CVC models with different structural parameters, and optimal connecting elements to understand the control performance of negative stiffness.
(2) Optimization solution on the location of the PNSD in the height of the connection elements using multi-story building models for the mainframe and subframe of CVC structures.
(3) To generalize the findings of this work, further experimental investigations would be conducted on PNSD with a larger displacement limit and snap-through phenomenon in MDOF-CVC structures subjected to ground motions.
(4) A study on robustness against parameter variation in the optimal tuning of CVC system with PNSD.

LIST OF RELATED PUBLISHED PAPERS

- **International peer-reviewed journal**

(1) Longjam S, Shirai K (2022) Numerical investigation of earthquake response reduction effects by negative stiffness connection for adjacent building structures. *Structures*, Vol. **38**, 672-688. https://doi.org/10.1016/j.istruc.2022.01.078

- **International peer-reviewed conference proceedings**

(1) Longjam S, Shirai K (2021) Use of negative stiffness for coupled vibration control structures: an analytical investigation. *The 17th World Conference on Earthquake Engineering*, September 27–October 2, 2021, Sendai, Japan.